UNIVERSIDAD DE SANTIAGO DE CHILE

FACULTAD DE CIENCIA
Departamento de Física

Circuit quantum electrodynamics in the ultrastrong coupling regime as resource for energy transport.

Francisco Andrés Cárdenas López

Profesores Guías:

Juan Carlos Retamal Abarzúa

Guillermo Esteban Romero Huenchuñir

Tesis para optar al grado de Doctor en Ciencia con Mención en Física.

Santiago – Chile

2018

Resumen

Este trabajo de tesis tiene como objetivo estudiar como un sistema luz-materia en el rgimen de acoplamiento ultra-fuerte, denominado sistema de Rabi cuntico (QRS) mejora el proceso de generacin y transporte de excitaciones cuando este sistema es considerado como mediador. La anarmnicidad en el espectro de energa y las reglas de seleccin de los operadores del sistema son un elemento clave en la mejora de estos procesos. El primer resultado de esta tesis consiste en estudiar como las caractersticas este sistema permiten implementar un protocolo para transferir excitaciones y estados cunticos aun cuando el sistema mediador (QRS) no posee coherencia cuntica. El segundo resultado consiste en estudiar como este sistema de Rabi acta como mediador en la generacin de estados fotnicos correlacionados y no correlacionados en cavidades de microondas. Aqu, la interaccin dispersiva entre las cavidades y el sistema mediador es posible obtener procesos de generacin paramtrica. Dependiendo del nmero de cavidades, los estados generados pueden ser no correlacionados o correlacionados. Adems, el tiempo de generacin de estos estados es inversamente proporcional al nmero de cavidades en el sistema. En ambos trabajos, se ha estudiado la dinmica del sistema fsico considerando parmetros experimentales consistentes con la plataforma de circuitos superconductores.

Keywords: Superconductividad, Circuitos Superconductores, Interacción Luz-Materia, Régimen de acoplamiento ultra fuerte.

Abstract

In this thesis, we addressed how a light-matter system in the ultra-strong coupling regime, termed as quantum Rabi system (QRS) improving the generation and the transport of excitation when this system is considered as a mediator. The anharmonicity of the energy spectrum and the selection rules of the system operators are a crucial element in these tasks. The first problem of this thesis concern with the development of a protocol to perform quantum state transfer between two-level systems even though the mediator (QRS) does not have quantum coherence. The second result concerns the generation of uncorrelated and correlated photonic quantum states in microwave cavities. Here, the dispersive interaction among the QRS and the cavities allow generating parametric process. Depending on the number of cavities this process permits to create uncorrelated or correlated copies of quantum states. Furthermore, the generation time of these states is inverse proportional to the number of cavities on the system. In both problems, we have studied the dynamics of the physical system with the environment considering consistent experimental parameters with near-term superconducting circuit technologies.

Keywords: Superconductivity, Superconducting Circuit, Light-Matter Interaction, Ultrastrong Coupling Regime.

To Margarita and Manuel

“Nothing great in the world has ever been accomplished without passion”

Friedrich Hegel.

Acknowledgment

I wish to thank Margarita and Manuel, my parents, whose support has been significant during every stage of my life. Furthermore, I also want to acknowledge to Cristina, my system, which recommended me to chose physics. On the other hand, I also want to thank my advisors, Juan Carlos Retamal and Guillermo Romero, The feedback given by them during my PhD helped me to grow as a scientist. Moreover, I also wish to acknowledge to Sebastian Allende for its useful aid and numerical tips, and that be a person ordered is very useful in science. Finally, I want to thank the support from Financiamiento Basal para Centros Científicos y Tecnológicos de Excelencia FB. 0807 and Dirección de Postgrado USACH, and FONDECYT under grant No. 1140194.

Table of Contents

Index of Tables

Index of Figures

Introduction

Quantum mechanics has radically changed our understanding of the physical phenomena at the fundamental scale. One of the most crucial aspects of this theory is that it forces us to recklessness concepts firmly rooted in our intuition as determinism and localization. In fact, concepts such as the quantum uncertainty [Hei27] and non-local properties as entanglement have a profound impact on the way we observe and understand the world. For this reason, the main feature of quantum mechanics is the capability to predict physical phenomena impossible to be described with classical theory. For instance, for an experiment involving atomic systems interacting with an external magnetic field as in the Stern-Gerlach (SG) experiment [GS89], the classical theory is not able to explain the preferential direction of deviation of the atomic particles observed in the experiment. Quantum mechanics thoroughly describes the experimental observations. Here, the physical systems can have discrete degrees of freedom. Therefore, the number of possible outcomes on the system is also discrete (In the SG experiment, the atomic particle can deviate upwards or downwards). Another exciting effect observed in this experiment is the impossibility to know a priori which will be the final state of the system. To know the final state of the system it is necessary to perform a measurement, that is, perturb the system. This fact shows that the possible outcomes on a quantum system are probabilistic instead of deterministic. In the SG experiment, the deviation probability of the atomic particle is equal to $P = 1/2$ (upwards and downwards). The following feature also shows that in a quantum system the possible outcomes are superposed. This phenomenon is known as the superposition principle and has been used to develop protocols within the information processing realm [Gro96; DJ92].

On the other hand, the development of a complete description about how light interacts with matter at the quantum level became an important achievement for this theory. The first step to develop the theory of light-matter interaction was done by P. Dirac and E. Fermi in the decade of the 1920 [Dir27; Fer32] with the development of quantum electrodynamics [Fey06]. In such case, light and matter interact via the minimal coupling in the Coulomb gauge [SZ97]. This coupling consid-

ers that light (either classical or quantum) coming from an external source interacts with an atom in the far wavelength limit [GAF10]. In this limit, the electromagnetic field only depends on the relative position of the atom and time. For the case where the light source is classical, and the atom is quantum (discrete energy levels), the model describing the light-matter interaction corresponds to the Rabi model [Rab37], obtained by applying perturbation theory to the minimal coupling and considering the dipole approximation [SZ97]. Differently, when the system is completely quantum (field source and the atom), the model describing the light-matter interaction corresponds to the quantum Rabi model [Rab36; Bra11]. In earlier quantum mechanics, this model was not solvable, and it had to be approximated using the rotating wave approximation [WY07], within this approximation, the Rabi model becomes the Jaynes-Cummings model [JC63; SK93; GKL13; Sho07; KM80]. The Jaynes-Cumming model has the property that the number of excitations on the system is a conserved quantity. Therefore, the model diagonalize in an effective 2×2 basis involving N excitations distributed either in the atom or the field mode. On the other hand, extensions of the light-matter interaction model beyond one atom have also been studied. We highlight two models involving multi-atom systems: the Dicke model [Dic54; Gar11] and the Tavis-Cummings model [TC68; TC69], which correspond to generalizations of the quantum Rabi model and the Jaynes-Cumming model for a set of N atoms interacting with a quantized electromagnetic field mode, respectively. Single and multi-atom models were implemented in quantum platforms as trapped ions [RSR07; Gut+01], and cavity quantum electrodynamics in both optical and microwave domain [Bru+87; SEW91; Bru+92; RBH01].

Given the proper nature of the quantum mechanics, one of the most important technological challenges is the construction of physical systems isolated from the environment. This can be accomplished by considering two different approaches: isolating natural systems or building artificial (hand-made) systems [Lan13; Sch07; Bis10; Bla+04]. The first approach considers physical systems which are already existing in nature, and by applying quantum engineering try to isolate specific degrees of freedom from the environment, as observed in experiments with confined photons into high-quality cavities, or trapped ions inside Paul traps, among others quantum platforms. The main disadvantage of this approach lies in the impossibility to perform quantum engineering on the system parameters as, for example, coupling strengths and energy gaps of two-level systems. The second alternative takes advantages of tailor-made physical systems whose behavior mimic the one of natural quantum systems. In this way, the technological progress to fabricate and design devices with quantum internal degrees of freedom has extensively grown the last three decades. A remarkable platforms are superconducting circuits, circuit quantum electrodynam-

ics [SG08; YN11; HTK12; DS13; Lan13; Sch07; Bis10; Bla+04], and lately microwave quantum photonics [Nak12; HJ+16; Gu+17]. In these platforms, the fundamental systems are constituted of electronic circuits whose natural frequencies are in the microwave regime. Artificial atoms [Dev+98; Koc+07; Orl+99; Wal+00; Yan+16] have been implemented in Josephson junction-based circuits. The Josephson junction is modeled by the RCL model [Tin04] i.e., as a capacitance connected in series with a non-linear inductor. This non-linear element introduces anharmonicity on the energy spectrum of the circuit, emulating the energy spectrum of an atomic system as the Hydrogen atom. Moreover, single and multi-mode microwave cavities have been implemented by using LC circuit, and in distributed circuit element as the strip-line and coplanar waveguide resonator [Sim04; Göp+08]. Advances on lithography techniques have permitted to build artificial atoms with dipole moment larger than the observed in alkaline and Rydberg atoms [TRK92; Bla+04]. Furthermore, it is also possible to build transmission line resonators whose vacuum Rabi splitting to be a least one hundred times larger than the one observed in 3D microwave cavities on cavity quantum electrodynamics [RBH01]. Also, it is possible to couple resonators through non-linear inductors. The coupling strength achieved in this setup has made possible to study effects not observed in atomic systems, for instance, it has been possible to observed enhanced Self and Cross Kerr effects between resonators [Ber+10; BGB10; Eic+11; Bou+12; Har+12]. Likewise, these fabrication techniques have also allowed to build both artificial atoms and photons sources with increasingly large coherence times [OW13; SSS17]. The combination of these improvements have allowed studying the light-matter interaction in electrical circuits.

The light-matter interaction between electrical circuits has been implemented using the charge and flux qubit. In both cases, the artificial atom is coupled to a transmission line resonator and the nature of light-matter interaction may change depending on the type of artificial atom. In fact, for charge or transmon qubit, the light-matter coupling is obtained via capacitive coupling [Bla+04; YTN03], whereas the light-matter coupling that involves a flux qubit is implemented either via mutual inductance [Izm+04; Plo+07; All+10] or galvanic coupling [YN03; NWF04]. Notice that these kinds of couplings are analog to the electric and magnetic dipole coupling in atomic systems, respectively [Gu+17]. Besides, the technological progress on material science and fabrication techniques have also made possible to achieved light-matter regimes that are not possible to obtain in standard quantum optics setups. We refer to as the ultra-strong coupling (USC) [CBC05; FD+16b; CC06; FD+10; AN10; Bau+16; Nie+10; BA17; Bos+17], and Deep strong coupling (DSC) regime [Cas+10a; Yos+16]. In these regimes, the ratio between the light-matter coupling becomes comparable to (USC) or larger than (DSC) the bare frequencies of the system components. As

a result, the rotating wave approximation breaks down, and the simplest model describing the light-matter interaction is the quantum Rabi model [Rab36; Bra11]. This model presents a discrete symmetry known as parity $\mathbb{Z}_2$. In such a case, the energy levels present specific selection rules for state transitions. These selection rules have been reported to be useful for performing quantum information processing and quantum simulations [NC11; Rom+12; Kya+15b; Kya+15a; Wan+16; AA+18].

In this thesis, by using the properties exhibited by light-matter systems in the ultra-strong coupling regime, termed as QRS, as anharmonic energy spectrum and internal selection rules, together with dispersive coupling between the system components, we address the problem of transport of energy. The first result obtained in this thesis concerns the high-fidelity quantum state transfer mediated by the QRS initialize in a thermal state. We demonstrate high-fidelity swap operations between qubits even though the quantum bus is thermally populated. . We discuss a possible physical implementation in a realistic circuit QED scheme that leads to the multimode Dicke model. The second result concerns the generation and transport of quantum copies of microwave photons. Our method considers two-photon processes that take place in a system composed of two extended cavities and an ultrastrongly coupled light-matter system. Under specific resonance conditions our method generates, in a deterministic manner, product states of uncorrelated photon pairs, Bell states, and W states. We demonstrate improved generation times when increasing the number of multi-mode cavities, and prove the generation of genuine multipartite-entangled states when coupling an ancillary system to each cavity.

Chapter 1

The Phenomenon of superconductivity

Superconductivity phenomenon was discovered in 1911 by Onnes [KO11]. Onnes observed the disappearance of the electrical resistance in metals such as mercury, lead, and tin when they are cooled down at a temperature below to their critical temperature. This temperature is characteristic of the metal [Tin04]. Another essential phenomenon observed in a superconductor is the emergence of a persistent current. It has been observed that this current may flow on the superconductor without decreasing in the time. In fact, it has been shown that the lifetime of this current is about 10^5 years [Tin04]. Both phenomena are usually known as *the perfect conductivity*.

Another critical phenomenon observed in a superconductor is the perfect diamagnetism or Meissner effect, discovered in 1933 by Meissner and Ochsenfeld [MO33]. The Meissner effect is related to the behavior of the magnetic field on the superconductor. As metal is cooled until its critical temperature, the magnetic field on the metal is expelled from the superconductor, and it is confined in the superconductor surface. Fritz and Heinz London studied both phenomena, perfect conductivity and perfect diamagnetism in 1935 [Rso]. They proposed a set of equations to describe the microscopic electromagnetic field on the superconductor. These equations are given by

$$\vec{E} = \frac{4\pi\lambda^2}{c^2}\frac{\partial \vec{J}_s}{\partial t} \tag{1.1}$$

$$\vec{h} = -\frac{4\pi\lambda^2}{c}(\nabla \times \vec{J}_s), \tag{1.2}$$

where c is the speed of light, and λ is the penetration depth of the superconductor. The penetration depth is a phenomenological parameter which quantifies how deep the magnetic field penetrates into the superconductor [Tin04]. Furthermore $\vec{J_s}$ is the current density of the superconductor. Finally, $\vec{h}$ is the microscopic magnetic field whose average corresponds to the macroscopic magnetic field $\vec{B}$. The Eq. (1.1) is related to the perfect conductivity. As the electric field is proportional to the derivative of the current density, any electric field on the superconductor accelerates the charge inducing a current. The Eq. (1.2) is associated with the perfect diamagnetism. Replacing the Eq. (1.2) in the Maxwell-Faraday equation i.e., $\nabla \times \vec{h} = 4\pi\vec{J_s}/c$ we obtain the equation $\nabla^2\vec{h} = \vec{h}/\lambda$. The solution of this equation corresponds to a microscopic magnetic field which exponentially decreases as the deep of the superconductor increases. Thus, the London equations provide a set of the equation which explains how a superconductor works.

Another step towards the understanding of the physics behind superconductivity is the development of the Bardeen-Cooper-Schrieffer (BCS) theory. The BCS theory was developed by J. Bardeen, L. N. Cooper, and J. R. Schrieffer at the end of the decade of 1950 [BCS57]. This theory explains how a metal suffers a phase-transition from a conductor to a superconductor. The phase transition occurs when a pair of electrons above the Fermi energy couple to each other due to an effective, attractive interaction produced by the virtual exchange of phonons in the metal. The superconductivity appears when the attractive interaction dominates over the repulsive Coulomb interaction. As a result, both electrons correlate yielding to a bosonic quantum state known as *Cooper pair*. Furthermore, the BCS theory shows that there is a minimum of energy $E_g = 3.528k_BT_c$ required to break a Cooper pair and create two uncoupled electrons depends on the metal temperature. This prediction provides one of the most evident verification of the microscopic theory of superconductors.

Other important results in superconductivity theory were obtained through the Ginzburg-landau theory in 1950 [Gin50]. The main idea in this theory is to associate the macroscopic wave function describing the superconductor as an order parameter in the second order phase transition. This order parameter is related with the macroscopic electron density and macroscopic phase by the relation $\psi(\vec{r},t) = \sqrt{n_s(\vec{r},t)}e^{i\theta(\vec{r},t)}$. With this order parameter, it is possible to write the free energy of the superconductor. Variational principle over this energy leads to a set of differential equations describing the superconductor. Unlike London equations, the Ginzburg-Landau theory could predict the non-linear effects on the electron density arising from the interaction with an external electromagnetic field. Even though the Ginzburg-Landau theory was initially constructed empirically, Gor'kov in 1959 [Gor59] demonstrates that the Ginzburg-Landau theory is a particular case

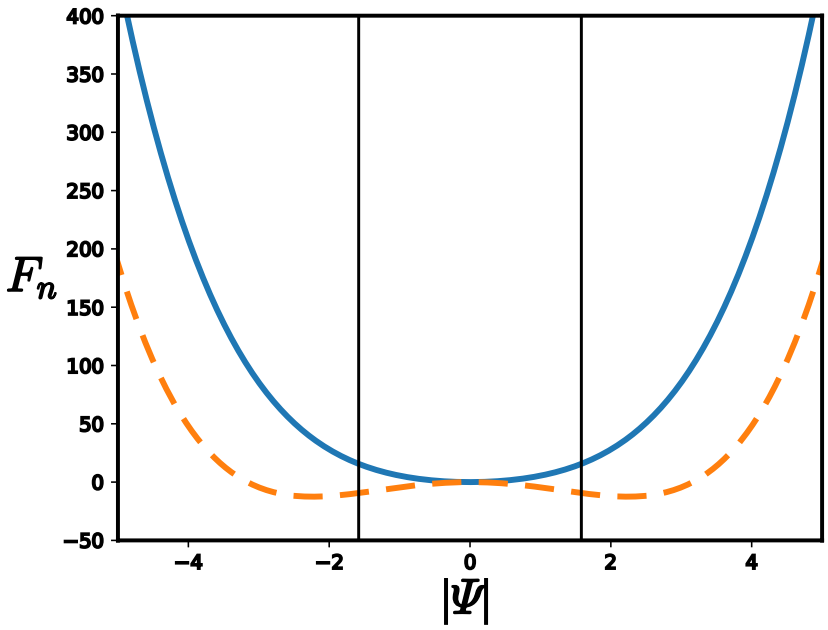

Figure 1.1: **Ginzburg-Landau potential** Given in Eq. (1.3), blue continuous line correspond to the free energy where $\alpha > 0$, this situation corresponds to a normal metal. The orange dashed line corresponds to the free energy where $\alpha < 0$. For this condition, the free energy looks like a double well potential with two stables minima.

of the BCS theory, making both theories complementary to each other.

This thesis chapter address fundamental results obtained on superconductivity theory at the macroscopic level using the Ginzburg-Landau theory. Based on this theory, we highlight two crucial results, that is, the quantization of the magnetic flux on a superconducting loop, and the Josephson effect on two weakly coupled superconductors.

1.1 The Ginzburg—Landau theory

The transition from metal to superconductor in the absence of external magnetic field at critical temperature T_c corresponds to a second-order phase transition [Cyr73]. The Landau-Lifshitz theory [LLP80] enunciates that there is an order parameter which must be zero after the transition, and finite before the phase transition. For superconductivity, the order parameter corresponds to the macroscopic complex wave function Ψ whose modulus is the Cooper pair density $n_s(\vec{r}) = |\Psi(\vec{r})|^2$. Near to the critical temperature where the phase transition may occur, the GL theory assumes that the free energy of the superconductor can be written as follows

$$F_s = F_n + \alpha|\Psi|^2 + \frac{\beta}{2}|\Psi|^4, \tag{1.3}$$

where F_n is the free energy of the metal in its normal state. This assumption is valid for a temperature range close to the critical temperature T_c. Notice that the free energy only contains even powers in ψ, this is due to the wave-function is complex and all the powers odd involves non-physical quantities (purely imaginary numbers). To obtain a bounded energy, it is required that $\beta > 0$. Besides, by fixing the sign of β, two conditions for the α parameter arises

- If $\alpha \geq 0$ the free energy F_s has a single minimum at $\psi = 0$, which corresponds to a normal metal state (see Fig. (1.1)).
- If $\alpha < 0$ the free energy F_s behaves as a double-well potential with two stables minimum at $\psi = \pm\sqrt{-\alpha/2\beta}$ (see Fig. (1.1)).

Now, let us consider the contribution to the free energy F_s done by the presence of an external magnetic field H_a on the superconductor. In such case, we write the free energy as

$$F_s = F_n + \alpha|\Psi|^2 + \frac{\beta}{2}|\Psi|^4 + \frac{1}{2m}\left|\left(-i\hbar\nabla - \frac{2e\vec{A}}{c}\right)\Psi\right|^2 + \frac{H_a^2}{8\pi} \tag{1.4}$$

The minimal action principle over ψ and $\vec{A}$ lead to the following differential equations

$$\alpha\Psi + \beta\Psi|\Psi|^2 + \frac{1}{2m}\left(-i\hbar\nabla - \frac{2e\vec{A}}{c}\right)^2\Psi = 0 \tag{1.5}$$

$$\frac{(\nabla^2\vec{A} - \nabla(\nabla\cdot\vec{A})) - \nabla\times H_a}{4\pi} = \frac{e\hbar}{imc}(\Psi^*\nabla\Psi - \Psi\nabla\Psi^*) - \frac{4e^2}{mc^2}\vec{A}|\Psi|^2. \tag{1.6}$$

The right hand of the Eq. (1.6) can be written in terms of the Noether current

$$\vec{J} = \frac{e\hbar}{imc}(\psi^*\nabla\psi - \psi\nabla\psi^*) - \frac{4e^2}{mc^2}\vec{A}|\psi|^2. \tag{1.7}$$

These equations have the following boundary conditions

$$(-i\hbar\nabla - \frac{2e}{c}\vec{A})\Psi\cdot\vec{s} = 0 \tag{1.8}$$

$$\nabla\times\vec{A} = H_a. \tag{1.9}$$

Where $\vec{s}$ is a vector normal to the superconducting surface. Thus, to obtain the physical description of a superconductor, it is necessary to solve the differential equations with the boundary conditions. Now by considering that the wavefunction has the following form $\Psi = \sqrt{n_s(\vec{r})}e^{i\theta(\vec{r})}$ we show that

the current density of the Cooper pair can be expressed in term of the spatial variation to the superconducting phase, replacing the expression of the wave-function into Eq. (1.7) the current density reads

$$\vec{J} = \frac{2e}{mc}\left(\hbar\nabla\theta - \frac{2e}{c}\vec{A}\right)n_s(\vec{r}). \tag{1.10}$$

With the expression for the current density previously obtained, it is possible to demonstrate that the magnetic flux enclosed in a superconducting loop is quantized. Let us consider region formed by a superconducting loop surrounded by a non-superconducting region. Afterward, we compute the integral of the current density as follows

$$\oint_C \vec{J}\cdot d\vec{l} = \oint_C \frac{2en_s}{mc}\left(\hbar\nabla\theta - \frac{2e}{c}\vec{A}\right)\cdot d\vec{l}, \tag{1.11}$$

where C is the integration path which considers a curve inside of the superconductor. Due to current is flowing on the superconductor surface. The integral in Eq. (1.11) is zero, implying

$$\oint_C \hbar\nabla\theta\cdot d\vec{l} = \oint \frac{2e}{c}\vec{A}\cdot d\vec{l}, \tag{1.12}$$

The left term on Eq. (1.12) Corresponds to the integral of the gradient of the superconducting phase. Therefore, the result of the integral corresponding to the phase evaluated at the edges of the curve, that is,

$$\oint_C \hbar\nabla\theta\cdot d\vec{l} = \hbar\lim_{\vec{r}_1\to\vec{r}_2}\big(\theta(\vec{r}_2) - \theta(\vec{r}_1)\big) = 2\hbar\pi n. \tag{1.13}$$

The right hand of the Eq. (1.12) can be solved by considering the Stokes' theorem. Thus, the write the line integral as a surface integral

$$\oint \frac{2e}{c}\vec{A}\cdot d\vec{l} = \frac{2e}{c}\int_{\partial C}(\nabla\times\vec{A})\cdot d\vec{S}. \tag{1.14}$$

Here, ∂C is the surface formed by the curve C and $d\vec{S}$ is a infinitesimal surface vector normal to the direction of $(\nabla\times\vec{A})$. The expression $(\nabla\times\vec{A}) = \vec{B}$ is simply the external magnetic field. By replacing on the Eq. (1.11) we obtain

$$\frac{2e}{c}\int_{\partial C}(\nabla\times\vec{A})\cdot d\vec{S} = \frac{2e}{c}\int_{\partial C}\vec{B}\cdot d\vec{S} = \frac{2e}{c}\Phi_B, \tag{1.15}$$

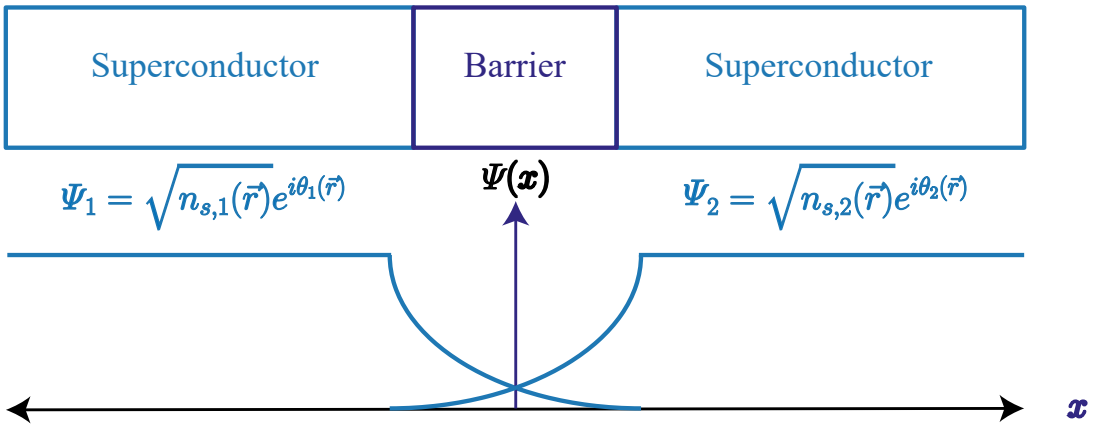

Figure 1.2: **Josephson effect**. Schematic representation of the Josephson effect. Two pieces of superconductors are coupled to a thin insulator barrier. The quantum tunneling of Cooper pair between superconductors is produced by the overlap of the wavefunction describing each superconductor.

where Φ_B is the external magnetic flux. Thus, by replacing the results of the integrals obtained in the Eq. (1.13) and Eq. (1.15) the fluxoid quantization relation arrives ($c = 1$)

$$2\hbar\pi n = 2e\Phi_B \rightarrow \Phi_B = \frac{h}{2e}n = n\phi_0. \tag{1.16}$$

Here, ϕ_0 is the flux quantum $\phi_0 = h/2e$. Experimental proof of this effect was observed in 1960 by R. Doll and co-authors [DN61] and B. S. Deaver and co-authors [DF61].

1.2 The Josephson effect in superconductors

The Josephson effect is a phenomenon in which a supercurrent appears as the result of the quantum tunneling of Cooper pair in an interface formed by two superconductors coupled through a thin insulator barrier as shown Fig. (1.2) (this interface is known as Josephson junction) discovered by Brian Josephson in 1962 [Jos62] and experimentally observed by Anderson and co-authors in 1963 [AR63]. To describe this effect we need to consider that each superconductor is described by a macroscopic wave function given by $\Psi_k(\vec{r}) = \sqrt{n_{s,k}(\vec{r})}e^{i\theta_k(\vec{r})}$ with $k = 1, 2$. Besides, we are assuming Cooper pair density is the same at edges and the bulk. Also, we assume that the length of each superconductor is smaller than its respective coherent length ($L \ll \xi$). These conditions impose the following constrain the wave function describing the interface superconductor-insulator

superconductor.

$$\Psi(x) = \sqrt{n_s(\vec{r})}e^{i\theta_1(\vec{r})}g(x) + \sqrt{n_s(\vec{r})}e^{i\theta_2(\vec{r})}(1 - g(x)), \tag{1.17}$$

Notice that $\Psi(x)$ must satisfy the following conditions

$$\Psi(x \to 0) \to \Psi_1, \quad \Psi(x \to L) \to \Psi_2, \tag{1.18}$$

The next step is to consider the first GL differential equation given in Eq. (1.5) without electromagnetic field and replace the wave function Ψ

$$-\frac{\hbar^2}{2m}\frac{\partial^2\Psi}{\partial x^2} + \alpha\Psi + \beta|\Psi|^2\Psi = 0 \tag{1.19}$$

Introducing the variables $\Psi(x) = |\Psi_\infty|f(x)$, where $|\Psi_\infty|^2 = -\alpha/\beta$, and $\xi^2 = \hbar^2/2m|\alpha|$, the differential equations becomes

$$\xi^2 f'' + f - |f|^2 f = 0 \tag{1.20}$$

To solve this differential equation, we consider that the terms f and f^3 are smaller than $\xi^2 f''$ because this term is proportional to $(\xi/L)^2 f \gg \{f, f^3\}$. Thus, the differential equation becomes in

$$f'' = 0 \to f(x) = c_1 + c_2 x, \tag{1.21}$$

By applying the constrains given in Eq. (1.18), the wave function is given by

$$\Psi(x) = \sqrt{n_s(\vec{r})}\left[e^{i\theta_1}\left(1 - \frac{x}{L}\right) + e^{i\theta_2}\frac{x}{L}\right]. \tag{1.22}$$

The current density is obtained by replacing the wavefunction $\Psi(x)$ into the Eq. (1.7) without electromagnetic field

$$|\vec{J}| = \frac{e\hbar}{mc}\frac{n_s}{L}\sin(\theta_2 - \theta_1). \tag{1.23}$$

The current is obtained by integrating the current density over the junction area

$$I = I_c \sin(\theta_2 - \theta_1), \tag{1.24}$$

where $I_c = e\hbar n_s A/mL$ is the persistent current on the Josephson junction. Integrating the free energy given in Eq. ((1.4) in the absence of electromagnetic field we obtain the free energy of the Josephson junction ($F_s = 0$)

$$E_J = \int_0^L \left[\alpha|\Psi|^2 + \frac{\beta}{2}|\Psi|^4 - \frac{\hbar^2}{2m}|\nabla\Psi|^2\right]. \tag{1.25}$$

In the limit ($\xi/L \ll 1$) the only contributing term correspond to the gradient $\nabla\Psi$ [Tin04]. In such a case, we write the energy as

$$E_J = \frac{\phi_0 I_c}{2\pi}\left[1 - \cos(\theta_2 - \theta_1)\right]. \tag{1.26}$$

Thus, the energy on the Josephson junction depends on the quantum flux, the persistent current, and the phase difference on the junction.

Chapter 2

Superconducting circuits

2.1 Macroscopic quantum mechanics

Superconducting quantum circuits [SG08; YN11; HTK12; DS13] consists into integrated devices whose size is larger than atomic systems (a conventional superconducting chip can size tens millimetres), but smaller than its respective operating wavelength. Hence, it is said that these devices operate within the lumped element description. In this case, both voltage and current on the circuit element do not vary with the position. As consequence, the circuit are considered as ideal (without resistance).

Superconducting circuits platform involves mainly two kinds of devices, i.e., non-linear circuits composed by Josephson junctions behaving as multilevel atoms, and LC circuits, strip-lines resonators and transmission line resonators working as microwave cavities. The main feature exhibited by superconducting circuits is the nature of its internal degrees of freedom. Unlike of circuit working at room temperature, where its internal degrees of freedom as current and voltage correspond to classical variables. The degrees of freedom on superconducting correspond to discrete variables. In fact, in some artificial atoms, the degrees of freedom correspond to an excess of Cooper pair in a superconducting island, or persistent current flowing on a superconducting loop. The main feature exhibited by superconducting circuits is the nature of its internal degrees of freedom. Therefore, it seems to be that the quantum nature of the degrees of freedom on the circuit is related with the temperature at which the circuit is cooled down. Here we address the question concerning with what does condition must satisfy a device for its internal degrees of freedom being considered as quantum variables? For electronic devices, the conditions to satisfies are (a) the

ultra-low temperature condition, and (b) the ultra-low dissipation condition, respectively.

The ultra-low temperature condition (a) is referred to the relationship among the operational circuit energy denoted as $\hbar\omega$, with ω with being the operational frequency of the circuit, and the thermal energy on the circuit i.e., $k_B T$, where k_B is the Boltzmann constant, and T is the circuit temperature. Formally, a circuit variable could be treated as a quantum degree of freedom when the condition $\hbar\omega \gg k_B T$ is fulfilled. Notice that this condition is not sufficient to treat a circuit variable as a quantum degree of freedom [Dev97; UM17]. Likewise, to treat the variables of a circuit as a quantum variable, the circuit also must satisfy the ultra-slow dissipation condition (b). This condition alludes to the relationship among the linewidth and the separation between each energy levels of the circuit. In the circuit, the spectral lines of the energy levels are not sharp because the energy levels have a finite lifetime. In fact, the linewidth of the spectral lines is proportional to $1/\tau$, with τ being the lifetime of the energy level. Thus, for energy levels with large linewidth (short lifetime), this energy levels could overlap. Therefore, the distinguishability of each energy levels is lost. This condition imposes that the variables on the circuit will be treated as quantum degree of freedom if the quality factor of the circuit $Q \gg 1$.

For example, let us consider a LC circuit whose parameters are given by $C = 10\ p\mathrm{F}$, and $L = 1\ n\mathrm{H}$ [Dev97; UM17]. The resonance frequency of this LC circuit is $\omega = 2\pi \times 1.59\ \mathrm{GHz}$. This energy corresponds to an effective Temperature of $T \approx 76\ \mathrm{mK}$. Hence, if the circuit is cooled down at temperature below of this T the ultra-low temperature condition is satisfied. In typical superconducting circuits the operational temperature is around of $T_o = 20 - 30\ \mathrm{mK}$ [SG08; YN11; HTK12; DS13]. On the other hand, the quality factor of the LC circuit connected in series is given by $Q = (1/R)\sqrt{L/C}$, with R being the effective resistance of the circuit. The ultra-slow dissipation condition is fulfilled when $Q \ll 1$.

2.2 Fundamentals of circuit theory

We consider an electrical circuit or network as a set of two-terminal elements and a set of nodes which are interconnected. We also identify each two-terminal element with a unique node, and every node is identified with at least one element terminal as shown in Fig. (2.1). The two-port elements are constituted by resistors, capacitors, inductors and Josephson junctions, and the nodes correspond to the point where these two-port elements meet, we denote the nodes as black dots. Another significant element on an electric circuit is the loop. The loop is defined as a closed path on the network which starts at a node, called n, passing through a set of nodes on

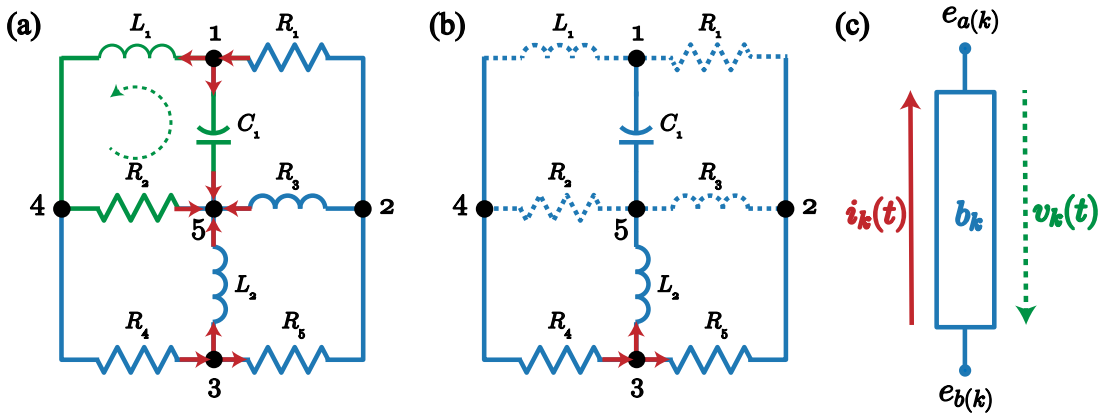

Figure 2.1: **Basic element on an electric circuit**. (a) The electronic circuit formed by two-port elements as resistors (R), inductors (L) and capacitors (C). The black dots represent the nodes on the network, whereas the red arrows stand for the current flowing on the circuit. (b) The spanning tree on the circuit. Continuous lines correspond to the twigs of the spanning tree, whereas, the dashed lines correspond to the link branches. (c) Schematic illustration for the current-voltage sign orientation for a circuit element placed at branch b.

the network and return to the initial node. In the circuit depicted in Fig. (2.1) the loop is formed by the set of nodes $\{1, 4, 5\}$. Further, we also define a tree or spanning tree of the network. The spanning tree is defined as a connected sub-network which contains all the nodes, but its branches (two-port element) do not form a loop, the tree is specified by enumerating its branches. The branches describing tree are called twigs denoted as $\mathcal{T}$, otherwise, are named links, denoted as $\bar{\mathcal{T}}$. For instance, for the depicted network, a possible spanning tree is formed by the elements $\mathcal{T} = \{R_4, R_5\}$ (blue continuous line), and the link are formed by $\bar{\mathcal{T}} = \{R_2, R_3, L_1, R_1\}$ (blue dashed line).

A passive circuit element corresponds to a two-terminal device such that we can write the current $I(t)$ and voltage $V(t)$ in the following form

$$V(t) = f(I, \dot{I}); \quad I(t) = g(V, \dot{V}). \tag{2.1}$$

Where $\dot{I}$ and $\dot{V}$ are the derivatives with respect to the time, for the current and voltage, respectively. These equations are known as the element equation [Naj10]. If these relations can be expressed as $I = g(V)$ or $V = f(I)$, the element is to be said resistive. Otherwise, the circuit elements are to be said dynamical. Depending on the element equation Eq. (2.1), we can identify the basic component in the electrical circuit, i.e., the resistor, the capacitor and the inductor [Naj10]. An element is said to be a resistor if this element equation is given by the Ohm's law $V = RI$ with R beings the resistance or $I = GV$ with G beings the conductance. The capacitor is a passive circuit

element such that the electrical charge $q(t)$ is a function of the voltage, i.e., $q(t) = CV(t)$, with C as the capacitance. Besides, the current on this device is $I(t) = dq/dt$. Finally, an inductor is a passive element such that we can relate the current with the magnetic field through the relation $\varphi(t) = LI(t)$, where L is the inductance of the device. Furthermore, the voltage on the inductor is $V(t) = LdI/dt$. We refer to an active circuit element as a device where either voltage and current coming from external sources.

The orientation of both current and voltage on the circuit are chosen in the following way: for the branch b_k the current i_{b_k} is positive if it flows from $e_{a(k)}$ to the node $e_{b(k)}$, where e are the node where the two-port element is connected. Otherwise, the current is negative. On the other hand, the voltage dropped on the branch v_k is considered positive if the electric potential is higher at node $e_{a(k)}$ than the node $e_{b(k)}$, as shown in Fig. (2.1)(c).

As we are interested in obtaining the Lagrangian and Hamiltonian of an electrical circuit, we need to compute the energy associated to each circuit element. The total energy absorbed by a circuit element on the branch b is given by

$$\mathcal{E}_b(t) = \int_{-\infty}^{t} dt' v_b(t') i_b(t') \tag{2.2}$$

Notice that the limit $t = -\infty$ assumes that at this time the circuit is switched-off, or equivalently, there is no electromagnetic field on the circuit. For the passive circuit element previously described, the total energy absorbed is given by

$$\mathcal{E}_C(t) = \frac{Cv_b^2(t)}{2}, \quad \mathcal{E}_I(t) = \frac{Li_b^2(t)}{2}, \quad \mathcal{E}_J(t) = E_J \cos\left(\frac{\Phi_b}{\phi_0}\right) \tag{2.3}$$

where, $v_b(t)$, $i_b(t)$, and Φ_b are the voltage dropped, the current flowing and the flux on the branch b, respectively.

2.3 Quantum description of superconducting circuits

To obtain the Lagrangian of any physical system, we need to fix a set of generalized coordinates, and with them compute the energy of each circuit element. In superconducting circuits, these coordinates correspond to the flux and the charge on the branch b, related to the voltage and the

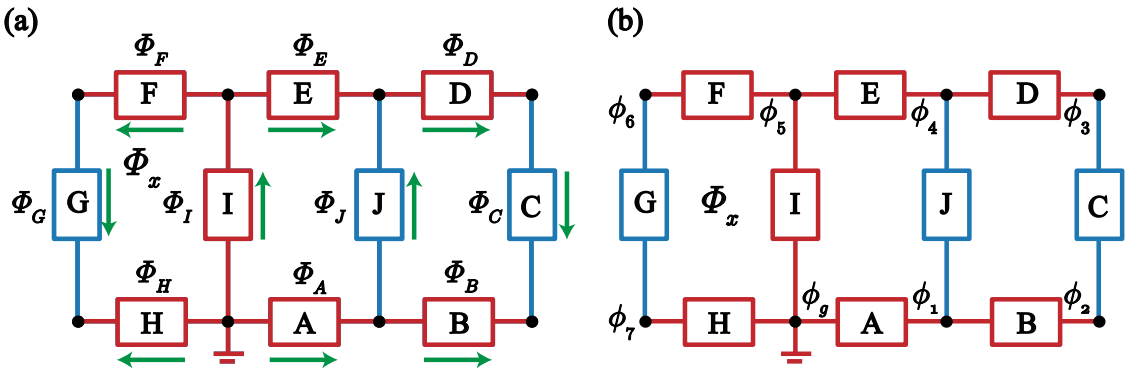

Figure 2.2: **The spanning tree method**. (a) Representation of an electrical circuit. Black dots correspond to the node on the network, the ground node is denoted as φ_g. Red line correspond to a chosen spanning tree which consider all the branches start from the ground node that does not form any loop. Blue line correspond to the branches that closing loop. Green arrows stand for the current on the circuit. The fluxes labeled with letters correspond to the fluxes describing each box. (b) Same representation of the electrical circuit than in (a), but with the difference that the fluxes describing the network are the node fluxes.

current on the respective branch [Dev97; UM17]

$$Q_b = \int_{-\infty}^{t} i_b(t')dt', \qquad \Phi_b = \int_{-\infty}^{t} v_b(t')dt'. \tag{2.4}$$

Regarding these generalized coordinates the energy terms given in Eq. (2.3) are rewritten regarding these coordinates

$$\mathcal{E}_C(t) = \frac{Q_b^2(t)}{2C}, \quad \mathcal{E}_I(t) = \frac{\Phi_b^2(t)}{2L}, \quad \mathcal{E}_J(t) = E_J \cos\left(\frac{\Phi_b}{\phi_0}\right), \tag{2.5}$$

The next step is to consider that the Kirchhoff's law for voltage and current on the branches do not provide linearly independent equations. Therefore, it could exist an overcount of the degrees of freedom on the circuit. To avoid that, we follow the procedure developed by M. H. Devoret [Dev97; UM17]. Instead of working with branches variables we choose the node variables. The advantages of choosing this method are that there are no superfluous variables, eliminating the overcounting of variables. In what follows, we describe the flux node method, and with this, we show how to obtain the circuit Lagrangian.

The method starts by choosing a reference node on the network; this node is called ground node as depicted in Fig. (2.2). We consider this node as the passive node, and it is neglect in the later calculations. The next step is to trace a spanning tree on the network. The spanning tree starts from the ground node and connects all the remaining nodes without form loops on the

network. We denote the set of branches forming the tree (twigs) by $\mathcal{T}$, and we called the set of branches forming the loops (links) as $\bar{\mathcal{T}}$. For the networks depicted in Fig. (2.2), the chosen spanning tree is formed by the set of branches $\mathcal{T} = \{\mathrm{A}, \mathrm{B}, \mathrm{D}, \mathrm{E}, \mathrm{F}, \mathrm{H}, \mathrm{I}\}$, and the loop branches are given by the set $\bar{\mathcal{T}} = \{\mathrm{C}, \mathrm{I}, \mathrm{J}\}$. Afterwards, we define the node fluxes φ_n, which is related with the branches fluxes Φ_b (cf. Fig. (2.2)) by the following relation

$$\varphi_n = \sum_b S_{nb}\Phi_b, \tag{2.6}$$

The matrix element S_{nb} can take the values $\{1, -1, 0\}$ depending whether the path traced from the ground node to the node n belonging to the spanning tree coincide $S_{nb} = 1$ or not $S_{nb} = -1$ with the orientation of the current at the branch b, or whether the branch b does not belong to the spanning tree $S_{nb} = 0$. For the circuit shown in Fig. (2.2) the node fluxes in term of the branches fluxes are given by

$$\varphi_1 = \Phi_\mathrm{A}, \varphi_2 = \Phi_\mathrm{A} + \Phi_\mathrm{B}, \tag{2.7a}$$

$$\varphi_3 = \Phi_\mathrm{D} + \Phi_\mathrm{E} + \Phi_\mathrm{I}, \varphi_4 = \Phi_\mathrm{E} + \Phi_\mathrm{I}, \tag{2.7b}$$

$$\varphi_5 = \Phi_\mathrm{I}, \Phi_6 = \Phi_\mathrm{I} + \Phi_\mathrm{F}, \varphi_7 = \Phi_\mathrm{H}. \tag{2.7c}$$

Likewise, we can obtain the flux on the branch b regarding the node fluxes φ_n and $\varphi_{n'}$, where n, and n' are the edges nodes of the branch b. Moreover, we need to differentiate between the branches forming the spanning tree (twigs) and the branches closing loop (links). For the branches closing the loop, we need to consider the fluxoid quantization rule. In such case, the fluxes on the branches follow the relation

$$\Phi_{b\in\mathcal{T}} = \varphi_n - \varphi_{n'} \tag{2.8}$$

$$\Phi_{b\in\bar{\mathcal{T}}} = \varphi_n - \varphi_{n'} + \Phi_x \tag{2.9}$$

For the circuit shown in Fig. (2.2), the flux on the branches Φ_b belonging to the spanning the tree is given by the relations

$$\Phi_\mathrm{A} = \varphi_1, \Phi_\mathrm{B} = \varphi_2 - \varphi_1, \Phi_\mathrm{D} = \varphi_3 - \varphi_4 \tag{2.10a}$$

$$\Phi_\mathrm{E} = \varphi_4 - \varphi_5, \Phi_\mathrm{F} = \varphi_6 - \varphi_5, \Phi_\mathrm{H} = \varphi_7, \Phi_\mathrm{I} = \varphi_5. \tag{2.10b}$$

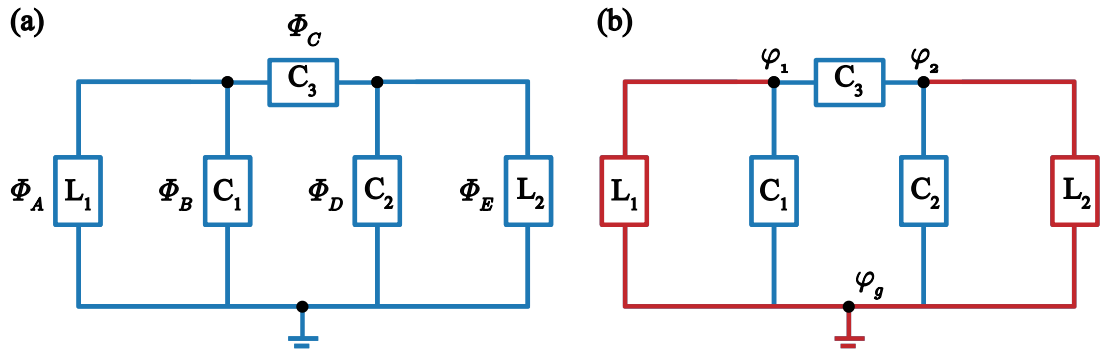

Figure 2.3: **An circuit example**.(a) schematic representation of a pair of LC circuit capacitively coupled through the capacitor C_3. (b) The spanning tree of the coupled LC circuit. The network contains one passive node, i.e., the ground φ_g and two active nodes.

For the branches closing loops (links), the flux is given by

$$\Phi_{\mathrm{C}} = \varphi_2 - \varphi_3, \Phi_{\mathrm{G}} = \varphi_7 - \varphi_6 + \Phi_x, \Phi_{\mathrm{J}} = \varphi_4 - \varphi_1. \tag{2.11a}$$

To obtain the Lagrangian of the circuit, we are assuming all capacitive elements on the network are linear [UM17]. As a consequence, we can write the capacitive energy regarding the derivative with respect to time of the flux on the branch, i.e., $\mathcal{E}_C = C\dot{\Phi}_b^2/2$. With this assumption, we write the energy of the circuit in term of the fluxes and the derivative concerning time; this is analogous to a mechanical system, where w can write the Lagrangian in term of the position and the velocity.

To exemplify how to obtain the circuit Lagrangian, Let us consider the circuit depicted in Fig. (2.3)(a) Consisting into two capacitively coupled LC resonator. We characterized k-th resonator by the capacitance C_k, and the inductance L_k. We start by tracing the spanning tree on the circuit depicted in red in the Fig. (2.3)(b). The tree is formed by the branches $\mathcal{T} = \{L_1, L_2\}$, and the links are given by the set $\bar{\mathcal{T}} = \{C_1, C_2, C_3\}$. The circuit is formed by five circuit elements; we have five branch variables denoted as Φ_b (b is the branch index). Also, from the choose spanning tree, we identify three nodes, the ground node φ_g and two active nodes φ_k, respectively. In such case, the branches fluxes are given by

$$\Phi_A = \Phi_B = \varphi_1, \quad \Phi_D = \Phi_E = \varphi_2, \quad \Phi_C = \varphi_2 - \varphi_1, \tag{2.12}$$

The next step is to compute the energy associated to each branch element using the node variables previously obtained. We obtain the Lagrangian as the difference between the capacitive energy with the potential energy, i.e., $\mathcal{L} = T - U$. Notice that we are considering the capacitive

energy as the kinetic energy because its form is like the kinetic energy on mechanical systems i.e., the energy is proportional to the derivative with respect of time of the generalized coordinate. Besides, we are assuming the inductors contributes to the potential energy of the circuit. In such case, the circuit Lagrangian reads

$$\mathcal{L} = \frac{C_1}{2}\dot{\varphi}_1^2 + \frac{C_2}{2}\dot{\varphi}_2^2 + \frac{C_3}{2}(\dot{\varphi}_1 - \dot{\varphi}_2)^2 - \frac{\varphi_1^2}{2L_1} + \frac{\varphi_2^2}{2L_2}. \tag{2.13}$$

At this point, we can compute the equations of motion of the circuit using the Euler-Lagrange equations. These equations correspond to the Kirchhoff's current and voltage law [Dev97]. Another way is to compute the Hamiltonian associated with this Lagrangian. To compute the Hamiltonian we need to compute the canonical momentum conjugate $Q_\ell = \partial\mathcal{L}/\partial[\dot{\varphi}_\ell]$. By defining the flux vector as $\vec{\varphi} = (\varphi_1, \varphi_2)$. The Lagrangian in the Eq. (2.13) can be written as a quadratic form

$$\mathcal{L} = \frac{1}{2}\dot{\vec{\varphi}}^{\,T}\hat{C}\dot{\vec{\varphi}} - \frac{1}{2}\vec{\varphi}^{\,T}\hat{L}^{-1}\vec{\varphi}, \tag{2.14}$$

where, $\hat{C}$ and $\hat{L}$ are the capacitance and the inductance matrix [UM17], respectively. For the studied circuit, these matrices have the following form

$$\hat{C} = \begin{pmatrix} C_1 & -C_3 \\ -C_3 & C_2 \end{pmatrix}, \qquad \hat{L}^{-1} = \begin{pmatrix} 1/L_1 & 0 \\ 0 & 1/L_2 \end{pmatrix}. \tag{2.15}$$

The canonical momentum conjugate vector $\vec{Q}$ is given by

$$\vec{Q} = \hat{C}\dot{\vec{\varphi}}. \tag{2.16}$$

Assuming that the capacitance matrix is regular, i.e., it has inverse $\hat{C}^{-1}$, it is possible to obtain $\dot{\vec{\varphi}}$ regarding the canonical momentum conjugate with the relation

$$\dot{\vec{\varphi}} = \hat{C}^{-1}\vec{Q}, \tag{2.17}$$

with this relation, we now apply the Legendre transformation $\mathcal{H} = \dot{\vec{\varphi}}^{\,T}\vec{Q} - \mathcal{L}$ on the circuit Lagrangian to obtain the circuit Hamiltonian $\mathcal{H}$

$$\mathcal{H} = \frac{1}{2}\vec{Q}^{\,T}\hat{C}^{-1}\vec{Q} + \frac{1}{2}\vec{\varphi}^{\,T}\hat{L}^{-1}\vec{\varphi}. \tag{2.18}$$

For the circuit shown in Fig. (2.3), the circuit Hamiltonian reads

$$\mathcal{H} = \frac{C_2}{2C^*}Q_1^2 + \frac{C_1}{2C^*}Q_2^2 + \frac{2C_3}{C^*}Q_1Q_2 + \frac{1}{2L_1}\varphi_1^2 + \frac{1}{2L_2}\varphi_2^2, \tag{2.19}$$

where, $C^* = C_1C_2 - C_3^2$ is the determinant of the capacitance matrix $\hat{C}$. The Hamiltonian $\mathcal{H}$ contains two terms, the first of them is the electrostatic energy stored on the capacitor as a function of the node charges Q_ℓ, whereas, the second terms are the electromagnetic energy as a function of the node fluxes φ_ℓ. Now, we are assuming that we are working in the ultra-low temperature and the ultra-slow dissipation approximation. Thus, we treated the circuit variables as quantum variables. Therefore, it is possible to quantize the Hamiltonian by promoting quantum operators instead of a function, i.e., $\varphi \to \hat{\varphi}$ and $Q \to \hat{Q}$. Furthermore, as the fluxes node and the charge node are canonical variables, the respective operators must satisfy the relation

$$[\hat{\varphi}_\ell, \hat{Q}_{\ell'}] = i\hbar\delta_{\ell,\ell'}. \tag{2.20}$$

Depending on the superconducting device, the set of quantum operators may change. For instance, in a superconducting LC circuit, the set of quantum operators are given by

$$\varphi_\ell = \sqrt{\frac{\hbar Z_{0,\ell}}{2}}(\hat{a}_\ell + \hat{a}_\ell^\dagger), \qquad Q_\ell = -i\sqrt{\frac{\hbar}{2Z_{0,\ell}}}(\hat{a}_\ell^\dagger - \hat{a}_\ell), \tag{2.21}$$

where $Z_{0,\ell} = \sqrt{L_\ell/C_\ell}$ is the impedance of the ℓ-th LC circuit, and $a_\ell^\dagger$ (a_n) is the boson operator, satisfying the commutation relation $[a_\ell, a_{\ell'}^\dagger] = \delta_{\ell,\ell'}$.For device as superconducting island coupled through a Josephson junction, the set of operators are given by

$$\varphi_\ell = -i\hbar\frac{\partial}{\partial\hat{N}_\ell}, \qquad Q_\ell \;\; = \;\; -2e\hat{N}_\ell. \tag{2.22}$$

Here, $\hat{N}_\ell$ is the Cooper pair operator with $2e$ being the Cooper pair charge. For devices composed by Josephson junctions interrupting a loop, the set of quantum operators are given by

$$\varphi_\ell = \hat{\varphi}_\ell, \qquad Q_\ell = -i\hbar\frac{\partial}{\partial\hat{\varphi}_\ell}. \tag{2.23}$$

In this example, as we are considering a set of coupled LC circuit, the quantum operators describing the system are the given in Eq. (2.19). In such case, the Hamiltonian corresponds to a pair of

coupled quantum harmonic oscillators

$$\mathcal{H} = \hbar\omega_1\left(a_1^\dagger a_1 + \frac{1}{2}\right) + \hbar\omega_2\left(a_2^\dagger a_2 + \frac{1}{2}\right) + \hbar g_{12}(a_1^\dagger - a_1)(a_2^\dagger - a_2). \tag{2.24}$$

Here, ω_ℓ is the frequency of the ℓ-th LC resonator. Moreover, $g_{12} = \sqrt{C_3^2/(C^*)^2 Z_{0,1} Z_{0,2}}$ is the coupling strength among both LC oscillators.

Chapter 3

Elements of superconducting circuits

3.1 The transmon qubit

The *transmon* qubit [Koc+07] is a superconducting artificial atom where its degree of freedom corresponds to an excess of Cooper pairs in two superconducting islands. Formally, the transmon qubit consists into two superconducting islands coupled through a pair of Josephson junctions. The key features observed in this artificial atom consists of an insensitive concerning the environmental offset charge. This improvement is achieved by coupling an additional shunt capacitance on the circuit. Thus, the ratio between the Josephson energy (junction) and the charge energy increase leading to an artificial atom with long coherence times. Furthermore, the inclusion of this capacitance also produces a decrease in the anharmonicity of the energy levels on the circuit. As a result, to measure the effective two-level system an additional energy level is required.

Figure. (3.1) shows the transmon circuit. The circuit is composed by two capacitors denoted as C_g and C_b, an external voltage source V_g and two Josephson junctions in a superconducting loop. We modeled each Josephson junction as an effective LC circuit with non-linear inductance [Tin04]. Also, the superconducting loop where both junctions are placed is threading with an external magnetic flux Φ_x. To obtain the Lagrangian, we note that the circuit contains five elements (two Josephson junctions, two capacitors, and a voltage source). Hence, we describe the system regarding five branch fluxes. Afterwards, we trace the spanning tree (see Fig. (3.1)(c)). The spanning tree is formed by the set of branches $\mathcal{T} = \{C_B, V_g\}$, while, the links are given by the set

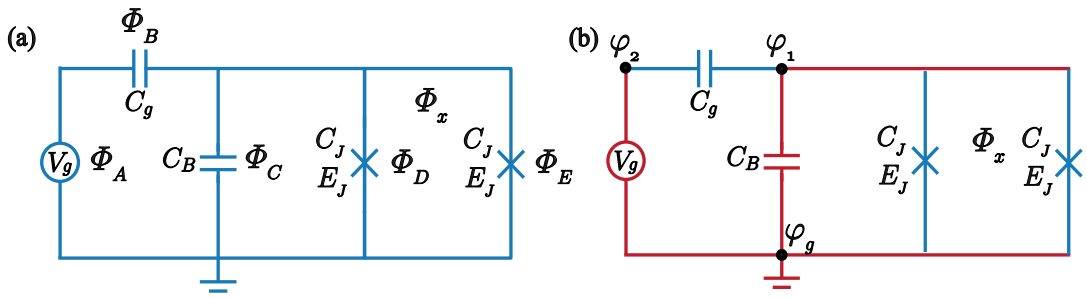

Figure 3.1: **Tranmon qubit circuit**. (a) Reduced circuit for the transmon qubit. The circuit contains a gate voltage V_g coupled to the superconducting island by a capacitor C_g which allow changing the offset charge in the circuit. Two identical Josephson junctions are connected in parallel to couple the two superconducting island. Additionally, a large shunted capacitance is connected in the circuit. This capacitor has the function to increase the ratio E_J/E_C. (c) Spanning tree chosen for the Lagrangian derivation, the black dots represent active nodes on the tree. Dashed lines stand for elements closing loops.

$\bar{\mathcal{T}} = \{C_g, C_J, C_J\}$. In this spanning tree, we found three nodes, the ground node and two active nodes φ_1 and φ_2 respectively. Thus, we write the branches nodes regarding the nodes fluxes by the relation

$$\Phi_A = \varphi_2, \quad \Phi_B = \varphi_1 - \varphi_2, \quad \Phi_C = \varphi_1, \quad \Phi_D = \varphi_1, \quad \Phi_E = \varphi_1 - \Phi_x \tag{3.1}$$

Notice that the node flux φ_2 corresponds to the flux associated with the voltage-biased V_g i.e, $\varphi_2 = \int_{-\infty}^{t} V_g(t')dt'$. On the other hand, To write the Josephson energy conveniently, we define the branch variable as $\Phi_+ = (\Phi_D + \Phi_E)/2$. Moreover, with the fluxoid quantization relation $\Phi_E - \Phi_D = \Phi_x$ it is possible to write the branch fluxes of the Josephson junctions as $\Phi_E = \Phi_+ + \Phi_x/2$, and $\Phi_D = \Phi_+ - \Phi_x/2$. Likewise, regarding the node variables, we obtain $\Phi_+ = \varphi_1$. Thus, the Lagrangian of the transmon reads

$$\mathcal{L} = \frac{C_\Sigma}{2}\dot{\varphi}_1^2 - C_g V_g \dot{\varphi}_1 + E_J(\Phi_x)\cos\left(\frac{\varphi_1}{\varphi_0}\right). \tag{3.2}$$

Here, $C_\Sigma = C_g + C_B + 2C_J$ is the total capacitance of the transmon, $\varphi_0 = \phi_0/2\pi$ is the reduced quantum flux, and V_g is the voltage-biased. We assume identical Josephson junction in this derivation. As result, the loop with both junctions are considered as an one junction with variable Josephson energy $E_J(\Phi_x) = 2E_J\cos(\Phi_x/\varphi_0)$. On the other hand, We neglect the terms proportional to V_g^2 because does not contribute to the system dynamics. To obtain the Hamiltonian of the

transmon, we compute the canonical momentum conjugate by the relation

$$Q_1 = \frac{\partial \mathcal{L}}{\partial \dot{\varphi}_1} = C_\Sigma \dot{\varphi}_1 - C_g V_g. \tag{3.3}$$

By inverting $\dot{\varphi}_1$, we obtain

$$\dot{\varphi}_1 = \frac{Q_1 + C_g V_g}{C_\Sigma}. \tag{3.4}$$

The circuit Hamiltonian is obtained by applying the Legendre transformation to the circuit Hamiltonian and replacing the flux derivative with the expression obtained in Eq. (3.3)

$$\mathcal{H} = \frac{(Q_1 - q_g)^2}{2C_\Sigma} - E_J(\Phi_x)\cos\left(\frac{\varphi}{\varphi_0}\right), \tag{3.5}$$

where, $q_g = C_g V_g$ is the offset charge. The perform circuit quantization by considering quantum operators instead of time-dependent functions. For the transmon qubit, the quantization is done by promoting the operators $\varphi_1 \to \hat{\varphi}_1$, and $Q_1 \to -2e\hat{n}_1$, where $\hat{n}_1$ is the Cooper pair operator. Thus, replacing the operator the Hamiltonian takes the following form

$$\mathcal{H} = 4E_C(\hat{n}_1 - n_g)^2 - E_J(\Phi_x)\cos\left(\frac{\hat{\varphi}_1}{\varphi_0}\right), \tag{3.6}$$

$E_C = e^2/C_\Sigma$ is the charge energy, which quantifies the required energy to place a single Cooper pair on the superconducting island at zero gate voltage. $n_g = q_g/2e$ is the offset charge energy, which provides Cooper pairs in the superconducting islands. The next step is to write the Hamiltonian in the charge basis.

$$\mathcal{H} = 4E_C \sum_{n=-\infty}^{+\infty} (n_1 - n_g)^2 |n\rangle\langle n| - E_J(\Phi_x) \sum_{n=-\infty}^{+\infty}\sum_{m=-\infty}^{+\infty} |n\rangle\langle n|\cos\left(\frac{\hat{\varphi}_1}{\varphi_0}\right)|m\rangle\langle m|, \tag{3.7}$$

to obtain the matrix element $\langle n|\cos(\hat{\varphi}_1/\varphi_0)|m\rangle$ it is necessary to use the commutation relation $[\hat{\phi}/\varphi_0, \hat{n}_1] = -i$, and the Baker-Hausdorff lemma. In such case, the exponential of the operator is written as $e^{\pm i\hat{\phi}_1/\varphi_0}|n\rangle = |n \mp 1\rangle$. Thus, replacing this expression on the Hamiltonian we arrive at

$$\mathcal{H} = \sum_{n=-\infty}^{+\infty} \left[4E_C(n_1 - n_g)^2 |n\rangle\langle n| - \frac{E_J(\phi_x)}{2}\Big(|n\rangle\langle n+1| + |n+1\rangle\langle n|\Big)\right]. \tag{3.8}$$

The second term on the Hamiltonian in Eq. (3.8) corresponds to the energy of the two Josephson

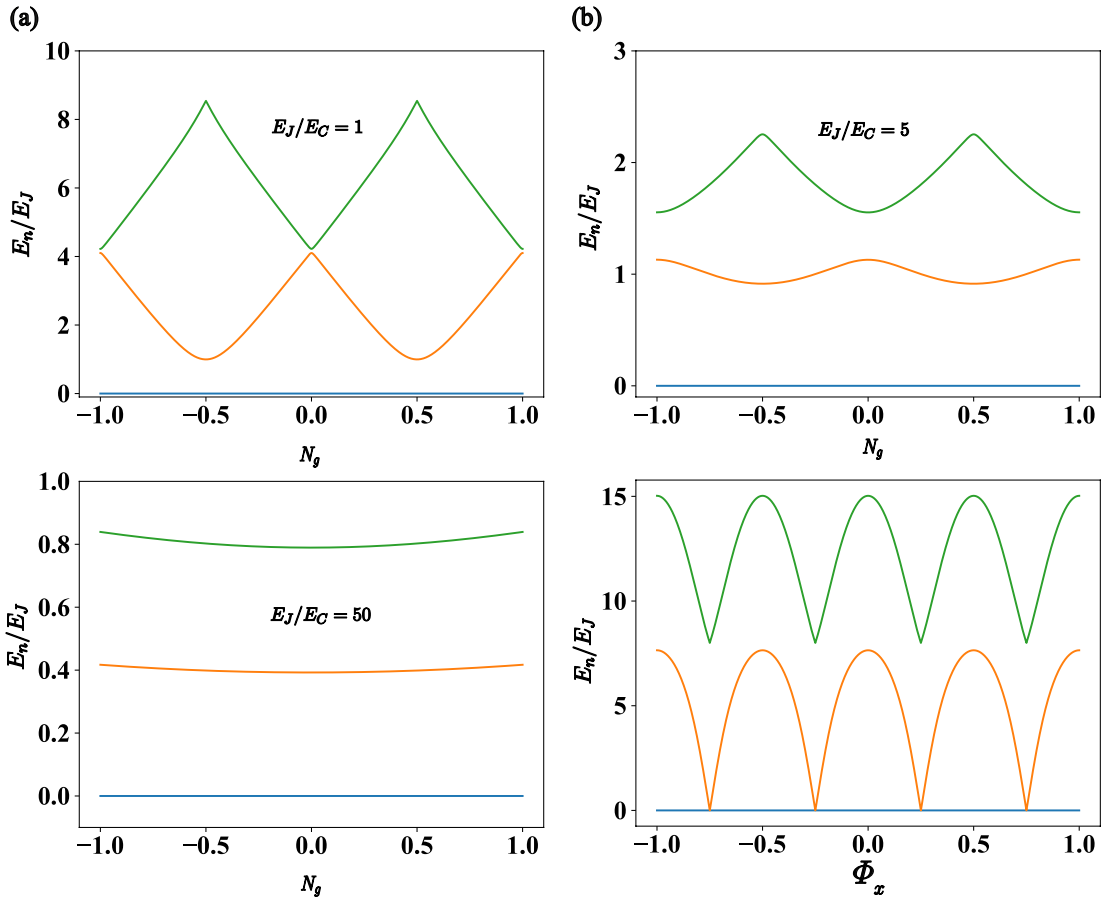

Figure 3.2: **Energy spectrum of the transmon for different Josephson energies**. (a)-(c) Energy spectrum for the transmon for different E_J/E_C ratios as a function of the effective offset charge N_g. Anharmonicity of the energy levels of the transmon depend on the ratio E_J/E_C. (d) Energy spectrum for the transmon qubit as function of the external magnetic flux ϕ_x for a fixed E_J/E_C ratio.

junction written in the charge basis. In this basis, this energy is the responsible of the transport of Cooper pair between the superconducting islands [NB09].

In Figure (3.2), we show the energy spectrum of the transmon qubit for several E_J/E_C ratios. Notice that, for large Josephson energy, and near to the sweet spot ($n_g \approx 1/2 + \delta n$) [NPT99]. In this limit, we can approximate the lowest energy levels as an effective two-level system.

$$\mathcal{H} = 4E_C\left[\left(\delta n + \frac{1}{2}\right)^2 |0\rangle\langle 0| + \left(\delta n - \frac{1}{2}\right)^2 |1\rangle\langle 1|\right] - \frac{E_J(\Phi_x)}{2}\left[|0\rangle\langle 1| + |1\rangle\langle 0|\right], \tag{3.9}$$

by expanding the binomial $(\delta n \pm 1/2)^2 \approx 1/4 \pm \delta n$, the Hamiltonian becomes

$$\mathcal{H} = 4E_C + 8E_C\delta n\sigma^z - \frac{E_J(\Phi_x)}{2}\sigma^x, \tag{3.10}$$

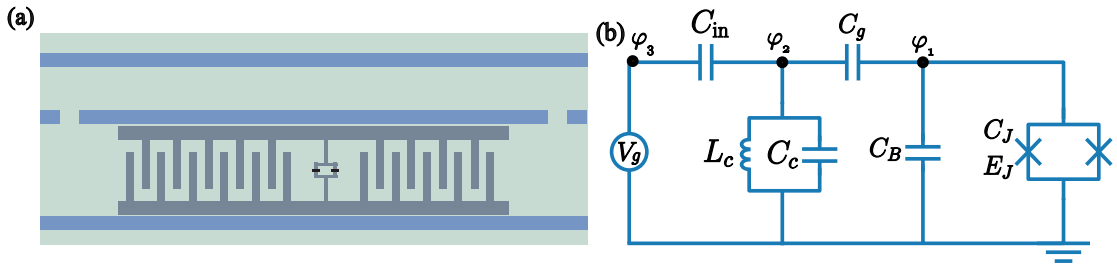

Figure 3.3: **Control and readout circuit**. (a) Schematic layout and the (b) equivalent circuit for a transmon coupled to a resonator to measure the transmon qubit.

In the sweet spot point $\delta n = 0$, the Hamiltonian in its diagonal basis takes the following form

$$\mathcal{H} = \frac{\omega_q(\Phi_x)}{2}\bar{\sigma}^z, \tag{3.11}$$

where $\omega_q = E_J(\Phi_x)$ is the flux-dependent two-level frequency. Changes on the qubits will be done changing the external magnetic flux. On the other hand, we can perform non-demolition measurement on the qubit measuring an ancillary system. For the transmon qubit, the measurement is node by coupling an ancillary resonator. The setup of this scenario is given by (see. Fig. (3.2)(d))

$$\mathcal{L}_{\text{read}} = \frac{C_\Sigma}{2}\dot{\varphi}_1^2 + E_J(\Phi_x)\cos\left(\frac{\varphi_1}{\varphi_0}\right) + \frac{C_R}{2}\dot{\varphi}_3^2 - \frac{\varphi_3^2}{2L_r} - C_g\dot{\varphi}_1\dot{\varphi}_3 - C_{\text{in}}V_g\dot{\varphi}_3. \tag{3.12}$$

Here, φ_3 is the flux node of the LC circuit. Moreover, $C_\Sigma = C_g + C_B + 2C_J$ is the total capacitance for the transmon, $C_R = C_{\text{in}} + C_r + C_g$ is the total capacitance of the LC circuit. To obtain the Hamiltonian of the coupled system, we express the Lagrangian as a quadratic form

$$\mathcal{L}_{\text{read}} = \frac{1}{2}\vec{\dot{\varphi}}^{\,T}\hat{C}\,\vec{\dot{\varphi}} - \vec{\dot{\varphi}}^{\,T}\hat{C}_g\vec{V} - U(\vec{\varphi}). \tag{3.13}$$

where $\vec{\varphi} = (\varphi_1, \varphi_3)^T$ is the flux vector and $\vec{V} = (0, V_g)^T$ is the voltage vector. $\hat{C}$ and $\hat{C}_g$ are the capacitance and gate capacitance matrix, respectively, and are defined as

$$\hat{C} = \begin{pmatrix} C_\Sigma & -C_g \\ -C_g & C_R \end{pmatrix}; \qquad \hat{C}_g = \begin{pmatrix} 0 & 0 \\ 0 & C_{\text{in}} \end{pmatrix}. \tag{3.14}$$

moreover, $U(\vec{\varphi})$ is the potential energy associated with the Josephson junction and the inductor.

$$U(\vec{\varphi}) = -E_J(\Phi_x)\cos\left(\frac{\varphi_1}{\varphi_0}\right) + \frac{\varphi_2^2}{2L_r}. \tag{3.15}$$

Now, we compute the canonical momentum conjugate vector $\vec{Q}$ through the relation

$$\vec{Q} = \frac{\partial \mathcal{L}_{\text{read}}}{\partial[\dot{\vec{\varphi}}]} = \hat{C}\dot{\vec{\varphi}} - \hat{C}_g\vec{V} \rightarrow \dot{\vec{\varphi}} = \hat{C}^{-1}(\vec{Q} + \hat{C}_g\vec{V}), \tag{3.16}$$

with this transformation together with the Legendre transformation $\mathcal{H} = \langle \vec{Q}, \dot{\vec{\varphi}} \rangle - \mathcal{L}(\vec{Q}, \vec{\varphi})$, we obtain the circuit Hamiltonian

$$\begin{aligned} \mathcal{H}_{\text{read}} &= \big(\vec{Q} + \hat{C}_g\vec{V}\big)^T(\hat{C}^{-1})^T\vec{Q} - \frac{1}{2}\big(\vec{Q} + \hat{C}_g\vec{V}\big)^T(\hat{C}^{-1})^T\hat{C}\hat{C}^{-1}\big(\vec{Q} + \hat{C}_g\vec{V}\big) \\ &- \big(\vec{Q} + \hat{C}_g\vec{V}\big)^T(\hat{C}^{-1})^T\vec{Q}_g + U(\vec{\varphi}). \end{aligned} \tag{3.17}$$

As the capacitance matrix by definition is a symmetric matrix, its inverse is also a symmetric matrix, hence $(\hat{C}^{-1})^T = \hat{C}^{-1}$. Thus the circuit Hamiltonian can be written as

$$\mathcal{H}_{\text{read}} = \frac{1}{2}\big(\vec{Q} + \hat{C}_g\vec{V}\big)^T\hat{C}^{-1}(\vec{Q} + \hat{C}_g\vec{V}) + U(\vec{\varphi}). \tag{3.18}$$

Where the inverse of the capacitance matrix $\hat{C}^{-1}$ is given by

$$\hat{C}^{-1} = \frac{1}{C^*}\begin{pmatrix} C_R & C_g \\ C_g & C_\Sigma \end{pmatrix}. \tag{3.19}$$

Here, $C^* = C_\Sigma C_R - C_g^2$ is the determinant of the capacitance matrix $\hat{C}$. Thus, the write the circuit Hamiltonian as

$$\begin{aligned} \mathcal{H}_{\text{read}} &= \frac{C_\Sigma}{2C^*}Q_3^2 + \frac{\varphi_3^2}{2L_r} + \frac{C_R}{2C^*}Q_1^2 - E_J(\Phi_x)\cos\left(\frac{\varphi_1}{\varphi_0}\right) \\ &+ \frac{C_g}{C^*}Q_1Q_3 + \frac{C_gC_{\text{in}}}{C^*}V_gQ_1 + \frac{C_\Sigma C_{\text{in}}}{C^*}V_gQ_3. \end{aligned} \tag{3.20}$$

Assuming $C_r \gg \{C_g, C_{\text{in}}, C_B\}$ [Koc+07], the Hamiltonian becomes

$$\mathcal{H}_{\text{read}} = \frac{(Q_1 + q_g)^2}{2C_\Sigma} - E_J(\Phi_x)\cos\left(\frac{\varphi_1}{\varphi_0}\right) + \frac{Q_3^2}{2C_r} + \frac{\varphi_3^2}{2L_r} + \frac{C_g}{C_rC_\Sigma}Q_1Q_3. \tag{3.21}$$

In this Hamiltonian, we identify three contributions; the first is the transmon Hamiltonian shown in Eq. (3.5). The second contribution corresponds to the LC circuit, and the last term is the capacitive

coupling among these systems. Thus, the quantum Hamiltonian reads

$$\mathcal{H}_{\rm read} = 4E_C(\hat{n}_1 - n_g)^2 - E_J(\Phi_x)\cos\left(\frac{\hat{\varphi}_1}{\varphi_0}\right) + \hbar\omega_r\left(a^\dagger a + \frac{1}{2}\right) - g_0\hat{n}_J(a^\dagger + a), \tag{3.22}$$

here $g_0 = 2e\beta V^0_{\rm rms}$ is the coupling strength between the transmon and the resonator. $\beta = C_g/C_\Sigma$ is the capacitance ratio and $V^0_{\rm rms} = \sqrt{\hbar\omega_r/2C_R}$ is the zero point fluctuation voltage of the resonator. The next step is to write the the transmon Hamiltonian in its diagonal basis

$$\mathcal{H}_{\rm read} = \hbar\omega_r\left(a^\dagger a + \frac{1}{2}\right) + \sum_{n=0}^{\infty}\hbar\omega_n|n\rangle\langle n| - \sum_{n,n'=0}^{\infty} g_{n,n'}|n\rangle\langle n'|(a^\dagger + a). \tag{3.23}$$

We obtain the readout Hamiltonian by considering the dispersive regime among the resonator and the transmon. This condition is achieved when $g_{n,n'}/\Delta_{n,n'} \ll 1$, where $\Delta_{n,n'} = \omega_n - \omega_{n'} - \omega_r$ is the qubit-resonator detuning. Notice that, due to the decrease of the anharmonicity of the energy levels on the transmon, the two-level approximation is not valid. In such case, the effective Hamiltonian is obtained by considering the following transformation $\mathcal{H}_{\rm eff} = U\mathcal{H}_{\rm read}U^\dagger$, where the transformation U is given by

$$U = e^{S-S^\dagger}; \qquad S = \sum_n \frac{g_{n+1,n}}{\Delta_{n+1,n}} a|n+1\rangle\langle n|. \tag{3.24}$$

Using the Baker-Campbell-Hausdorff formula [LL73] and keeping terms up to second order in $g_{n+1,n}/\Delta_{n+1,n}$, we obtain the effective Hamiltonian

$$\begin{aligned}\mathcal{H}_{\rm eff} &= \sum_{l=0}^{\infty}\hbar\omega_n|n\rangle\langle n| + \hbar\omega_r a^\dagger a + \sum_n \hbar\chi_{n,n+1}|n+1\rangle\langle n+1| - \chi_{0,1}a^\dagger a|0\rangle\langle 0| \\ &+ \sum_n \hbar(\chi_{n-1,n} - \chi_{n,n+1})a^\dagger a|n\rangle\langle n|.\end{aligned} \tag{3.25}$$

Where, $\chi_{\ell,\ell'} = g^2_{\ell,\ell'}/\Delta_{\ell,\ell'}$ is the effective dispersive shift. By truncating the Hamiltonian **??** up to the first two energy levels of the transmon, the readout Hamiltonian is given by

$$\mathcal{H}_{\rm eff} = \frac{\hbar\omega'_q(\Phi_x)}{2}\sigma^z + \hbar(\omega'_r + \chi\sigma^z)a^\dagger a. \tag{3.26}$$

Here, $\omega_q^{`} = \omega_q + \chi_{01}$, and $\omega_r - \chi_{1,2}/2$ are the normalized qubit and resonator frequency, respectively. Moreover, $\chi = \chi_{0,1} - \chi_{1,2}/2$ is the effective Stark-shift on the qubit. This Hamiltonian shows that by measuring the resonator it is possible to know the qubit state.

3.2 The flux qubit

Superconducting persistent current qubit, or flux qubit [Orl+99] is a type of superconducting artificial atom whose energy levels correspond to the circulating current in a superconducting loop. This artificial atom is composed by a loop interrupted by three asymmetric Josephson junctions; the three junctions increase the total inductance of the loop. Therefore, the superconducting phase on the loop does not fluctuate much as the charge on the circuit. Thus, the degree of freedom describing the system corresponds to the superconducting phase instead of the charge as in the transmon. On the other hand, as the circuit corresponds to a superconducting loop, the state of the qubit can be modified by considering an external magnetic flux threading the superconducting loop.

In Figure. (3.4) we depict the flux qubit circuit. The flux qubit is composed by a loop interrupted by three Josephson junctions. We are assuming asymmetric junctions i.e., $E_{J1} = E_{J2} = E_J$, and $E_{J3} = \alpha E_J$. Furthermore, the circuit is connected to two gate voltages through the capacitor C_g. Finally, we are considering the loop is threaded by an external magnetic field Φ_x. Regarding the node variables, the circuit Lagrangian is given by

$$\begin{aligned}\mathcal{L} &= \frac{C_\Sigma}{2}(\dot{\varphi}_1^2 + \dot{\varphi}_2^2) - 2\alpha C\dot{\varphi}_1\dot{\varphi}_2 - \gamma C(\dot{\varphi}_1 V_A + \dot{\varphi}_2 V_B) \\ &+ E_J\left[2 + \alpha - \cos\left(\frac{\varphi_1}{\phi_0}\right) - \cos\left(\frac{\varphi_2}{\phi_0}\right) - \alpha\cos\left(\frac{\Phi_{x1} + \varphi_1 - \varphi_2}{\varphi_0}\right)\right]. \end{aligned} \tag{3.27}$$

Here, $C_\Sigma = (1+\alpha+\gamma)C$ is the equivalent capacitance on the circuit. Furthermore, we eliminate the terms proportional to $V_{A(B)}^2$ because do not contribute to the system dynamics. The study starts by considering the classical analysis from the potential energy given in Eq. (3.27). We will show that one critical point of the potential corresponds to two fluxes circulating in the opposite direction. These states define our qubit. The potential energy corresponds to the Josephson contributions given by

$$U/E_J = 2 + \alpha - \cos\left(\frac{\varphi_1}{\phi_0}\right) - \cos\left(\frac{\varphi_2}{\phi_0}\right) - \alpha\cos\left(\frac{\Phi_{x1} + \varphi_1 - \varphi_2}{\varphi_0}\right). \tag{3.28}$$

The critical points correspond to flux variables $(\varphi_1^*, \varphi_2^*)$ vanishing its respective derivatives

$$\frac{\partial U}{\partial \varphi_1} = \sin\left(\frac{\varphi_1}{\varphi_0}\right) + \alpha\sin\left(\frac{\Phi_{x1} + \varphi_1 - \varphi_2}{\varphi_0}\right) = 0. \tag{3.29}$$

$$\frac{\partial U}{\partial \varphi_2} = \sin\left(\frac{\varphi_1}{\varphi_0}\right) - \alpha\sin\left(\frac{\Phi_{x1} + \varphi_1 - \varphi_2}{\varphi_0}\right) = 0. \tag{3.30}$$

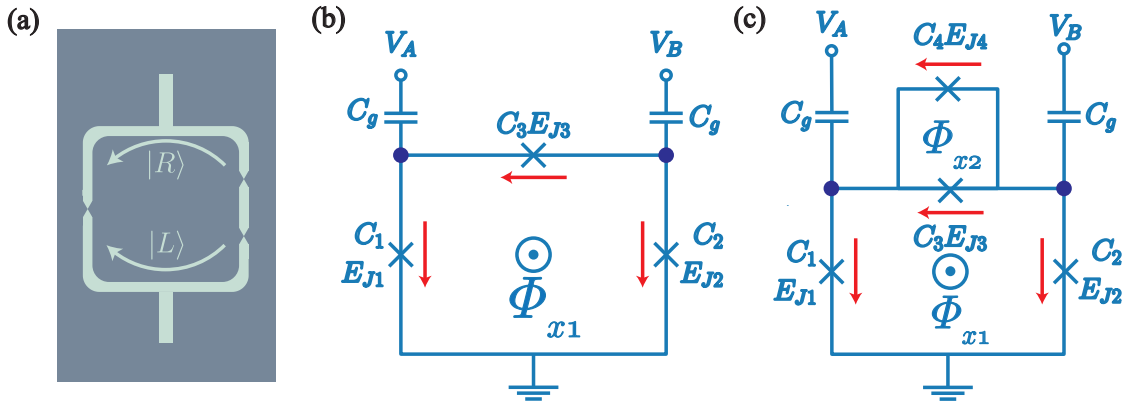

Figure 3.4: **Flux qubit circuit**. (a) Three Josephson junction connected in series in a superconducting loop composed our flux qubit. At each node of the circuit represented by the blue dots, external sources have been connected to obtain off-set charges. (b) Four junction qubits. Two Josephson junction form a SQUID which has Josephson energy and capacitance βC and βE_J, respectively. The SQUID has the function to modify the energy levels of the flux qubit.

These solution correspond to

$$\sin\left(\frac{\varphi_1^*}{\varphi_0}\right) = -\sin\left(\frac{\varphi_2^*}{\varphi_0}\right) \rightarrow \varphi_1^* = -\varphi_2^*. \tag{3.31}$$

$$\sin\left(\frac{\varphi^*}{\varphi_0}\right) = -\alpha\sin\left(\frac{2\Phi_{x1}+2\varphi^*}{\varphi_0}\right). \tag{3.32}$$

The first critical point represents two fluxes circulating with opposite direction, i.e., our qubits. To show that this critical point is a minimum of U, we compute the determinant of the Hessian matrix and evaluate this determinant with the critical point. The determinant of the Hessian matrix is given by [RJ95]

$$\mathrm{Det}[\mathbf{H}] = \frac{\partial^2 U}{\partial\varphi_1^2}\frac{\partial^2 U}{\partial\varphi_2^2} - \left(\frac{\partial^2 U}{\partial\varphi_1\partial\varphi_2}\right)^2. \tag{3.33}$$

$$\mathrm{Det}[\mathbf{H}] = \alpha\cos\left(\frac{\Phi_{x1}+\varphi_1-\varphi_2}{\varphi_0}\right)\left(\cos\frac{\varphi_1}{\varphi_0}+\cos\frac{\varphi_2}{\varphi_0}\right)+\cos\frac{\varphi_1}{\varphi_0}\cos\frac{\varphi_2}{\varphi_0}. \tag{3.34}$$

By replacing the critical point given in Eq. (3.33) in the Eq. (3.38), we obtain $\mathrm{Det}[H] > 0$ and $\partial^2 U/\partial\varphi_\ell^2 > 0$, so the critical point $\varphi_1^* = -\varphi_2^*$ is a minimum of U. The surface of potential is plotted in Fig. (3.5)(a). The 2D projection on Fig. (3.5)(b) shows the two minimum corresponding to the circulating current state. To obtain the Hamiltonian of the circuit it is convenient to write it as a quadratic

$$\mathcal{L} = \frac{1}{2}\vec{\dot{\varphi}}^{\,T}\hat{C}\,\vec{\dot{\varphi}} - \vec{\dot{\varphi}}^{\,T}\hat{C}_g\vec{V} - U(\vec{\varphi}). \tag{3.35}$$

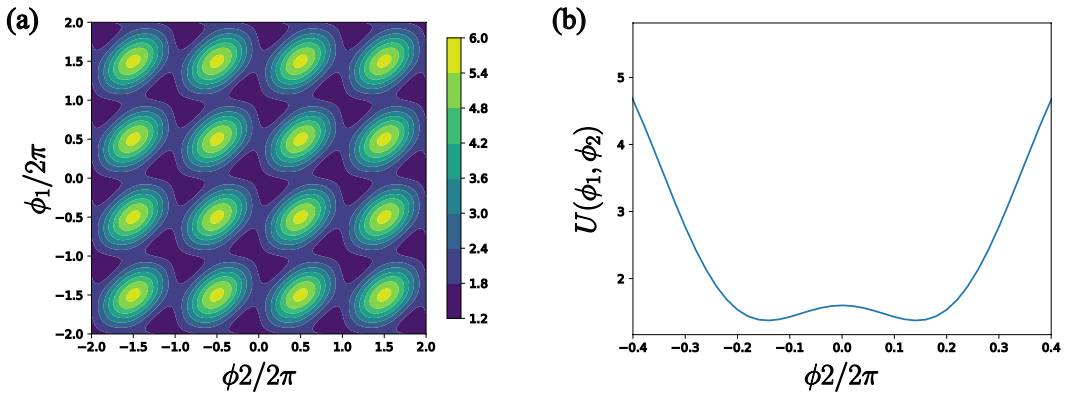

Figure 3.5: **Flux qubit potential**. (a) Surface graphic for the potential energy $U(\varphi_1, \varphi_2)$, for $f = 1/2$ and $\alpha = 0.8$ as a function of the flux parameters. (b) 2D plot for the energy potential as function of φ_2. In this case, we are considering $\varphi_1 = -\varphi_2$. As we can see the potential exhibit two minimum, which correspond to two fluxes circulating in opposite direction.

Here, we have defined the capacitance matrix $\hat{C}$ and the gate capacitance matrix $\hat{C}_g$ as

$$\hat{C} = C \begin{pmatrix} 1+\alpha+\gamma & -\alpha \\ -\alpha & 1+\alpha+\gamma \end{pmatrix}; \qquad \hat{C}_g = \gamma C \begin{pmatrix} 1 & 0 \\ 0 & 1 \end{pmatrix}, \tag{3.36}$$

where, $\vec{\dot{\varphi}}^{\,T} = (\dot{\varphi}_1, \dot{\varphi}_2)$ and $\vec{V}^T = (V_A, V_B)$ correspond to the flux and gate voltage vector respectively. The canonical conjugate momentum is obtained with the relation $\vec{Q} = \partial\mathcal{L}/\partial\vec{\dot{\varphi}}$.

$$\vec{Q} = \hat{C}\vec{\dot{\varphi}} - \hat{C}_g\vec{V}, \tag{3.37}$$

Thus, as $\hat{C}$ is invertible, we can also invert the flux vector $\vec{\dot{\varphi}}$

$$\vec{\dot{\varphi}} = \hat{C}^{-1}(\vec{Q} + \vec{q}_g). \tag{3.38}$$

where, $\vec{q}_g = \hat{C}_g\vec{V}$ is the offset charge. The Hamiltonian is obtained by performing the Legendre transformation $\mathcal{H} = \langle\vec{Q}, \vec{\dot{\varphi}}\rangle - \mathcal{L}(\vec{Q}, \vec{\varphi})$, and we replace the expression $\vec{\dot{\varphi}}$ from Eq. (3.38)

$$\begin{aligned} \mathcal{H} &= (\vec{Q} + \vec{q}_g)^T(\hat{C}^{-1})^T\vec{Q} - \frac{1}{2}(\vec{Q} + \vec{q}_g)^T(\hat{C}^{-1})^T\hat{C}\hat{C}^{-1}(\vec{Q} + \vec{q}_g) \\ &- (\vec{Q} + \vec{q}_g)^T(\hat{C}^{-1})^T\vec{q}_g + U(\vec{\varphi}). \end{aligned} \tag{3.39}$$

$$\mathcal{H} = \frac{1}{2}(\vec{Q} + \vec{q}_g)^T\hat{C}^{-1}(\vec{Q} + \vec{q}_g) + U(\vec{\varphi}). \tag{3.40}$$

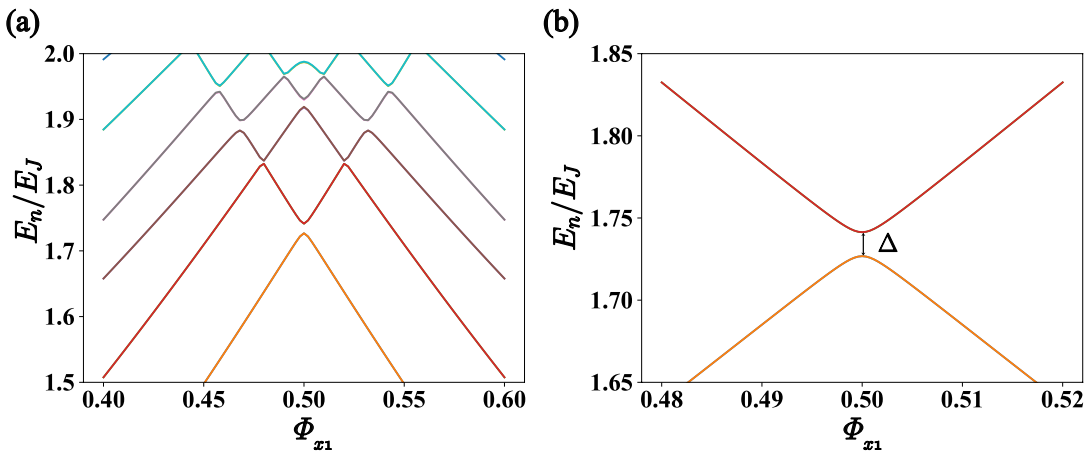

Figure 3.6: **Energy levels of the flux qubit**. Energy spectrum as a function of the external magnetic flux f for $E_J/E_c = 80$, $\alpha = 0.8$ and $\gamma = 0.02$. At the point $f = 0.5$, we observe that the first two energy levels are closed to each other, allowing made an effective two-level approximation.

Where we write the inverse of the capacitance matrix $\hat{C}^{-1}$ as

$$\hat{C}^{-1} = \frac{1}{C(\gamma+1)(1+2\alpha+\gamma)} \begin{pmatrix} 1+\alpha+\gamma & \alpha \\ \alpha & 1+\alpha+\gamma \end{pmatrix}. \tag{3.41}$$

We perform the quantization of the circuit Hamiltonian by considering operators instead of function. These operators must satisfy canonical commutation relation. For the flux qubit, as the charge fluctuates much than the flux. The quantization is done promoting $\vec{Q} \to i\hbar\nabla_\varphi$

$$\mathcal{H} = \frac{1}{2}\left(i\hbar\vec{\nabla}_\varphi - \vec{q}_g\right)^T \hat{C}^{-1}\left(i\hbar\vec{\nabla}_\varphi - \vec{q}_g\right) + U(\vec{\varphi}). \tag{3.42}$$

This Hamiltonian can be written in a simpler way considering the following form of the wave function $\Psi(\vec{\varphi}) = e^{i(k_A\varphi_1 + k_B\varphi_2)}\psi(\vec{\varphi})$, with $k_\ell = -\gamma C V_\ell$. Thus, the Hamiltonian reads

$$\mathcal{H} = \frac{-\hbar^2}{2}\vec{\nabla}_\varphi^{\,T}\hat{C}^{-1}\vec{\nabla}_\varphi + U(\vec{\varphi}). \tag{3.43}$$

By performing the transformation $\varphi_p = (\varphi_1+\varphi_2)/2$ and $\varphi_m = (\varphi_1-\varphi_2)/2$ the Hamiltonian becomes

$$\mathcal{H} = -\frac{\hbar^2}{2M_p}\partial^2_{\varphi_p} - \frac{\hbar^2}{2M_m}\partial^2_{\varphi_m} - E_J\left[2+\alpha-2\cos\frac{\varphi_p}{\varphi_0}\cos\frac{\varphi_m}{\varphi_0} - \alpha\cos\left(\frac{\Phi_{x1}+2\varphi_m}{\varphi_0}\right)\right]. \tag{3.44}$$

Here, $M_p = 2C(1+\gamma)$ and $M_m = 2C(1+2\alpha+\gamma)$ are the effective capacitance. The energy spectrum of the Hamiltonian corresponds to bands energy, corresponding to the solutions of the

central equation [Kit66]. The energy spectrum of the Hamiltonian in Eq. (3.44) is shown in Fig. (3.6) as function of the external flux Φ_{x1}. Near the point, $\Phi_{x1} = \phi_0/2$ the first two energy levels of the flux qubit are close to each other, and hence the system can be truncated as an effective two-level system. To quantify the energy of this effective two-level system, we consider the tight-binding approximation [Orl+99; Wal+00], where the wavefunction is written as $\Psi = c_+u^+ + c_-u^-$, here, $u^\pm$ corresponds to the solution on each well on the potential U. The wavefunction Ψ must satisfy the following Shrödinger equation

$$\begin{pmatrix} H_{u^+,u^+} & H_{u^+,u^-} \\ H_{u^-,u^+} & H_{u^-,u^-} \end{pmatrix} \begin{pmatrix} c_+ \\ c_- \end{pmatrix} = E \begin{pmatrix} c_+ \\ c_- \end{pmatrix}. \tag{3.45}$$

The diagonal matrix elements correspond to the energy of each well as shown in Fig (3.5)(b). At the degeneracy point $\Phi_{x1} = \phi_0/2$ both wells have the same energy i.e., $H_{u^\pm,u^\pm} = \pm E_0 = 2I_p(\Phi_x - \phi_0/2)$ with I_p being the persistent current on the loop and ϕ_0 is the flux quantum. Moreover, the non-diagonal terms correspond to the tunnelling energy denoted as Δ. Thus, the effective two-level Hamiltonian is given by

$$\begin{pmatrix} E_0 & -\Delta \\ -\Delta & -E_0 \end{pmatrix} = E_0\sigma^z - \Delta\sigma^x, \tag{3.46}$$

Written this Hamiltonian in its diagonal form, we arrive at the flux-qubit Hamiltonian

$$\mathcal{H} = \sqrt{\Delta^2 + E_0^2}\sigma^z = \frac{\hbar\omega}{2}\sigma^z. \tag{3.47}$$

The energy gap of the flux-qubit depends directly on the external magnetic flux and the tunnelling between nearest neighbour. Hence by modifying these parameters, it is possible to manipulate the qubit. We modify the qubit frequency by changing the external magnetic flux Φ_{x1} threading the loop, whereas, the modification of the tunnelling energy is through the area on the third junction. However, this is not possible in the experimental situation. In such case, the manipulation qubit gap and tunnelling parameter are modified by including a superconducting loop interrupted by a Josephson junction with capacitance $C_{J4} = \alpha C$, and Josephson energy $E_{J4} = \alpha E_J$. On the other hand, the branch variable of this junction is related with active node variables through the fluxoid quantization rule given by $\Phi_J = \varphi_1 - \varphi_2 - \Phi_{x1} - \Phi_{x2}$. The Lagrangian of the system is given by

($V_A = V_B = 0$)

$$\begin{aligned}\mathcal{L} &= \frac{C_{eq}}{2}(\dot{\varphi}_1^2 + \dot{\varphi}_2^2) - 4\alpha C\dot{\varphi}_1\dot{\varphi}_2 \\ E_J &\left[2 + 2\alpha - \cos\frac{\varphi_1}{\varphi_0} - \cos\frac{\varphi_2}{\varphi_0} - \alpha\cos\left(\frac{\varphi_1 - \varphi_2 + \Phi_{x1}}{\varphi_0}\right)\right. \\ - &\left.\alpha\cos\left(\frac{\varphi_1 - \varphi_2 - \Phi_{x1} - \Phi_{x2}}{\varphi_0}\right)\right],\end{aligned} \tag{3.48}$$

where $C_{eq} = (1 + 2\alpha + \gamma)$ is the total capacitance of the system. By performing the transformation $\varphi_1 = \varphi_p + \varphi_m$. The Lagrangian reads

$$\begin{aligned}\mathcal{L} &= \frac{C(1+\gamma)}{2}\dot{\varphi_p}^2 + \frac{C(1+2\alpha+\gamma)}{2}\dot{\varphi_m}^2 \\ E_J &\left[2 + 2\alpha - \cos\frac{\varphi_p}{\varphi_0}\cos\frac{\varphi_m}{\varphi_0} - 2\alpha\cos\left(\frac{\Phi_{x2}}{2\varphi_0}\right)\cos\left(\frac{2\varphi_m + \Phi_{x1}}{\varphi_0} - \frac{\Phi_{x2}}{2\varphi_0}\right)\right].\end{aligned} \tag{3.49}$$

Notice that this Lagrangian is like the obtained in Eq. (3.27), but now, the parameter alpha is pondered with a term proportional to the external magnetic flux threading on the second loop. Thus, we obtain a flux-qubit with controllable tunnelling energy. This tunability allows manipulating the states of the flux qubit. The Hamiltonian for this Lagrangian is given by

$$\begin{aligned}\mathcal{H} &= -\frac{\hbar^2}{2C_p}\partial^2_{\varphi_p} - \frac{\hbar^2}{2C_m}\partial^2_{\varphi_m} \\ &+ E_J\left[2 + 2\alpha - \cos\frac{\varphi_p}{\varphi_0}\cos\frac{\varphi_m}{\varphi_0} - 2\alpha\cos\left(\frac{\Phi_{x2}}{2\varphi_0}\right)\cos\left(\frac{2\varphi_m + \Phi_{x1}}{\varphi_0} - \frac{\Phi_{x2}}{2\varphi_0}\right)\right].\end{aligned} \tag{3.50}$$

where $C_p = 2C(1+\gamma)$, and $C_m = 2C(1+4\alpha+\gamma)$. To obtain the Hamiltonian, we are considering that both external magnetic flux i.e., $\Phi_{x1} = \phi_0 + \delta_1$ and $\Phi_{x2} = \phi_0 + \delta_2$. Thus, with the tight-binding approximation, the effective two-level Hamiltonian reads

$$\bar{\mathcal{H}} = \sqrt{\phi_0^2 + \Delta^2}\sigma^z + \mathcal{H}_1. \tag{3.51}$$

$$\mathcal{H}_1 = r_1\left(\delta_1 + \frac{\delta_2}{2}\right)\big(\cos\theta_0\sigma^z - \sin\theta_0\sigma^x\big) - s_2\delta_2\big(\sin\theta_0\sigma^z + \cos\theta_0\sigma^x\big), \tag{3.52}$$

where $r_1 = 2\pi E_J\sqrt{1 - 1/(4\alpha)}$ and $s_2 = 3.5\Delta\sqrt{E_J/E_C}$ [Orl+99; Wal+00] and $\theta_0 = \Delta/f_0$. Thus, by adding an additional loop interrupted with a Josephson junction it is possible to manipulate the states of the flux qubit.

3.3 The coplanar waveguide resonator

Another essential element in superconducting circuits is the photon sources. Many efforts have been made to build electrical circuits behaving as, for example, Faby-Perot cavity in cavity quantum electrodynamics [Boa+07]. In superconducting circuits, several devices have been proposed as possible photon sources, devices as, LC resonators [Gir11] and strip-line resonator [Ito74]. However, these devices do not offer cavities with high-quality factors. Technological progress on fabrication techniques has made possible to design superconducting cavities with high-quality factors. A remarkable device is the coplanar waveguide resonator (CWR) [Göp+08]. Coplanar waveguide resonator has proven to be an excellent device to generate photons. Flexible fabrication techniques have allowed designing resonators operating at the microwave regime (1 $\sim$10 GHz) with quality factors around of $Q \ll 10^6$ [Sag+11], and a lifetime of ($T_\kappa \sim 2.5\mu s$) [Wan+09]. Moreover, the vacuum field achieved in this resonator is at least one hundred times larger than the achieved in 3D cavities in cavity quantum electrodynamics [RBH01]. This increase on the vacuum field have permitted to implement the light-matter interaction among an artificial superconducting atom with microwave resonator.

Figure (3.7) shows the circuit of the coplanar waveguide resonator. The device is considered as a set of N (N approaching to infinite) LC circuit connected in series each of them characterized by their capacitance and inductance per unit of length $c\ dz$, and $l\ dz$, respectively. Under this assumption each LC circuit is modelled within the lumped circuit element description [Poz09] i.e., both current and voltage do not vary with the position. Thus, the circuit Lagrangian for the CWR reads

$$\mathcal{L} = \sum_{n=1}^{N} \frac{cdz}{2}\dot{\psi}_n^2 - \sum_{n=1}^{N-1} \frac{1}{2ldz}(\psi_{n+1} - \psi_n)^2. \tag{3.53}$$

where the flux node on the n-th LC resonator is defined as $\psi_n = \int_{-\infty}^{t} v_n(t')dt'$, with $v(t')$ being the voltage drop through the specific branch component. The next step in the derivation is to consider the *continuum limit*. In this limit, we assume that the number of resonator approaches to infinite and the length $dz \to 0$. Under this condition, we assume that the flux on the coplanar waveguide resonator is a smooth function on the position $\psi(z,t)$. In this limit, we obtain

$$\psi_{n+1} = \psi(z_{n+1},t) \quad = \quad \psi(z_n,t) + \partial_z\psi(z_n,t)dz. \tag{3.54}$$

$$\lim_{\Delta z\to 0}\sum_n \Delta z \quad \to \quad \int dz. \tag{3.55}$$

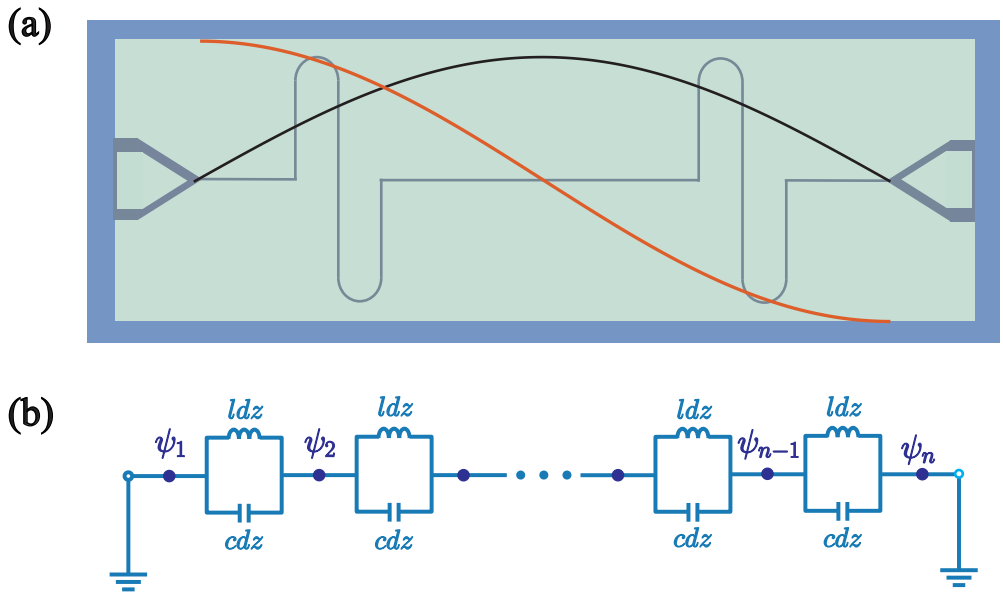

Figure 3.7: **Coplanar waveguide resonator**. Diagram for superconducting coplanar waveguide resonator. (a) Illustration for a $\lambda/2$ transmission line resonator, which consists in three pieces of superconducting metal. At both edges of the resonator, there are breaks; these breaks correspond to a capacitor which has the function to vanish the current at the edges of the resonator. (b) Lumped-element circuit for the $\lambda/2$ coplanar waveguide. The resonator is divided into many LC resonator, each of them is characterized by the capacitance and the inductance per unit of length cdz and ldz, respectively.

Replacing these relations on Eq. (3.53), the circuit Lagrangian takes the following form

$$\mathcal{L} = \int_0^L dz \left[\frac{c}{2} [\partial_t \psi(z,t)]^2 - \frac{1}{2l} [\partial_z \psi(z,t)]^2 \right]. \tag{3.56}$$

To obtain the profile of the current and the voltage on the resonator, we solve the equation of motion associated with the Lagrangian in Eq. (3.56). The equation of motion is given by

$$\partial_t^2 \psi(z,t) - v^2 \partial_z^2 \psi(z,t) = 0, \tag{3.57}$$

This equation corresponds to the wave equation for an electric wave propagating with group velocity $v = 1/\sqrt{lc}$. The boundary conditions for the flux $\psi(z,t)$ depends whether the ends of the resonator are open or not. In superconducting circuit, there are two types of resonators. One of them corresponds to the *half-wavelength* resonator which has both edges open. Thus, the current on the edges is zero, and the voltage, in the end, reaches its maximal value at this point. The second resonator is the *quarter-wavelength* which contains only one end open. In the open end, there is no current, and the voltage reaches its maximal value. In the closed end, there is no

voltage, and the current reaches its maximal value. These boundary conditions are represented by: Half-wavelength transmission line resonator

$$\partial_z \psi(z=0,t) = \partial_z \psi(z=L,t) = 0, \tag{3.58}$$

For the quarter-wavelength transmission line resonator, we have the followings boundary conditions

$$\partial_z \psi(z=0,t) = \partial_t \psi(z=L,t) = 0. \tag{3.59}$$

We solve the wave equation considering the following assumption for the flux $\psi(z,t)$

$$\psi(z,t) = \sum_{\ell=0}^{\infty} \left[\mathcal{A}_\ell e^{i(k_\ell z - \omega_\ell t)} + \mathcal{B}_\ell e^{-i(k_\ell z - \omega_\ell t)} \right], \tag{3.60}$$

Where $\mathcal{A}_\ell$ and $\mathcal{B}_\ell$ are coefficient determined by the boundary conditions in Eq. (3.58), and Eq. (3.58). Replacing this normal-mode expansion in the wave equation given in Eq. (3.57) we obtain

$$\psi(z,t) = \sqrt{\frac{2}{L}} \sum_{\ell=0}^{\infty} \cos(k_\ell z) e^{-i\omega_\ell t}, \tag{3.61}$$

where k_ℓ is the wave number for the electrical wave. We obtain the value of the wavenumber with the boundary conditions given in Eq. (3.58), and Eq. (3.59). For the half-wavelength and quarter-wavelength resonator, the wave vector is given by $k_\ell = \pi\ell/L$ and $k_\ell = \pi(2\ell+1)/L$, respectively. We obtain the expression for voltage and current through the following constitutive relations

$$v(z,t) = \frac{\partial \psi(z,t)}{\partial_t} = \sqrt{\frac{2}{L}} \sum_{\ell=0}^{\infty} \omega_\ell \cos(k_\ell z) e^{-i\omega_\ell t}. \tag{3.62}$$

$$i(z,t) = -\frac{1}{l} \frac{\partial \psi(z,t)}{\partial_z} = -\sqrt{\frac{2}{L}} \sum_{\ell=0}^{\infty} \frac{k_\ell}{l} \sin(k_\ell z) e^{-i\omega_\ell t}. \tag{3.63}$$

On the other hand, to obtain the circuit Hamiltonian, we compute the canonical conjugate momenta $\mathcal{Q}$ through the relation

$$\mathcal{Q} = \frac{\partial \mathcal{L}}{\partial[\partial_t \psi]} = c\partial_t \psi(z,t). \tag{3.64}$$

The canonical momentum corresponds to the charge on the waveguide. Afterwards, we perform

the Legendre transformation $\mathcal{H} = \mathcal{Q}\partial_t\psi - \mathcal{L}$ obtaining the following system Hamiltonian

$$\mathcal{H} = \int_0^L dz \left[\frac{1}{2c}\mathcal{Q}^2 + \frac{1}{2l}[\partial_z \psi]^2 \right]. \tag{3.65}$$

Now, we proceed to quantize the waveguide Hamiltonian. As both, fluxes and charges are time-dependent functions, it is convenient to quantize the waveguide in the Heisenberg picture. Thus, the operators $\hat{\mathcal{Q}}$ and $\hat{\psi}$ are time-independent and satisfy the following commutation relation

$$[\hat{\mathcal{Q}}(z), \hat{\psi}(z')] = i\hbar\delta(z - z'), \quad [\hat{\mathcal{Q}}(z), \hat{\mathcal{Q}}(z')] = 0, \quad [\hat{\psi}(z), \hat{\psi}(z')] = 0. \tag{3.66}$$

Thus, we represent both operators as

$$\hat{\psi}(z) = \sum_{k_\ell=0}^{\infty} \sqrt{\frac{\hbar}{2cL\omega_\ell}} \left[\hat{a}_\ell e^{ik_\ell z} + \hat{b}_\ell e^{-ik_\ell z} \right]. \tag{3.67}$$

$$\hat{\mathcal{Q}}(z) = \sum_{k_\ell=0}^{\infty} -i\sqrt{\frac{\hbar c\omega_\ell}{2L}} \left[\hat{a}_\ell e^{ik_\ell z} - \hat{b}_\ell e^{-ik_\ell z} \right]. \tag{3.68}$$

In these expression, $\hat{a}_\ell$ and $\hat{b}_\ell$ correspond to boson operators. As we are considering the quantization of a transmission line, the propagating waves must be real waves. This condition implies that we can describe the flux operator as a real scalar field [Pes18].

$$\hat{\psi}(z,t) = \sum_{k_\ell=0}^{\infty} \sqrt{\frac{\hbar}{2cL\omega_\ell}} \left[\hat{a}_\ell e^{ik_\ell z} + \hat{a}_\ell^\dagger e^{-ik_\ell z} \right]. \tag{3.69}$$

$$\hat{\mathcal{Q}}(z,t) = \sum_{k_\ell=0}^{\infty} -i\sqrt{\frac{\hbar c\omega_\ell}{2L}} \left[\hat{a}_\ell e^{ik_\ell z} - \hat{a}_\ell^\dagger e^{-ik_\ell z} \right]. \tag{3.70}$$

By replacing these operators on the Hamiltonian in Eq. (3.65) we arrive at the quantum Hamiltonian of the transmission line resonator

$$\mathcal{H} = \sum_{k_\ell=0}^{\infty} \hbar\omega_\ell \left(a_\ell^\dagger a_\ell + \frac{1}{2} \right). \tag{3.71}$$

Thus, the coplanar waveguide resonator Hamiltonian corresponds to an infinite set of quantum harmonic oscillators of frequency ω_ℓ.

Chapter 4

The quantum Rabi model

4.1 Energy spectrum

The quantum Rabi model was introduced at the end of the decade of 1930, describing the interaction of an atom with a highly oscillating weak magnetic field [Rab36]. Likewise, the quantum Rabi model describes the simplest interaction between an atom with a quantized electromagnetic field mode. The interaction between those systems correspond to the dipole interaction, i.e., the energy levels of the atom interact with the quadrature of the electromagnetic field. In the far-wavelength approximation (field does not depend on the position) [SZ97]. In superconducting circuits (the scope of this theses) the dipole interaction is obtained through the galvanic coupling between a flux-qubit with a coplanar waveguide resonator [Abd+08; Chi+04], or as the capacitive coupling between a transmon qubit with a transmission line resonator [Wal+04; TRK92]. The quantum Rabi Hamiltonian is given by

$$\mathcal{H}_{\mathrm{QRS}} = \hbar\omega_{\mathrm{cav}} a^{\dagger}a + \frac{\hbar\omega_q}{2}\sigma^z + \hbar g(\sigma^{+} + \sigma^{-})(a^{\dagger} + a). \tag{4.1}$$

Here, ω_{cav} is the frequency of the quantized field mode, ω_q is the frequency gap of the two-level system, and g is the dipolar coupling between the two-level system and the field mode. Besides, $a^{\dagger}$ (a) correspond to the creation (annihilation) boson operator describing the field mode, and σ^z, $\sigma^{\pm}$ are the Pauli matrices describing the two-level system.

In the strong-coupling regime, $0 < g < 0.01\omega_{\mathrm{cav}}$ the quantum Rabi model can be approximated with the rotating wave approximation, leading to the renamed Jaynes-Cummings model [Sho07; KM80]. The Jaynes-cummings model has the number of excitation operator $N_e = a^{\dagger}a + \sigma^{+}\sigma^{-}$

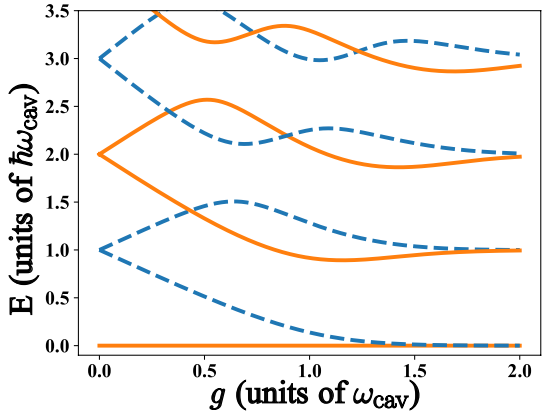

Figure 4.1: **Energy spectrum of the quantum Rabi system**. (a) Energy spectrum of the quantum Rabi model as a function of the coupling g for the qubit ad the resonator in resonance $\omega_q = \omega_{\rm cav}$. Orange lines correspond to states with parity $p = +1$, and blue dashed lines stand for eigenstates with parity $p = +1$.

as a conserved quantity, imposing a continuous symmetry $U(1)$. In such a case, the model can diagonalise in an effective 2×2 basis involving one excitation either in the atom and the field. This basis is usually known as the Jaynes-cummings doublet [SZ97]. On the other hand, in the perturbative ultra-strong coupling regime $0.01 < g < 0.03\omega_{\rm cav}$, the counter-rotating terms on the Jaynes-Cumming model $g(a^\dagger\sigma^+ + a\sigma^-)$ become significant. However, it is possible to obtain their contributions with perturbation theory. Moreover, in the non-perturbative regime, i.e., $0.3 \leq g/\omega_{\rm cav} \leq 1$ the counter-rotating terms cannot be expressed as perturbative contributions of the Jaynes-Cummings model. Instead, it is necessary to diagonalise the fully Rabi model. Several ways have been taken to obtain the energy spectrum and the energy states of the quantum Rabi model. D. Braak did the most significant achievement [Bra11; Lee+17] by diagonalising the quantum Rabi model. In such a case, the Hamiltonian is written in the Bogoliubov space [Bra11; Lee+17], leading to a set of coupled differential equations. The eigenvalues of this set of the equation are divided into two types: regular and exceptional. The former corresponds to the energy spectrum of the uncoupled system, and the latter stands to the quantum Rabi model energy spectrum [Bra11].

As we said before, the quantum Rabi model in the strong-coupling regime, there is a continuous symmetry allows diagonalising the model in 2×2 basis. However, the counter-rotating terms arising in the ultra-strong coupling regime breaks down this symmetry, and the continuous symmetry is changed by a discrete ones known as parity $\mathbb{Z}_2$. The parity symmetry is defined by the parity operator defined as $\mathcal{P} = -\sigma^z \otimes e^{i\pi a^\dagger a}$ with eigenvalues $p = \pm 1$. Notice that the parity operator commutes with the quantum Rabi Hamiltonian, i.e., $[\mathcal{H}_{\rm QRS}, \mathcal{P}] = 0$. As a result, we can

simultaneously diagonalise both operators on a common basis $\{|\sigma, p\rangle\}_{\sigma=0}^{\infty}$. Thus, we can label each energy level concerning their energy σ, and their parity p. This labelling permits to divide the whole Hilbert space into two orthogonal subspaces (as shown in Fig. (4.1)), the even subspace $p = +1$ and the odd subspace $p = -1$, respectively. We can expand each subspace in terms of the following chains

$$|g, 0\rangle \leftrightarrow |e, 1\rangle \leftrightarrow |g, 2\rangle \leftrightarrow |e, 3\rangle \leftrightarrow ... \quad (p = +1), \tag{4.2}$$

$$|e, 0\rangle \leftrightarrow |g, 1\rangle \leftrightarrow |e, 2\rangle \leftrightarrow |g, 3\rangle \leftrightarrow ... \quad (p = -1). \tag{4.3}$$

where $|g(e)\rangle$ is the ground (excited) state of the two-level system, and $|n\rangle$ is the n-th Fock state of the field mode. Therefore, from the energy spectrum depicted in Fig. (4.1) the lowest energy levels have parity $p = +1$, and $p = -1$, respectively. Thus, we can write these states as follows

$$|0, +\rangle = \sum_{n=0}^{\infty} a_n |g, 2n\rangle + b_n |e, 2n + 1\rangle \tag{4.4}$$

$$|1, -\rangle = \sum_{n=0}^{\infty} c_n |g, 2n + 1\rangle + d_n |e, 2n\rangle \tag{4.5}$$

Notice that the low-lying energy spectrum of the Rabi model correspond to entangled light-matter states. On the other hand, The parity symmetry $\mathbb{Z}_2$ presents on the Rabi model in the ultra-strong coupling regime give rise to selection rules between energy transition, which are not appreciable in the strong-coupling regime [FD+16a]. In fact, in the quantum Rabi model, there are interactions which couple states with identical or distinct parity. For instance, it has demonstrated that driving lasers as $\mathcal{H}_d = (a + a^{\dagger})$, and $\mathcal{H}_d = \sigma^x$ connect states belonging to different parity subspaces because the matrix element $\langle \sigma, \pm|\mathcal{H}_d|\sigma', \mp\rangle \neq 0$. Likewise, driving laser as $\mathcal{H}_d = \sigma^z$ couples states belonging to the same parity subspace due to the matrix element $\langle \sigma, \pm|\mathcal{H}_d|\sigma', \pm\rangle \neq 0$. The emergence of these selection rules does not exhibit in the Jaynes-Cummings model have a profound impact in the development of this thesis.

4.2 Description of the dissipation

All quantum systems unavoidable interacts with their environment producing detrimental effects as energy relaxation and loss of coherence. Master equation formalism deals with the study of these detrimental effects [SZ97]. For systems whose light-matter coupling strength is within the

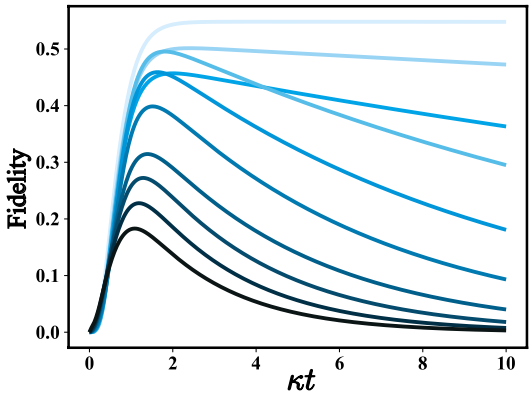

Figure 4.2: **Dissipation of the quantum Rabi system under the standard master equation**. Evolution of the Fidelity between the state $\rho_{st} = |g,0\rangle\langle g,0|$ with the ground state of the QRS obtained through the standard master equation for different coupling constants $g = (0.01, 1)$. As the coupling strength decreases, the Fidelity between the ground state with ρ_{st} approaches to one. The system parameter is given by $\omega_{\rm cav} = 2\pi \times 10$ GHz, $\omega_q = \omega_{\rm cav}$, and $\gamma_a = \gamma_{\sigma^x} = 0.1\omega_{\rm cav}$.

strong coupling regime, the master equation formalism assumes that all system components (light and matter) evolve under independent channels. For the Jaynes-cummings model, the dissipative dynamics is governed by the following master equation

$$\dot{\rho} = -i[\mathcal{H}_{JC}, \rho] + \mathcal{L}_a(\rho) + \mathcal{L}_d(\rho) + \mathcal{L}_{dn}(\rho), \tag{4.6}$$

$$\mathcal{H}_{JC} = \hbar\omega_{\rm cav} a^\dagger a + \frac{\hbar\omega_q}{2}\sigma^z + \hbar g(\sigma^+ a + \sigma^- a^\dagger), \tag{4.7}$$

$$\mathcal{L}_{\mathcal{O}}(\rho) = \frac{\gamma_{\mathcal{O}}}{2}(\bar{n}_{\mathcal{O}} + 1)(2\mathcal{O}\rho\mathcal{O}^\dagger - \{\mathcal{O}^\dagger\mathcal{O}, \rho\}) + \frac{\gamma_{\mathcal{O}}}{2}\bar{n}_{\mathcal{O}}(2\mathcal{O}^\dagger\rho\mathcal{O} - \{\mathcal{O}\mathcal{O}^\dagger, \rho\}), \tag{4.8}$$

$$\mathcal{L}_{dn}(\rho) = \gamma_{dn}(\sigma^z\rho\sigma^z - \rho), \tag{4.9}$$

where $\mathcal{H}_{JC}$ is the Jaynes-Cummings Hamiltonian. Moreover, $\mathcal{L}_{\mathcal{O}}$, ($\mathcal{O} = a, \sigma^-$) is the Lindblad operator, which describe the effect of the thermal reservoir on the two-level system (σ^-) and on the cavity (a), at rate $\gamma_{\mathcal{O}}$. Furthermore, the two-level system additionally interacts with the damping reservoir (σ^z) at rate γ_{dn}. Under this dynamics, a system initially prepared in an excited state should evolve to its ground state if the reservoir is at zero temperature. Likewise, the system prepared in the ground state should evolve to the thermal state at temperature T whether the reservoir is at finite temperature T. However, for system whose light-matter coupling strength is comparable or larger than the bare frequencies of the system component this description fails. For instance, in the dissipative dynamics of the quantum Rabi model, the independent channel description is not valid anymore. Thus, the dissipative and non-dissipative channels must be considered as a whole. Furthermore, we need also to take into account the anharmonic nature of

the energy spectrum of the quantum Rabi model. Therefore, by considering the standard master equation formalism, some unphysical results should appear. In the Reference [Wer+08], the uses of this master equation produces that starting from the state $|g,0\rangle$ (Jaynes-Cummings ground state), the system can generate photons even though the system is at zero temperature. This effect is mainly produced by the fact the dark state at which the standard master equation converges, i.e., $\rho_{st} = |g,0\rangle\langle g,0|$ is not the true ground state of the quantum Rabi model (see Eq. (4.4), and Eq. (4.5)), as a result the system at zero temperature converges to a superposition of excited state [BGB11]. Fig (4.2) shows the evolution of the fidelity between the ground state of the Jaynes-Cummings model with the ground state of the Rabi model computed with the standard master equation as a function of the light-matter coupling strength. Notice that as the coupling strength increases, the fidelity among the steady state obtained with the master equation and the ground state of the quantum Rabi system decreases.

The master equation for systems operating beyond the strong coupling regime will need to consider additional factors not considered before, as the anharmonicity of the energy spectrum of the light-matter system, besides, the ground state of the system contains photons. The first approach toward describing the dissipative dynamics of the quantum Rabi model has been made through of the second-order time-convolutionless projection operator method [BP+02; DL+09], In such a case, the master equation takes into account the coloured bath approximation, i.e., each energy levels have its respective decay rates. With this considerations, the new master equation reads

$$\dot{\rho} = -i[\mathcal{H}_{\rm QRS}, \rho] + \sum_{\ell}(\hat{U}_{\ell}\rho\hat{S}_{\ell} + \hat{S}_{\ell}\rho\hat{U}_{\ell}^{\dagger} - \hat{S}_{\ell}\hat{U}_{\ell}\rho - \rho\hat{U}_{\ell}^{\dagger}\hat{S}_{\ell}). \tag{4.10}$$

Here, $\mathcal{H}_{\rm QRS}$ is the quantum Rabi Hamiltonian, $\hat{S}_{\ell} = (\mathcal{O} + \mathcal{O}^{\dagger})$, $(\ell = a, \sigma^{-})$ is the effective collapse operator taking into account the interaction among the Rabi system with the thermal reservoir of the two-level system and the cavity. Furthermore, $\hat{U}_{\ell}$ is described by

$$\hat{U}_{\ell}(t) = \int_0^{\infty} v_{\ell}(t')e^{-it'\mathcal{H}_R}\hat{S}_{\ell}e^{it'\mathcal{H}_R}dt', \tag{4.11}$$

$$v_{\ell}(t) = \int_0^{\infty} \frac{\gamma_{\ell}(\omega)}{2\pi}(\bar{n}_{\ell}(\omega)e^{i\omega t'} + [\bar{n}_{\ell}(\omega)+1]e^{-i\omega t'})d\omega, \tag{4.12}$$

where $\gamma_{\ell}(\omega)$ is the energy-dependent loss rate for both qubit and cavity, usually, these decay rates depend on the density of states at energy $\hbar\omega$ and must be equal to zero at negative frequencies. The next step is to write the master equation in the dressed basis. Write the master equation in the

quantum Rabi system basis permit to solve the problem associated with the presence of photons in the QRS ground state as well as obtain that the system evolves to the true ground state when the reservoir is at zero temperature. We write the quantum Rabi model in its diagonal form as follows $\mathcal{H}_{\rm QRS} = \sum_{\sigma}^{\infty} \nu_{\sigma} |\sigma, p\rangle\langle\sigma, p|$. Hence, the master equation is given in Eq. (4.10) is expressed as

$$\dot{\rho} = -i \sum_{\sigma=0} [\nu_{\sigma} |\sigma, p\rangle\langle\sigma, p|, \rho] + \sum_{\ell} (\hat{U}_{\ell} \rho \hat{S}_{\ell} + \hat{S}_{\ell} \rho \hat{U}_{\ell}^{\dagger} - \hat{S}_{\ell} \hat{U}_{\ell} \rho - \rho \hat{U}_{\ell}^{\dagger} \hat{S}_{\ell}), \tag{4.13}$$

where, the operator $\hat{S}_{\ell}$, and $\hat{U}_{\ell}$ have been expressed in the Rabi basis

$$\hat{S}_{\ell} = \sum_{\sigma', \sigma > \sigma'} \Big[\langle \sigma, p | S_{\ell} | \sigma', p' \rangle |\sigma, p\rangle\langle\sigma', p'| + \langle \sigma', p' | S_{\ell} | \sigma, p \rangle |\sigma', p'\rangle\langle\sigma, p| \Big], \tag{4.14}$$

$$\hat{U}_{\ell} = \sum_{\sigma', \sigma > \sigma'} \frac{\gamma_{\ell}(\nu_{\sigma\sigma'})}{2} \langle \sigma, p | S_{\ell} | \sigma', p' \rangle |\sigma, p\rangle\langle\sigma', p'| \tag{4.15}$$

At this point, several assumptions have been made, the first concerns with the selection rules of the QRS operators. As the operators $a + a^{\dagger}$, and σ^{x} only connect states belonging to different parity subspaces, we obtain that there are no diagonal contributions to the master equation produced by this operators. In other words, we obtain $\langle \sigma, \pm | S_{\ell} | \sigma', \pm \rangle = 0$ for all σ, σ'. Furthermore, we write the summation in such a way that term with negative frequencies are not allowed. The next step into the derivation is to express the master equation in the interaction picture. We perform this procedure to eliminate via secular approximation all the terms whose oscillation be smaller than the dressed decay rate, i.e., $\Gamma_{\ell}^{\sigma,\sigma'}(\nu_{\sigma,\sigma'}) = \gamma_{\ell}(\nu_{\sigma,\sigma'}) |S_{\ell}^{\sigma,\sigma'}|^2/2$. After this approximation, we arrive at the master equation in the dressed basis for the quantum Rabi model in the ultra-strong coupling regime [BGB11]

$$\dot{\rho} = -i[\mathcal{H}_{\rm QRS}, \rho] + \sum_{\ell} \sum_{\sigma', \sigma > \sigma'} \Gamma_{\ell}^{\sigma,\sigma'}(\nu_{\sigma,\sigma'}) \Big[|\sigma, p\rangle\langle\sigma', p'| \rho |\sigma', p'\rangle\langle\sigma, p| - \frac{1}{2} \Big\{ |\sigma, p\rangle\langle\sigma, p|, \rho \Big\} \Big]. \tag{4.16}$$

In implementation based on circuit quantum electrodynamics [Rid+12], the usual form for the coloured decay rate is given by

$$\Gamma_{\ell}^{\sigma,\sigma'}(\nu_{\sigma,\sigma'}) = 2\pi d_{\ell}(\nu_{\sigma,\sigma'}) \alpha_{\ell}^{2}(\nu_{\sigma,\sigma'}) |S_{\ell}^{\sigma,\sigma'}|^2, \tag{4.17}$$

where, $d_{\ell}(\nu_{\sigma,\sigma'})$ is the spectral density of the bath at frequency $\nu_{\sigma,\sigma'}$, $\alpha_{\ell}^{2}(\nu_{\sigma,\sigma'})$ is the system-

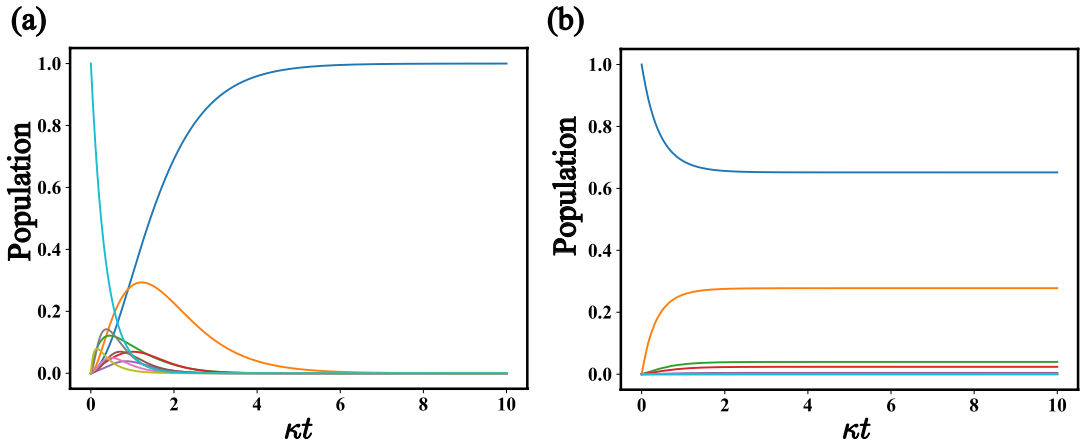

Figure 4.3: **Dissipation dynamics into the dressed states master equation**. Evolution of the population, computed with the master equation given in Eq. (4.16) for the Rabi system initialized in the 20-th excited state (a), and the ground state (b), and the environment at low temperature ($T = 10$ mK in (a)), and high temperature ($T = 200$ mK in (b)). The system parameter is given by $\omega_{\rm cav} = 2\pi \times 10$GHz, $\omega_q = \omega_{\rm cav}$, and $\gamma_a = \gamma_{\sigma^x} = 0.1\omega_{\rm cav}$.

environment coupling strength, which also depend on the energy transition (coloured bath approximation). The shape of both spectral density and the system-bath coupling strength depends on how the superconducting elements coupled to the reservoir. For circuit quantum electrodynamics, the resonator coupled through the quadratures. Hence, the spectral density can be considered constant i.e, $d_\ell(\nu_{\sigma,\sigma'}) = \gamma_\ell/\omega_\ell$, with ω_ℓ being the bare frequency of the system composing the Rabi system, and the system-environment coupling is linear in the energy transition $\alpha^2_\ell(\nu_{\sigma,\sigma'}) = \nu_{\sigma,\sigma'}$. Therefore, the coloured decay rate for this master equation is given by

$$\Gamma_\ell^{\sigma,\sigma'}(\nu_{\sigma,\sigma'}) = \frac{\gamma_\ell \nu_{\sigma,\sigma'}}{\omega_\ell} |S_\ell^{\sigma,\sigma'}|^2. \tag{4.18}$$

Figure (4.3) show the evolution of the population of the eigenstate of the quantum Rabi model for the system evolving under the master equation given in Eq. (4.16). The evolution of the population is in agreement with the expected result of a master equation i.e., the system prepared in a higher state at low temperature decay into the ground state (see (a)), whereas, for a system prepared in the ground state evolves to the thermal state where the bath is a finite temperature (see (b)).

4.3 Implementation of the quantum Rabi model in superconducting circuits

We study how to achieve the ultra-strong coupling regime (USC) in a superconducting circuit composed by a superconducting artificial atom (flux-qubit) directly coupled to a coplanar waveguide resonator [Abd+08] as shown in Fig. (4.4). The coupling strength increases between both subsystems in two ways: By considering a non-uniform coplanar waveguide resonator. The change of the shape on the resonator at the position where we place the flux qubit [Bou+09], and couples an additional Josephson junction at the wire shared between the qubit and the resonator [Ber+05; Nis+07]. As a consequence, the inductance of the resonator increases allowing to achieve the ultra-strong coupling regime. Figure (4.4) shown the effective circuit, which is composed of a $\lambda/2$ coplanar waveguide where coupled at the middle with a four-junction flux qubit. The Lagrangian of the circuit is given by

$$\mathcal{L}=\int_{-L}^{L}dz\left[\frac{c}{2}[\partial_t\psi(z,t)]^2-\frac{1}{2l}[\partial_z\psi(z,t)]^2\right]+\sum_{k=0}^{4}\left[\frac{C_{J_k}}{2}\dot{\varphi}_k^2+E_{J_k}\cos\left(\frac{\varphi_k}{\phi_0}\right)\right]. \tag{4.19}$$

Here, c and l correspond to the capacitance and inductance per unit of length of the CWR, respectively. Moreover, C_{J_k} and E_{J_k} are the Josephson capacitance and energy for the k-th junction, respectively. Furthermore, We assume the coupling junction is placed at the position z_1 and z_2. Thus, the flux on the junction corresponds to the phase difference of the CWR $\Delta\psi=\psi(z_2)-\psi(z_1)$. Besides, the fluxoid quantization relation on the loop forming the flux-qubit is given by

$$\varphi_1+\varphi_2-\varphi_3-\Delta\psi=\phi_{\rm x} \tag{4.20}$$

Replacing this relation on the Lagrangian given in Eq. (4.19), we obtain

$$\mathcal{L} \;=\; \mathcal{L}_{\rm CPW}+\mathcal{L}_{\rm q}+\mathcal{L}_{\rm int}, \tag{4.21}$$

where the Lagrangian of the CWR with the embedded junction $\mathcal{L}_{\rm CPW}$ is given by

$$\mathcal{L}_{\rm CPW}=\int_{-L}^{L}dz\left[\frac{c}{2}[\partial_t\psi(z,t)]^2-\frac{1}{2l}[\partial_z\psi(z,t)]^2\right]+\frac{C_J(\alpha+\gamma)}{2}(\partial_t\Delta\psi)^2+\gamma E_J\cos\left(\frac{\Delta\psi}{\phi_0}\right) \tag{4.22}$$

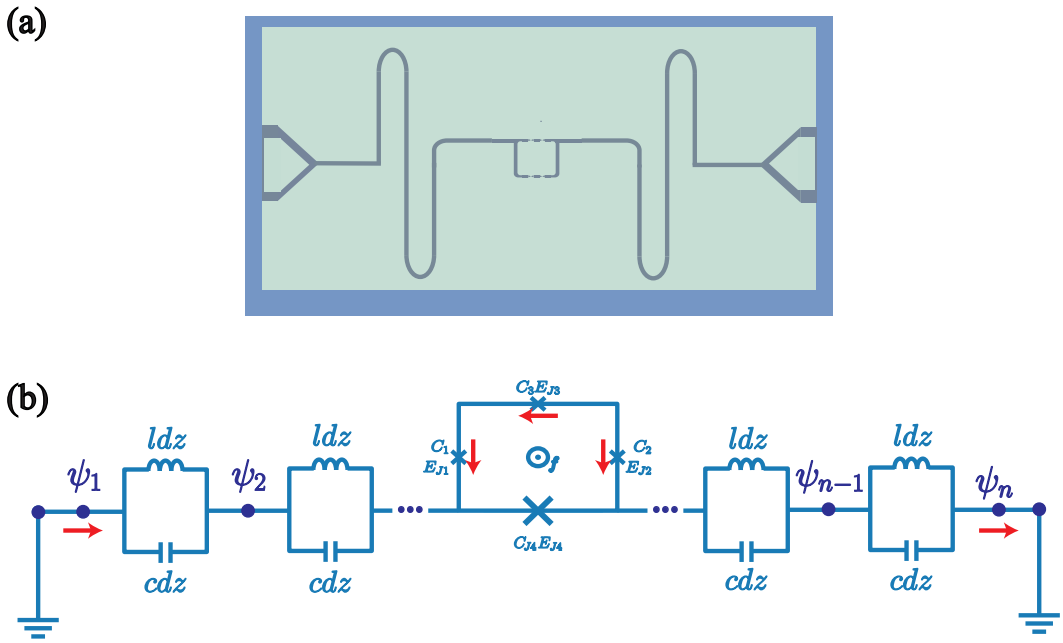

Figure 4.4: **Flux qubit coupled to a resonator**. (a) Illustration of a four-junction qubit coupled at the middle $z = 0$ of a $\lambda/2$ coplanar waveguide resonator. (b) Discretized lumped element representation for the for the $\lambda/2$ coplanar waveguide resonator interrupted at the middle with a four-junction flux qubit.

$\mathcal{L}_{\rm q}$ is the four-junction flux qubit Lagrangian

$$\begin{aligned}\mathcal{L}_{\rm q} &= \frac{C_J(1+\alpha)}{2}(\dot{\varphi}_1^2+\dot{\varphi}_2^2)+\alpha C_J\dot{\varphi}_1\dot{\varphi}_2 \\ &+ E_J\left[\cos\left(\frac{\varphi_1}{\phi_0}\right)+\cos\left(\frac{\varphi_2}{\phi_0}\right)+\alpha\cos\left(\frac{\varphi_1+\varphi_2-\phi_{\rm x}}{\phi_0}\right)\cos\left(\frac{\Delta\psi}{\phi_0}\right)\right].\end{aligned} \tag{4.23}$$

In this derivation, we have considered the following parameters $C_{J_1}=C_{J_2}=C_J$, $E_{J_1}=E_{J_2}=E_J$, $C_{J_3}=\alpha C_J$ $E_{J_3}=\alpha E_J$, and $C_{J_4}=\gamma C_J$. Finally, the interaction Lagrangian is given by

$$\mathcal{L}_{\rm int}=\alpha C_J(\partial_t\Delta\psi)(\dot{\varphi}_1+\dot{\varphi}_2)+\alpha E_J\sin\left(\frac{\varphi_1+\varphi_2-\phi_{\rm x}}{\phi_0}\right)\sin\left(\frac{\Delta\psi}{\phi_0}\right). \tag{4.24}$$

Let us consider that the presence of the flux-qubit does not perturb the mode structure of the CWR. We achieve this considering small Josephson capacitances [Bou+09]. As the capacitive terms induce Stark-shift on the resonator mode, neglecting this term leads to unperturbed field mode. Another condition imposed is that the total inductance of the flux qubit is larger than the inductance of the shared wire on the resonator, i.e., $ldz \ll \sum_k L_k$, with $L_{J_k}=\phi_0^2/E_{J_k}$. This fact physically means that most of the current flowing through the resonator instead of the loop forming (this assumption is valid for small junctions). Finally, we also assume that $\Delta\psi/\phi_0 \ll 1$ [Bou+09].

Thus, all the terms proportional to $\Delta\psi/\phi_0$ are up to its lower power. In such a case, we write the Lagrangian as

$$\begin{aligned}
\mathcal{L}_{\rm CWR} &= \int_{-L}^{L} dz\left[\frac{c}{2}[\partial_t\psi(z,t)]^2 - \frac{1}{2l}[\partial_z\psi(z,t)]^2\right] + \frac{C_J(\alpha+\gamma)}{2}(\Delta\partial_t\psi)^2 + \frac{1}{2L_J}(\Delta\psi)^2. \\
\mathcal{L}_{\rm q} &= \frac{C_J(1+\alpha)}{2}(\dot\varphi_1^2+\dot\varphi_2^2) + \alpha C_J\dot\varphi_1\dot\varphi_2 \qquad (4.25)\\
&+ E_J\left[\cos\left(\frac{\varphi_1}{\phi_0}\right)+\cos\left(\frac{\varphi_2}{\phi_0}\right)+\alpha\cos\left(\frac{\varphi_1+\varphi_2-\phi_{\rm x}}{\phi_0}\right)\right]. \qquad (4.26)\\
\mathcal{L}_{\rm int} &= \alpha E_J\sin\left(\frac{\varphi_1+\varphi_2-\phi_{\rm x}}{\phi_0}\right)\frac{\Delta\psi}{\phi_0}. \qquad (4.27)
\end{aligned}$$

Notice that, in the $\mathcal{L}_{\rm int}$ the capacitive terms have been neglected due to the previous condition imposing small capacitance values. Therefore, the galvanic coupling dominates the coupling interaction. To obtain the Hamiltonian of the CWR, we follow the procedure developed in Chapter (3.3), where the equation of motion for the flux $\psi(z,t)$ obeys the wave equation. Thus, we write the flux $\psi(z,t)$ as

$$\psi(z,t) = \sum_{\ell=0}^{\infty}\mathcal{U}_\ell(z)\mathcal{G}_\ell(t), \qquad (4.28)$$

where $\mathcal{U}_\ell(z)$ is given by

$$\mathcal{U}_\ell(z) = \left\{\begin{array}{ll}\mathcal{A}_\ell\cos(k_\ell(z+L)) & -L\le z\le 0\\ \mathcal{B}_\ell\cos(k_\ell(z-L)) & 0\le z\le L\end{array}\right\}, \qquad (4.29)$$

where $k_\ell=\omega_\ell/v$ is the wave-vector of the resonator, with $v=1\sqrt{lc}$ being the group velocity of the wave transmitted on the resonator. $\mathcal{G}_\ell(t)$ is a function satisfying $\ddot{\mathcal{G}}(t) = -\omega_\ell^2\mathcal{G}_\ell(t)$. Replacing the expression of $\psi(z,t)$ on the Lagrangian we arrive at

$$\mathcal{L}_{\rm CPW} = \sum_\ell\left[\frac{C_{\Sigma_\ell}}{2}\dot{\mathcal{G}}_\ell^2 - \frac{C_{\Sigma_\ell}\omega_\ell^2}{2}\mathcal{G}_\ell^2\right]. \qquad (4.30)$$

where C_Σ is the effective capacitance defined as

$$C_{\Sigma_\ell} = \int_{-L}^{L} dz\, c\,\mathcal{U}_\ell^2(z) + C_J(\alpha+\gamma)\Delta\mathcal{U}_\ell^2(z) \qquad (4.31)$$

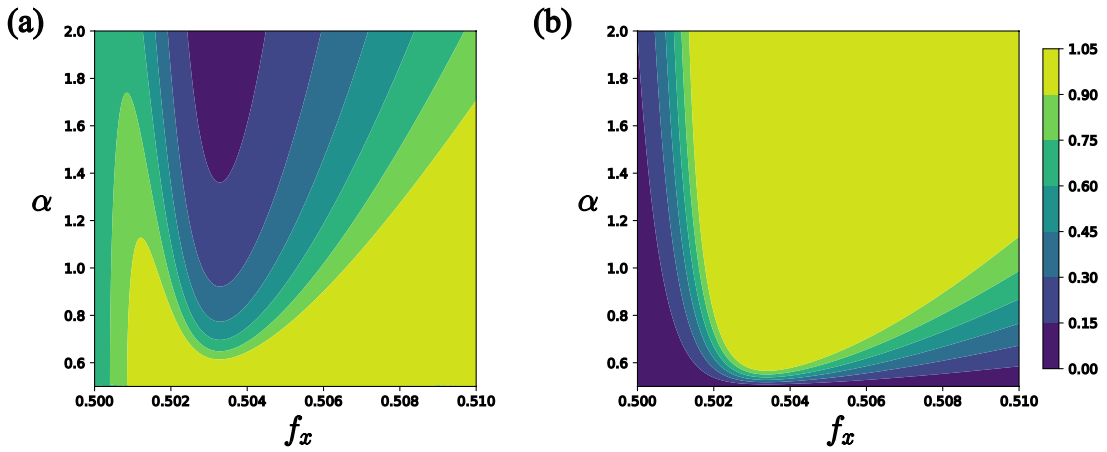

Figure 4.5: **Coupling strength contributions**. Coupling strength associated to the operators σ^x(a) and σ^z (b) as function of the asymmetric Josephson parameter α and as function of the external magnetic flux ϕ_x near from the symmetry point i.e., $\phi_{\rm x} \approx \phi_0/2$. As shown the figure, close of this point the contribution is mainly provided by σ^x.

and the resonator frequency is obtained through the following transcendental equation

$$k_\ell = \frac{l}{L_J}\cot(k_\ell L)\left(1 - \frac{(\alpha+\gamma)\omega_\ell^2}{\omega_{\rm p}^2}\right). \tag{4.32}$$

Here, $\omega_{\rm p} = 1/\sqrt{L_J C_J}$ is the plasma frequency of the fourth junction. The Hamiltonian is obtained by applying the Legendre transformation $\mathcal{H}_{\rm CPW} = P\dot{\mathcal{G}} - \mathcal{L}$, with $P_\ell = \partial\mathcal{L}^{\rm CWR}/\partial\dot{\mathcal{G}}_\ell$ being the canonical conjugate momentum.

$$\mathcal{H}_{\rm CPW} = \sum_\ell \left[\frac{P_\ell^2}{2C_{\Sigma_\ell}} + \frac{C_{\Sigma_\ell}\omega_\ell^2}{2}\mathcal{G}_\ell^2\right]. \tag{4.33}$$

Finally, the quantum Hamiltonian for the resonator is given by

$$\mathcal{H}_{\rm CPW} = \sum_\ell \hbar\omega_\ell\left(a_\ell^\dagger a_\ell + \frac{1}{2}\right), \tag{4.34}$$

Now, we focus on the flux-qubit Lagrangian

$$\begin{aligned}\mathcal{L}_{\rm q} &= \frac{C_J(1+\alpha)}{2}(\dot{\varphi}_1^2 + \dot{\varphi}_2^2) + \alpha C_J\dot{\varphi}_1\dot{\varphi}_2 \\ &+ E_J\left[\cos\left(\frac{\varphi_1}{\phi_0}\right) + \cos\left(\frac{\varphi_2}{\phi_0}\right) + \alpha\cos\left(\frac{\varphi_1+\varphi_2-\phi_{\rm x}}{\phi_0}\right)\right].\end{aligned} \tag{4.35}$$

The realisation of the complete derivation for the flux-qubit Hamiltonian in the Chapter (3.2). With this derivation, we obtain the following Hamiltonian

$$\mathcal{H}_{\rm q} = \frac{\hbar\omega}{2}\sigma^z, \tag{4.36}$$

where, $\sqrt{\Delta^2 + E_0^2}$ is the flux-dependent qubit frequency. Finally, numerical calculations showed that close to the symmetry point $\phi_x = \phi_0/2$ the term $\sin$ on the interacting Hamiltonian can be expressed as a σ^x operator in the effective two-level basis of the flux-qubit. Thus the interacting Hamiltonian reads

$$\mathcal{H}_{\rm int} = \sum_{\ell=0}^{\infty} g_\varphi^\ell \sigma^x (a_\ell^\dagger + a_\ell). \tag{4.37}$$

here, g_φ^ℓ is the galvanic qubit-resonator coupling defined as

$$g_\varphi^\ell = \frac{\alpha E_J \Delta\mathcal{U}_\ell}{2\phi_0}\sqrt{\frac{\hbar}{2C_{\Sigma_\ell}\omega_\ell}}\langle e|\sin\left(\frac{\varphi_1+\varphi_2-\phi_{\rm x}}{\phi_0}\right)|g\rangle \tag{4.38}$$

with $|g\rangle$, and $|e\rangle$ as the ground and first excited state of the flux-qubit, respectively. Thus, in the single mode limit $\ell = 0$, the quantum Rabi Hamiltonian can be written as

$$\mathcal{H} = \sum_{\ell=0}^{\infty}\hbar\omega_\ell\left(a^\dagger a + \frac{1}{2}\right) + \frac{\hbar\omega_{\rm q}}{2}\sigma^z + \sum_{\ell=0}^{\infty}\hbar g_\varphi \sigma^x (a_\ell^\dagger + a_\ell). \tag{4.39}$$

The first experimental realisation of a circuit quantum electrodynamics device operating at the ultrastrong coupling regime (USC) was reported in [Nie+10]. The system is constituted by a λ transmission line resonator made of Niobium, where a part of it was replaced by a narrow aluminium strip interrupted by a large area junction. Moreover, the flux qubit is formed by a superconducting loop embedded with three Josephson junctions, which is threaded by external magnetic flux to tune the qubit frequency. A false scanning electron microscope (SEM) image for the chip is shown in Fig. (4.4)(a). Spectroscopy on the chip permits to obtain the values for the internal system parameters of the system, demonstrating the system operates at the ultrastrong coupling regime. For instances, in this work the system to be considered is the same as the showed in Eq. (4.39) for $\ell = 0, 1, 2$ modes. The experimental value obtained by the spectroscopy are given by $\omega_0 = 2\pi \times 2.782$ GHz, $\omega_1 = 2\pi \times 5.357$ GHz and $\omega_2 = 2\pi \times 7.777$ GHz, $\Omega = 2\pi \times 2.25$ GHz, $g_\varphi^{010} = 2\pi \times 314$ MHz, $g_\varphi^{011} = 2\pi \times 636$ MHz and $g_\varphi^{012} = 2\pi \times 568$ MHz. Hence, the ratio defined as $r_\ell = |g_\varphi^{01\ell}/\omega_\ell|$ are the following: $r_0 = 0.112$, $r_1 = 0.118$ and $r_2 = 0.073$. These ratios

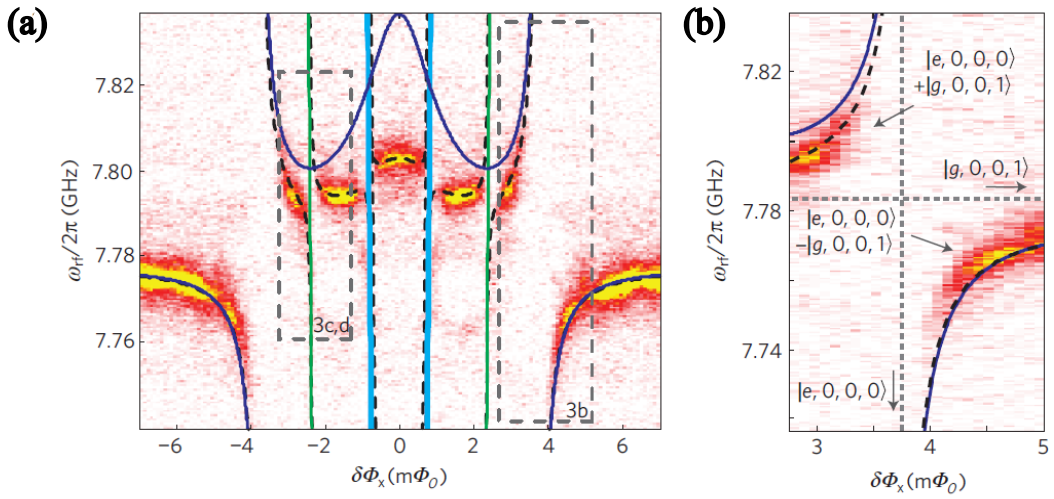

Figure 4.6: **Experimental evidence for breaking of the rotating-wave approximation**. (a) Cavity spectroscopy as function of the external magnetic flux. Black dashed lines stand for the energy spectrum of the Hamiltonian (4.39). Whereas green $|e,1,0,0\rangle$, light blue $|e,0,1,0\rangle$ and dark blue $|e,0,1,0\rangle$ ($|g,2,0,0\rangle$) stand for the energy levels of the Jaynes-Cummings model, respectively. (b) enlarged level crossing produced by the states $|e,1,0,0\rangle$ and $|e,0,1,0\rangle$. These states are generated from the counter rotating terms presents on the quantum Rabi Hamiltonian (4.39). The figure has been extracted from [Nie+10] and slightly modified.

demonstrate that the system is operating on the ultrastrong coupling regime. This experimental realisation consists into the study the energy spectrum of the Hamiltonian in Eq. (4.39) by measuring the power transmission on the resonator as a function of the external magnetic flux as shown in Fig. (4.6). The spectroscopy for this transmission shows that there are lines on the energy spectrum which does not appear on the Jaynes-Cummings model. This contribution corresponds to generation of two excitations on the system, i.e., one excitation on the qubit and other on the resonator or, additionally, two excitations are generated on the resonator. This process appears due to the presence of the counter-rotating terms on the quantum Rabi model, but not on the Jaynes-Cummings Hamiltonian, evidencing that there are unexplored physics beyond the rotating wave approximation.

Chapter 5

Incoherent-mediator for quantum state transfer in the ultrastrong coupling regime

We study quantum state transfer between two qubits coupled to a common quantum bus that is constituted by an ultrastrong coupled light-matter system. By tuning both qubit frequencies on resonance with a forbidden transition in the mediating system, we demonstrate a high-fidelity swap operation even though the quantum bus is thermally populated. We discuss a possible physical implementation in a realistic circuit QED scheme that leads to the generalized Dicke model. This proposal may have applications on hot quantum information processing within the context of ultrastrong coupling regime of light-matter interaction.

5.1 Introduction

The exchange of information between nodes of a quantum network is a necessary condition for large-scale quantum information processing (QIP) and networking. Many physical platforms have been proposed to implement high-fidelity quantum state transfer (QST) such as, coupled cavities [Cir+97; ECZ97; OIK08; Fel+14], spin chains [Chr+04; Chr+05], trapped ions [CZ95; HRB; SWM10], photonic lattices [PL+13], among others. In the majority of cases, a necessary condition to carry out the transfer protocol is accessing to a highly controllable mediator. However, several protocols have been proposed to perform QST even though the mediator system is not

controlled [Bos03; Yao+11], or it is initialized in a thermally populated state [SMFZ99; SM99; SM00; Cas+10b; Sch+17].

Likewise, the state-of-the-art quantum technologies has also proven useful for other quantum information tasks such as quantum computing [Lad+10] and quantum simulations [GAN14]. As important representatives of quantum devices we can mention superconducting circuits [CW08] and circuit quantum electrodynamics (QED) [Bla+04; CW08; Chi+04; SG08]. These technologies have also pushed forward to achieve the ultrastrong coupling (USC) [Bou+09; Nie+10; FD+10; FD+16b; BA17; FD+16a; Bau+16] and deep strong coupling (DSC) [Cas+10a; Yos+16] regimes of light-matter interaction, where the coupling strength becomes comparable to or larger than the frequencies of the cavity mode and two-level system. In this case, the light-matter coupling is well described by the quantum Rabi model (QRM) [Rab36; Bra11] and features a discrete parity symmetry. It has been proven that the above symmetry may be useful for quantum information tasks in the USC regime [NC11; Rom+12; Kya+15b; Kya+15a; Wan+16].

We propose a protocol for performing high-fidelity QST between qubits coupled to a common mediator constituted by a two-qubit quantum Rabi system (QRS) [RLM13; Guo+14], see Figure.5.1. The QST relies on the tuning of qubit frequencies on resonance with a forbidden transition of the QRS, provided by the selection rules imposed by its parity symmetry. We demonstrate that high-fidelity QST occurs even though the QRS is thermally populated and the whole system experiences loss mechanisms. We also discuss a possible physical implementation of our QST protocol for a realistic circuit QED scheme that leads to the generalized Dicke model [RCLV15] as mediating system. This proposal may bring a renewed interest on hot quantum computing [SMFZ99; SM99; SM00] within state-of-art light-matter interaction in the USC regime.

5.2 The model

Our proposal for quantum state transfer is schematically shown in Figure. 5.1. We consider a pair of two-level systems with transition frequencies $\omega_{q,i}$ $(i = 1, 2)$, ultrastrongly coupled to a single cavity mode of frequency $\omega_{\rm cav}$. This situation is described by the two-qubit quantum Rabi model [RLM13; Guo+14]

$$H_{\rm QRS} = \hbar\omega_{\rm cav}a^{\dagger}a + \sum_{i=1}^{N=2}\frac{\hbar\omega_{q,i}}{2}\sigma_i^z + \hbar g_i\sigma_i^x(a^{\dagger}+a). \tag{5.1}$$

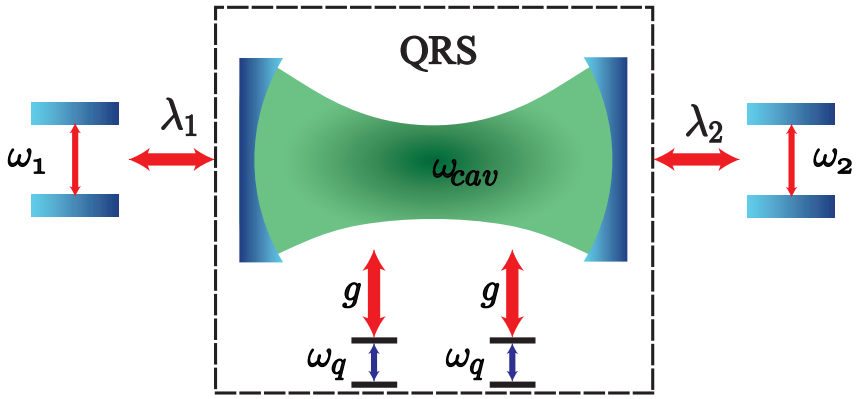

Figure 5.1: **Schematic representation of the model**. Two qubits with frequency gaps ω_1 and ω_2 are coupled to a QRS via dipolar coupling with strengths λ_1 and λ_2, respectively. The QRS is constituted by a pair of two-level systems ultrastrongly coupled to a single cavity mode of frequency $\omega_{\rm cav}$.

Here, $a(a^\dagger)$ is the annihilation (creation) bosonic operator for the cavity mode. The operators σ_i^z and σ_i^x stand for Pauli matrices describing each two-level system. Also, $\omega_{\rm cav}$, $\omega_{q,i}$, and g_i, are the cavity frequency, ith qubit frequency, and ith qubit-cavity coupling strength, respectively. Furthermore, two additional qubits with frequency gaps ω_n $(n = 1, 2)$, are strongly coupled to the QRS through the cavity mode with coupling strengths λ_n. The Hamiltonian for the whole system depicted in Figure. 5.1 reads

$$\mathcal{H} = \mathcal{H}_{\rm QRS} + \sum_{j=1}^{N=2} \frac{\hbar\omega_j}{2}\tau_j^z + \hbar\lambda_j\tau_j^x(a^\dagger + a), \tag{5.2}$$

where $\tau_j^{x,z}$ are Pauli matrices associated with the additional qubits. In what follows, we will discuss about the parity symmetry of the two-qubit quantum Rabi model (5.1), and their corresponding selection rules.

5.3 Selection rules in the two-qubit quantum Rabi model.

An important result in quantum physics are the selection rules imposed by the electric and magnetic dipole transitions. Similarly, the parity symmetry ($\mathbb{Z}_2$) of the Hamiltonian (5.1) imposes selection rules for state transitions. The $\mathbb{Z}_2$ symmetry can be seen if we replace $\sigma_i^x \to -\sigma_i^x$ and $(a^\dagger + a) \to -(a^\dagger + a)$ in the Hamiltonian (5.1) such that it remains unchanged. In other words, this symmetry implies the existence of a parity operator $\mathcal{P}$ that commutes with the Hamiltonian, $[H_{\rm QRS}, \mathcal{P}] = 0$. In this way both operators can be simultaneously diagonalized in a basis

$\{|\sigma, p\rangle\}_{\sigma=0}^{\infty}$. In particular, for the two-qubit quantum Rabi model Eq. (5.1), the parity operator reads $\mathcal{P} = \sigma_1^z \otimes \sigma_2^z \otimes e^{i\pi a^\dagger a}$, such that $\mathcal{P}|\sigma, p\rangle = p|\sigma, p\rangle$, with $p = \pm 1$, and $\mathcal{H}_{\rm QRS}|\sigma, p\rangle = \hbar\nu_\sigma|\sigma, p\rangle$, where ν_σ is the σth eigenfrequency.

The selection rules associated with the parity symmetry appear when considering a cavity-like driving, proportional to $a^\dagger + a$, or qubit-like driving $\propto \sigma^x$ or σ^z [FD+16a; Wan+16]. We are interested in the former case since each qubit in Figure. 5.1 couples to the QRS via the field quadrature $X = a^\dagger + a$. It is noteworthy that for the single-qubit quantum Rabi model [Bra11], it is possible to demonstrate that matrix elements $q_{\sigma,\sigma'} = \langle\sigma, p|(a^\dagger + a)|\sigma', p'\rangle$ are different from zero when $p \neq p'$, whereas $q_{\sigma,\sigma'} = 0$ when $p = p'$ [Fel+15]. In addition, for the two-qubit quantum Rabi model we need to take into account additional features. In this case, if one considers identical qubits and coupling strengths in the Hamiltonian (5.1), the spectrum features an invariant subspace formed by tensor products of pseudo spin and Fock states $\{|\downarrow,\uparrow, N\rangle, |\uparrow,\downarrow, N\rangle\}$, whose eigenstates are.

$$|\phi_N\rangle = \frac{1}{\sqrt{2}}\big(|\downarrow\uparrow\rangle - |\uparrow\downarrow\rangle\big)|N\rangle. \tag{5.3}$$

This is a dark state (DS) where the spin singlet is decoupled from the cavity mode [MCCM14; Hao+15; Sol+17]. Figure 5.2(a) shows the energy spectrum of the Hamiltonian (5.1) for identical qubits ($\omega_{q,1} = \omega_{q,2}$) as a function of the coupling strength $g_1 = g_2 = g$. Blue (dot-dashed) lines stand for states with parity $p = +1$, while red (continuous) for states with parity $p = -1$. The dark states (5.3) appear with constant energies whose gaps correspond to the cavity mode frequency. The selection rules in the two-qubit quantum Rabi system need to take into account the emergence of dark states. In this case, each DS has definite parity as shown in Figure. 5.2(a); however, the matrix elements between a DS and remaining states are null, $X_{\phi_N k} = \langle\phi_N|(a^\dagger + a)|\sigma, p\rangle = 0$, since states $|\sigma, p\rangle$ can be written as linear superpositions of products of symmetric states for the pseudo spins and Fock states, that is, $|\sigma, p\rangle = \sum_{N=0}^{\infty}\sqrt{N!}\{a_N(|\uparrow\uparrow\rangle \pm (-1)^N|\downarrow\downarrow\rangle) + b_N(|\uparrow\downarrow\rangle \pm (-1)^N|\downarrow\uparrow\rangle)\}|N\rangle$, where $\pm$ stands for parity $p = \pm 1$ [DHC15; Wan+14]. In the light of the above forbidden transitions, we will show that they become a key feature for our quantum state transfer protocol.

5.4 Parity assisted excitation transfer

We study the QST between two qubits that are coupled to a common QRS system [cf. Figure. 5.1]. We focus on the situation where frequencies of the leftmost and rightmost qubits are resonant with

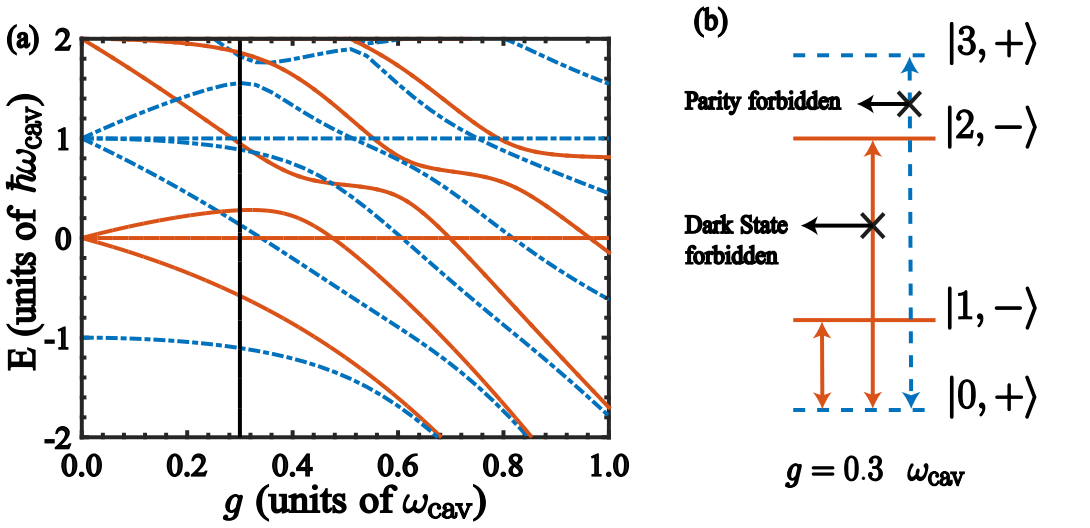

Figure 5.2: **Energy Spectrum of the two-qubit quantum Rabi system**. (a) Energy spectrum of the Hamiltonian (5.1) with parameters $\omega_{q,1} = \omega_{q,2} = \omega_{\rm cav}$, as a function of the coupling strength g. Blue (dot-dashed) lines stand for states with parity $p = +1$. Red (continuous) lines stand for states with parity $p = -1$. The straigth lines in the spectrum stand for dark states $|\phi_N\rangle$. (b) Schematics of the level structure at $g = 0.3\ \omega_{\rm cav}$ corresponding to the vertical solid line in (a). It is shown the allowed and forbidden transitions ruled by the parity symmetry of the two-qubit quantum Rabi model.

a forbidden transition of the QRS. For instance, if we consider the case $g = 0.3\ \omega_{\rm cav}$ as denoted by the vertical solid line in Figure. 5.2(a), we choose $\omega_1 = \omega_2 = \nu_3 - \nu_0$. It is clear that the matrix element $X_{03} = \langle 0,+|a+a^\dagger|3,+\rangle = 0$ because states $|0,+\rangle$ and $|3,+\rangle$ have parity $p = +1$. Also, the matrix element $X_{02} = 0$ since $|2,-\rangle = |\phi_0\rangle$ is a dark state. The allowed and forbidden transitions for the lowest energies of the Hamiltonian (5.1), for $g/\omega_{\rm cav} = 0.3$, are schematically shown in Figure. 5.2(b).

In view of the above conditions, and considering the QRS initialized in its ground state, we realize that the only transmission channel that would participate in a QST protocol between qubits corresponds to the first excited state of the QRS, since the matrix element $X_{01} \neq 0$, as $|0,+\rangle$ and $|1,-\rangle$ have opposite parity. However, both qubits are far-off-resonance with respect to this allowed transition. In this case, one can demonstrate that the QST occurs in a second-order process, as qubits interact dispersively with the QRS resulting in an effective qubit-qubit interaction. The latter can be seen in the spectrum of the Hamiltonian (5.2), as depicted in Figure. 5.3(a). Specifically, around the region $E/\hbar\omega_{\rm cav} \approx 1.2386$ appears an avoided level crossing, enlarged in Figure. 5.3(b), where states $|0,+\rangle|\uparrow\downarrow\rangle$ and $|0,+\rangle|\downarrow\uparrow\rangle$ hybridize to form maximally entangled states well approximated by $|0,+\rangle(|\uparrow\downarrow\rangle + |\downarrow\uparrow\rangle)/\sqrt{2}$ and $|0,+\rangle(|\uparrow\downarrow\rangle - |\downarrow\uparrow\rangle)/\sqrt{2}$. This hybridization resembles the two-body interaction mediated by a single-qubit quantum Rabi model [Kya+17]. The effective qubit-

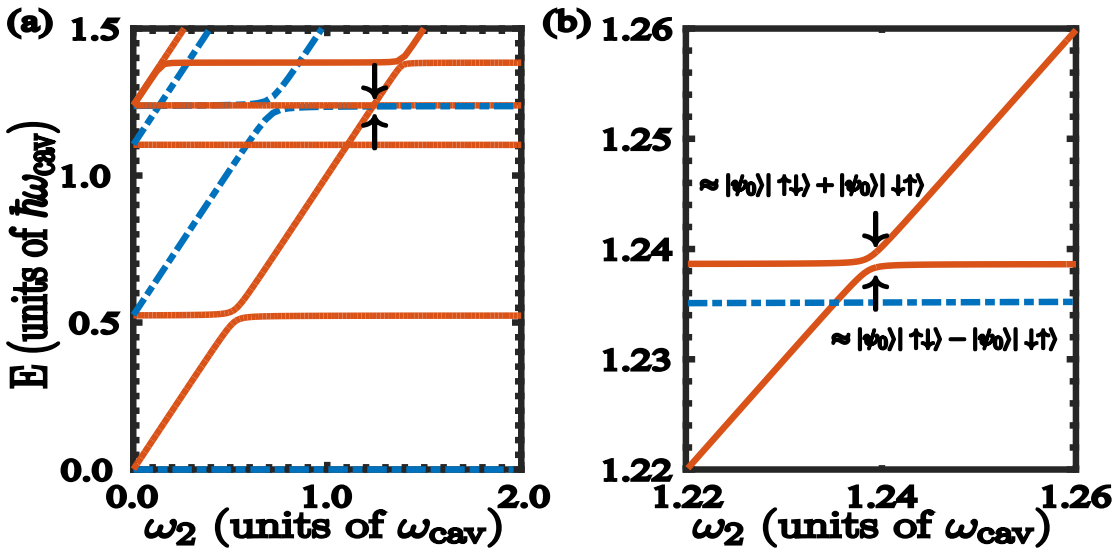

Figure 5.3: **Spectrum of the complete model**. (a) Energy differences from the spectrum of Hamiltonian (5.2), as a function of the rightmost qubit frequency ω_2. Blue (dot-dashed) lines stand for states with parity $p = +1$, while red (continuous) lines stand for states with parity $p = -1$. At frequency $\omega_2 = \omega_1$ an avoided energy crossing appears. (b) Enlarged view of the energy spectrum shown in (a) around the region $\omega_2 = \omega_1 = \nu_3 - \nu_0$. The numerical calculation was performed with the same parameters used in Figure. 5.2.

qubit interaction can be obtained from the total Hamiltonian (5.2) via a dispersive treatment beyond rotating-wave approximation [Kya+17; Zue+09]. In this case, the effective qubit-qubit interaction reads

$$\mathcal{H}_{\text{eff}} = \mathcal{H}_0 + \frac{\hbar}{2}|\chi_{10}|^2 \mathbf{Z}_p \otimes \mathbf{S}_{12}, \tag{5.4}$$

where

$$|\chi_{10}|^2 = |\langle 0,+|(a^\dagger + a)|1,-\rangle|^2 \tag{5.5}$$

$$\mathbf{Z}_p = |1,-\rangle\langle 1,-| - |0,+\rangle\langle 0,+| \tag{5.6}$$

$$\mathbf{S}_{12} = \lambda_1\lambda_2\left(\frac{1}{\mu_{10}^1} + \frac{1}{\mu_{10}^2} - \frac{1}{\Delta_{10}^1} - \frac{1}{\Delta_{10}^2}\right)\tau_1^x\tau_2^x + 2\sum_{j=1}^{2}\lambda_j^2\left(\frac{\tau_j^+\tau_j^-}{\Delta_{10}^j} - \frac{\tau_j^-\tau_j^+}{\mu_{10}^j}\right), \tag{5.7}$$

and $\tau_n^\pm = (\tau_j^x \pm i\tau_j^y)/2$. The detunings are defined as $\Delta_{10}^j = \omega_j - \nu_{10}$ and $\mu_{10}^j = \omega_j + \nu_{10}$, where ω_j corresponds to the jth qubit frequency that interacts with the QRS, see Figure. 5.1, and ν_{10} stands for the frequency difference between the two lowest energy states of the QRS. Figure 5.4(a) shows the population inversion between states $|0,+\rangle|\uparrow\downarrow\rangle$ and $|0,+\rangle|\downarrow\uparrow\rangle$ calculated from the full Hamiltonian (5.2), and from the dispersive Hamiltonian (5.4), see Figure. 5.4(b). In

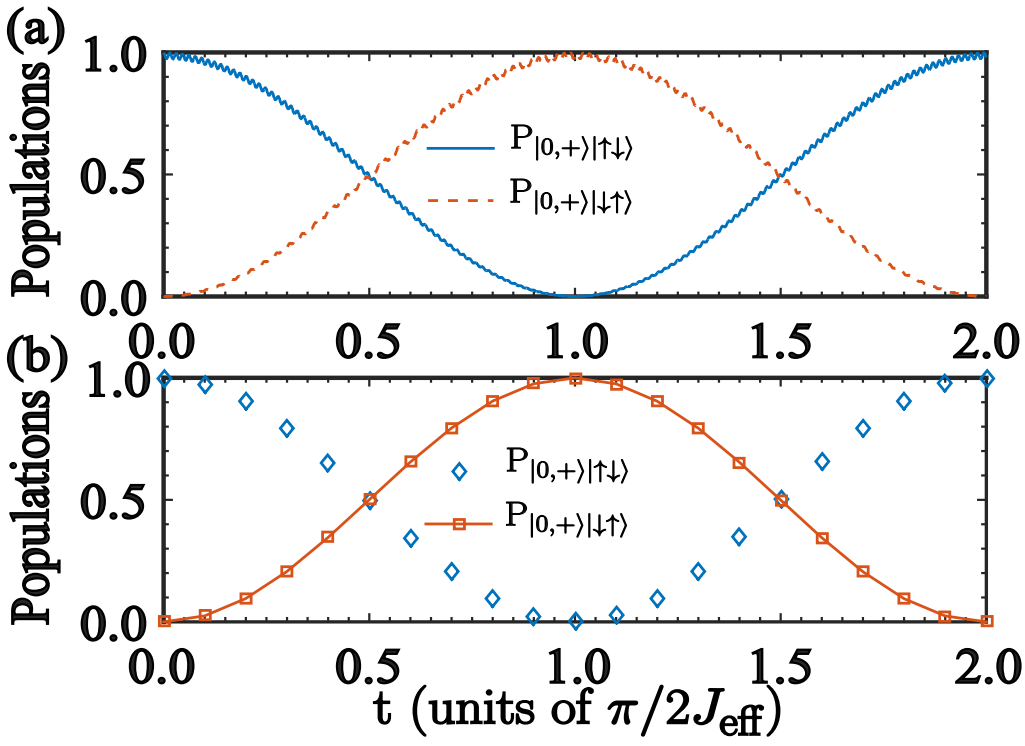

Figure 5.4: **Population evolution**. (a) Population inversion of the states $|\psi_0\rangle|\uparrow\downarrow\rangle$ and $|\psi_0\rangle|\downarrow\uparrow\rangle$, numerically calculated from the *ab initio* model (5.2). (b) Population inversion calculated from the effective Hamiltonian (5.4). These numerical calculations have been performed with parameters, $\omega_{q,i} = \omega_{\text{cav}}$, $g = 0.3\ \omega_{\text{cav}}$, $\omega_1 = \omega_2 = \nu_3 - \nu_0$ and $\lambda_1 = \lambda_2 = 0.02\ \omega_{\text{cav}}$.

both cases, the qubit-qubit exchange occurs within a time scale proportional to the inverse of the effective coupling constant $J_{\text{eff}} = |\chi_{10}|^2\lambda_1\lambda_2(1/\mu_{10}^1 + 1/\mu_{10}^2 - 1/\Delta_{10}^1 - 1/\Delta_{10}^2)$. For parameters, $\omega_{q,i} = \omega_{\text{cav}}$, $g = 0.3\ \omega_{\text{cav}}$, $\omega_1 = \omega_2 = \nu_3 - \nu_0$ and $\lambda_1 = \lambda_2 = 0.02\ \omega_{\text{cav}}$, we obtain $|\chi_{10}| = 1.0325$, $\mu_{10}^1 = \mu_{10}^2 = 1.7632\ \omega_{\text{cav}}$ and $\Delta_{10}^1 = \Delta_{10}^2 = 0.7141\ \omega_{\text{cav}}$. These values lead to an effective coupling strength $2J_{\text{eff}} \approx 0.0011\ \omega_{\text{cav}}$. In addition, if we consider typical values for microwave cavities such as $\omega_{\text{cav}} = 2\pi \times 8.13$ GHz [FD+16a], the excitation transfer happens within a time scale of about $t = \pi/2J_{\text{eff}} \approx 56$ [ns].

Additionally, we also study quantum correlations in our system. Figure 5.5 shows the Entanglement of Formation (EoF) for the subsystem composed by the leftmost and rightmost qubits, and the von Neumann entropy, $S(\rho)$, for the reduced density matrix of the QRS. $S(\rho)$ shows a negligible correlation between the bipartition composed by QRS and the additional qubits. This behavior can be predicted from the effective Hamiltonian (5.4), which shows an effective qubit-qubit interaction while it is diagonal in the QRS basis. Therefore, the QRS will not evolve and the quantum

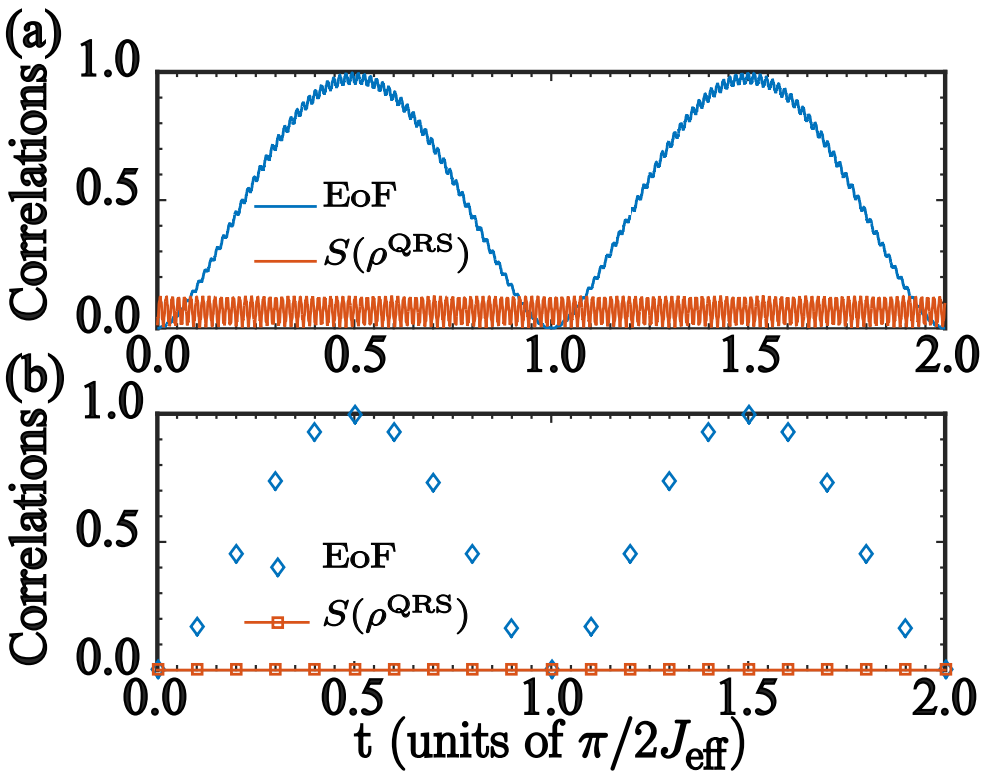

Figure 5.5: **Correlation evolution**. (a) Entanglement dynamics for the reduced system composed by the leftmost and rightmost qubits, and the von Neumann entropy $S(\rho^{\mathrm{QRS}})$ for the reduced QRS system, numerically calculated from the *ab initio* model (5.2). (b) Entanglement of formation and von Neumann entropy numerically calculated from the effective Hamiltonian (5.4). We have used the parameters from Figure. 5.4.

correlations between it and additional qubits is negligible. At the same time, the EoF between the leftmost and rightmost qubits has an oscillating behavior whose minimum value is reached when the excitation transfer has been completed.

5.5 Incoherent mediator for quantum state transfer

Notably, the above described mechanism allows us for quantum state transfer between qubits even though the QRS is initially prepared in a thermal state at finite temperature. Let us describe how our system governed by Eq. (5.2) is initialized in a thermally populated state. Since the frequencies of the additional qubits are larger than the lowest energy transition of the QRS, we should expect that thermal population associated with both qubits are concentrated only in their ground states. In order to ascertain the latter, we compute the fidelity $\mathcal{F}$ between the Gibbs state obtained from the

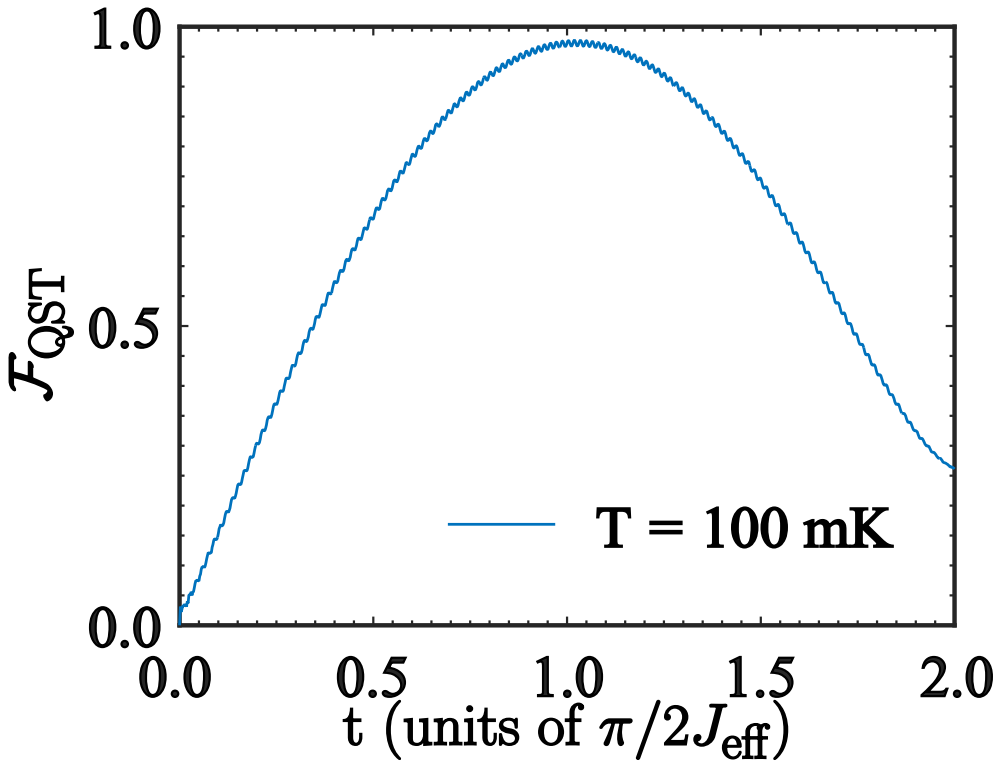

Figure 5.6: **Fidelity of the QST process**. Time-evolution of the QST fidelity $\mathcal{F}_{\rm QST}$ between the states $|\chi\rangle = \cos\theta|\uparrow\rangle + \sin\theta e^{i\phi}|\downarrow\rangle$ and $\rho_{Q_2}(t)$, averaged over the Bloch sphere. We have considered the QRS initialized in a thermal state at $T = 100$mK.

Hamiltonian (5.2), $\rho_{\rm Gibbs} = e^{(-H/k_BT)}/Z$, where $Z = \sum_m \exp(-\hbar\epsilon_m/k_BT)$ is the partition function, and the probe state defined by $\rho_{\rm p} = \rho_{\rm th}^{\rm QRS} \otimes |\downarrow\downarrow\rangle\langle\downarrow\downarrow|$, where $\rho_{\rm th}^{\rm QRS}$ is the Gibbs state for the QRS. Notice that $\hbar\epsilon_j$ corresponds to the jth eigenvalue of the Hamiltonian (5.2), $H|m\rangle = \hbar\epsilon_m|m\rangle$. Taking parameters from Figure. 5.4 and $T = 100$ mK, we obtain the fidelity $\mathcal{F} = {\rm tr}(\rho_{\rm Gibbs}\rho_{\rm p}) = 0.9951$. Therefore, the Gibbs state is a tensor product between the additional qubits in their ground states and the QRS in an thermal state. For the purpose of QST of an arbitrary qubit state, we need to excite either the leftmost or rightmost qubit, see Figure. 5.1. This can be done by applying an external driving on the leftmost (rightmost) qubit $H_d(t) = \hbar\Omega\cos(\nu t + \phi)\tau_1^x(\tau_2^x)$ resonant with the qubit frequency gap ω_1 (ω_2) and far off-resonance with both the QRS and rightmost (leftmost) qubit. For example, one can initialize the whole system in the state

$$\rho_{\rm QST} = \rho_{\rm th}^{\rm QRS} \otimes |\chi\rangle\langle\chi| \otimes |\downarrow\rangle\langle\downarrow|, \tag{5.8}$$

where $|\chi\rangle = \cos\theta|\uparrow\rangle + \sin\theta e^{i\phi}|\downarrow\rangle$. We study the QST under dissipative mechanisms in a way that is consistent with a circuit QED implementation based on a flux qubit coupled to an on-chip microwave cavity in the USC regime [Nie+10], and including the effect of a finite temperature. The treatment that we use has also been applied to a recent implementation of the QRM at finite temperature [FD+16a]. Moreover, the leftmost and rightmost qubits could be implemented by means of transmon qubits [Koc+07; Sai+14] coupled to the edges of the microwave cavity. The dissipative dynamics is governed by the microscopic master equation in the Lindblad form [BGB11]

$$\frac{d\rho(t)}{dt} = \frac{i}{\hbar}[\rho,\mathcal{H}] + \sum_{\sigma,\sigma'>\sigma}(\Gamma_X^{\sigma,\sigma'} + \Gamma_\gamma^{\sigma,\sigma'})\mathcal{D}[|\sigma,p\rangle\langle\sigma',p'|]\rho + \sum_{j=1}^{N=2}\gamma_j\mathcal{D}[\tau_j^x]\rho + \sum_{j=1}^{N=2}\gamma_{\phi_j}\mathcal{D}[\tau_j^z]\rho, \tag{5.9}$$

where the Hamiltonian $\mathcal{H}$ is given by Eq. (5.2), and $\mathcal{D}[O]\rho = 1/2(2O\rho O^\dagger - \rho O^\dagger O - O^\dagger O\rho)$. Here, γ_j corresponds to the relaxation rate for the external qubit and γ_{ϕ_j} stands for the qubit pure dephasing rate. Also, $\Gamma_X^{\sigma,\sigma'}$ is the dressed photon leakage rate for the resonator, $\Gamma_\gamma^{\sigma,\sigma'}$ corresponds to the dressed qubit relaxation rate for the qubit-cavity system, both dressed rates are defined as follows

$$\Gamma_X^{\sigma,\sigma'} = \frac{\kappa}{\omega_{\rm cav}}\nu_{\sigma,\sigma'}|X_{\sigma,\sigma'}|^2 \quad \Gamma_\gamma^{jk} = \frac{\gamma}{\omega_{q,i}}\nu_{\sigma,\sigma'}|\sigma^x_{\sigma,\sigma'}|^2, \tag{5.10}$$

where κ and γ are the bare decay rates for the cavity mode and the two-level systems that belong to the QRS, $\nu_{\sigma,\sigma'} = \nu_\sigma - \nu'_\sigma$, and $|X_{\sigma,\sigma'}|^2 = |\langle\sigma,p|(a+a^\dagger)|\sigma',p'\rangle|^2$, $|\sigma^x_{jk}|^2 = |\langle\sigma,p|\sigma^x_i|\sigma',p'\rangle|^2$. The QST fidelity $\mathcal{F}_{\rm QST} = \langle\chi|\rho_{Q_2}(t)|\chi\rangle$, where $\rho_{Q_2}(t)$ is the density matrix of the rightmost qubit, is numerically calculated from Eq. (5.9) for 4000 input states $|\chi\rangle$, uniformly distributed over the Bloch sphere. Figure 5.6 shows the evolution of $\mathcal{F}_{\rm QST}$ as a function of time and for a system temperature of $T = 100$ mK. As the QST time is shorter than any decay rate in the system, the dissipation should not affect the performance of QST. We see that the main detrimental effect on QST is produced by the distribution of the thermally populated states in the mediator. The numerical calculations have been performed for the QRS parameters given in Ref. [FD+16a], that is, $\kappa/2\pi = 0.10$ MHz, $\gamma/2\pi = 15$ MHz, and for the leftmost and rightmost qubits we choose $\gamma_j/2\pi = 0.48$ MHz, $\gamma_{\phi_j}/2\pi = 0.15$ MHz given in Ref. [Sai+14]. At temperature $T = 100$ mK we obtain maximum fidelity of about $\mathcal{F}_{\rm QST} = 0.9785$. It is worth mentioning that the validity of our QST protocol relies on the range of temperatures in which the system can be initialized as a product state $\rho_{\rm p}$.

5.6 Conclusion

We have shown that a system composed by two qubits connected to an incoherent QRS mediator, allows us to carry out high fidelity QST of single-qubit states even though the mediator system is in a thermally populated state. The QST mechanism involves the tuning of qubit frequencies resonant to a parity forbidden transition in the QRS such that an effective qubit-qubit interaction appears. Numerical simulations with realistic circuit QED parameters show that QST is successful for a broad range of temperatures. We have also discussed a possible physical implementation of our QST protocol for a realistic circuit QED scheme that leads to the generalized Dicke model. Our proposal may be of interest for hot quantum information processing within the context of ultrastrong coupling regime of light-matter interaction.

Chapter 6

Parity-assisted generation of nonclassical states of light in superconducting circuits

We propose a method to generate non-classical states of light in multi-mode microwave cavities. Our approach considers two-photon processes that take place in a system composed of two extended cavities and an ultrastrongly coupled light-matter system. Under specific resonance conditions, our method generates, in a deterministic manner, product states of uncorrelated photon pairs, Bell states, and W states. We demonstrate improved generation times when increasing the number of multi-mode cavities, and prove the generation of genuine multipartite-entangled states when coupling an ancillary system to each cavity. Finally, we discuss the feasibility of our proposal in superconducting circuits.

6.1 Introduction.

The state-of-the-art of devices exhibiting quantum behaviour has grown extensively in the last two decades. Remarkable platforms such as superconducting circuits [SG08; YN11; HTK12; DS13] and circuit quantum electrodynamics (QED) [SG08; YN11; HTK12; DS13; Lan13; Sch07; Bis10; Bla+04] have allowed the implementation of microwave quantum photonics [Nak12; HJ+16; Gu+17], where superconducting electrical circuits mimic the behavior of atoms and cavities [Orl+99; Mar+02; DWM04; Koc+07; Göp+08]. Here, the capability of tailoring internal circuit parameters to

obtain devices with long coherence times and switchable coupling strengths have allowed reproducing quantum optics experiments such as electromagnetically induced transparency [Abd+10], and photon blockade [Lan+11; Hof+11; Eic+14], to name but a few. A distinctive aspect of microwave photonics are the inherent nonlinearities coming from Josephson junction devices that makes possible to build photonic crystals with Kerr and Cross-Kerr nonlinearities much larger than the one observed in optical devices [Ber+10; BGB10; Eic+11; Bou+12; Har+12], thus enhancing processes such as parametric down conversion [Mar07; Kos09; Liu+14; SB+16], and the generation of non-classical states of light [Yur+89; Eve+04; Zag+08; Yur+88; MG05; DQB14]. Likewise, the notable features of superconducting circuits have also triggered a bunch of proposals for microwave photon generation in systems composed of a large number of cavities. In this context, it is possible to find proposals for the generation of entangled photon states such as NOON and MOON [Str12; Zha+16; WK10; SJS10; Wan+11; SYZ14; Xio+15] states, studies of correlated photons emitted from a cascade system [Gas+17], the implementation of a CNOT gate between qubits encoded in a cavity [CI+18], among other applications [Ros+18; Nar+16; Kur+18].

On the other hand, circuit QED has also made possible to achieve light-mater coupling strengths such as the ultrastrong (USC) [Bou+09; Nie+10; FD+10; FD+16b; BA17; FD+16a; Bau+16] and deep-strong coupling regime (DSC) regimes [Cas+10a; Yos+16]. In both cases, as the coupling strength between the light and matter becomes comparable (USC) or larger than the frequency of the field mode (DSC), the rotating wave approximation breaks down and the simplest model that describes the physical situation is the quantum Rabi model (QRS) [Rab36; Bra11]. This model exhibits a discrete parity symmetry and an anharmonic energy spectrum that provide a set of resources for quantum information tasks and quantum simulations [NC11; Rom+12; Kya+15b; Fel+15; Kya+15a; Wan+16; AA+18].

Based on the latest developments in superconducting circuits, here we propose a method to generate non-classical states of light in multi-mode microwave cavities. Our approach considers two-photon processes that take place in a system composed of two extended cavities and an ultrastrongly coupled light-matter system hereafter called quantum Rabi system (QRS). Under specific resonance conditions, our method allows a deterministic generation of product states of uncorrelated photon pairs, Bell states, and W states of photons with different frequencies. We demonstrate improved generation times when increasing the number of multi-mode cavities, and show the generation of genuine multipartite-entangled states when coupling an ancillary system to each cavity.

This paper is organized as follows: In the section 6.2 we introduce our physical scheme. In

section 6.3, we discuss about the main aspects of the physics of QRS, that is, its parity symmetry and the underlying selection rules for states transitions. In section 6.4, we discuss on the two-photon processes presented in our physical system, and the generation of non-classical states of light. In section 6.5, we show that our model allow generating copies density matrices. In section 6.6, we study swapping processes for the generation of genuine multipartite entanglement. Finally, in sec. 6.7, we present our concluding remarks.

6.2 The Model

Let us consider a two-level system of frequency ω_q interacting with a quantized electromagnetic field mode of frequency $\omega_{\rm cav}$ in the USC regime. This system is described by the quantum Rabi Hamiltonian [Rab36; Bra11] ($\hbar = 1$)

$$\mathcal{H}_{\rm QRS} = \omega_{\rm cav} a^\dagger a + \frac{\omega_q}{2}\sigma^z + g\sigma^x(a^\dagger + a). \tag{6.1}$$

Here, $a^\dagger(a)$ is the creation (annihilation) boson operator for the field mode, the operators σ^x and σ^z are the Pauli matrices describing the two-level system, and g is the light-matter coupling strength. In addition, N multi-mode resonators [EW13; Sun+15], each supporting $M = 2$ modes of frequencies ω_1^ℓ and ω_2^ℓ, are coupled to the edges of the QRS through field quadratures. Notice that each mode couples to the QRS with coupling strengths J_1^ℓ and J_2^ℓ, respectively, see Fig.6.1. This physical situation will be described by the Hamiltonian

$$\mathcal{H} = \mathcal{H}_{\rm QRS} + \mathcal{H}_{\rm c} + \mathcal{H}_I, \tag{6.2}$$

$$\mathcal{H}_{\rm c} = \sum_{\ell=1}^{N} (\omega_1^\ell b_\ell^\dagger b_\ell + \omega_2^\ell c_\ell^\dagger c_\ell), \tag{6.3}$$

$$\mathcal{H}_I = \sum_{\ell=1}^{N} \left[J_1^\ell (b_\ell^\dagger + b_\ell) + J_2^\ell (c_\ell^\dagger + c_\ell)\right](a + a^\dagger), \tag{6.4}$$

where $b_\ell^\dagger(b_\ell)$ and $c_\ell^\dagger(c_\ell)$ are the creation (annihilation) boson operators for the first and second field mode of the ℓth cavity, respectively. Notice that the coupling strength between resonators $J_{1,2}^\ell$ can be several order of magnitude smaller than $\omega_{1,2}^\ell$ [Und+12]. Hence, the counter-rotating terms present in Eq. (B.3) can be neglected through the rotating wave approximation (RWA) leading to

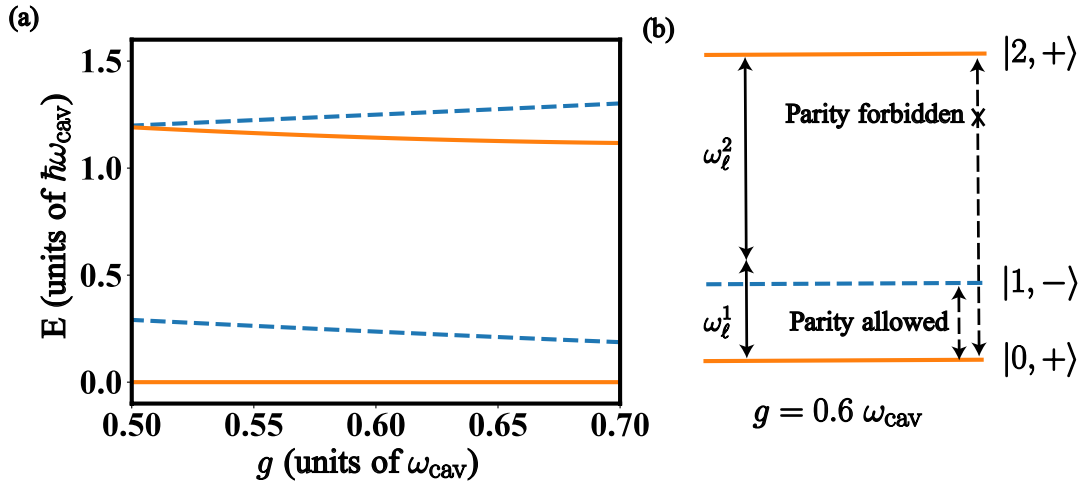

Figure 6.1: **QRS energy spectrum**. (a) Energy spectrum of the Hamiltonian in Eq. (6.1) as a function of the coupling strength g. Blue dashed lines stand for states with parity $p = +1$. Orange continuous lines correspond to states with parity $p = -1$. (b) Diagram of the energy levels at $g = 0.6\ \omega_{\rm cav}$. In these numerical calculations we use $\omega_q = 0.8\ \omega_{\rm cav}$.

the following interaction Hamiltonian

$$\mathcal{H}_I = \sum_{\ell=1}^{N} \left[(J_1^\ell b_\ell + J_2^\ell c_\ell) a^\dagger + (J_1^\ell b_\ell^\dagger + J_2^\ell c_\ell^\dagger) a \right]. \tag{6.5}$$

In what follows, we will discuss the features of the energy spectrum of the QRS, that is, its anharmonicity and the internal symmetry arising in the USC regime.

6.3 Parity symmetry $\mathbb{Z}_2$ and selection rules

The energy spectrum of the QRS presents interesting features which have proven useful in performing quantum information processing [NC11; Rom+12; Kya+15b; Fel+15; Kya+15a; Wan+16]. These features correspond to the anharmonicity of the energy levels and the selection rules imposed by the $\mathbb{Z}_2$ symmetry arising in the USC regime. In Fig. 6.1 we show the first four energy levels of the QRS as a function of $g/\omega_{\rm cav}$, where we see an anharmonic energy spectrum. Moreover, in the QRS it is possible to define the parity operator $\mathcal{P} = -\sigma^z \otimes e^{i\pi a^\dagger a}$ which has discrete spectrum $p = \pm 1$. Notice that $\mathcal{P}$ commutes with the QRS Hamiltonian, $[H_{\rm QRS}, \mathcal{P}] = 0$, thus enabling the diagonalization of both operators in a common basis $\{|\sigma, p\rangle\}_{\sigma=0}^{\infty}$. We label each quantum state regarding two quantum numbers, σ corresponds to the energy level while p denotes its parity value. In Fig. 6.1 states with parity $+1(-1)$ are denoted by the continuous orange (dashed blue) line. As

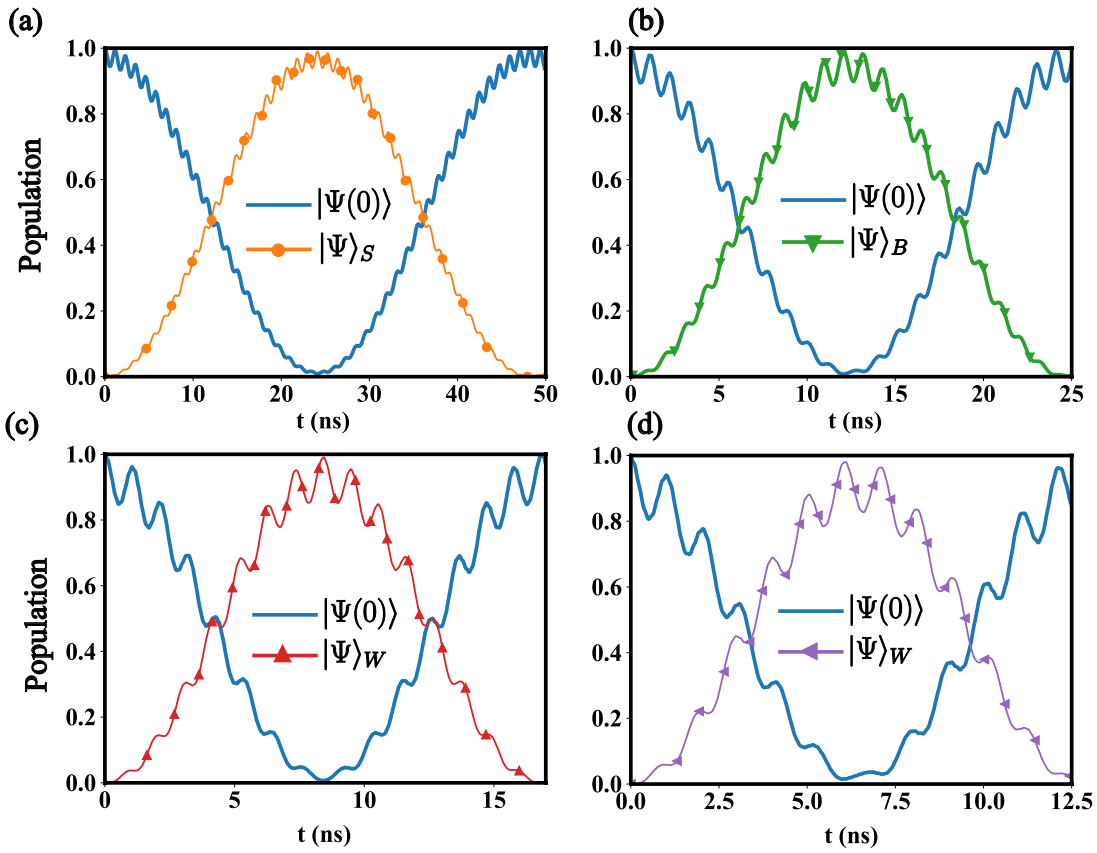

Figure 6.2: **Population evolution**. Population evolution for the *ab initio* model Eq. (6.2) for the initial state $|\Psi(0)\rangle = |2,+\rangle \bigotimes_{\ell,n}^{N,M} |0_\ell^n\rangle$ for the cases $N = 1$ (a), $N = 2$ (b), $N = 3$ (c), and $N = 4$ (d) multi-mode cavities. Blue continuos line is the evolution of the initial state $|\Psi(0)\rangle$. (a) Orange dotted line stands the population of $|\Psi\rangle_S = |0,+\rangle \otimes |1_{\omega_1}\rangle \otimes |1_{\omega_2}\rangle$. (b) Green dotted line stands for the population of $|\Psi\rangle_B = |0,+\rangle \otimes |\Psi^+_{\omega_1}\rangle \otimes |\Psi^+_{\omega_2}\rangle$, and (c) red dotted line stands for $|\Psi\rangle_W = |0,+\rangle \otimes |W_{\omega_1}\rangle \otimes |W_{\omega_2}\rangle$. The parameters for these numerical calculations are described in the main text.

a consequence, the Hilbert space of the QRS is divided into two parts, the even and the odd parity subspaces. This allows, depending on the kind of driving, the possibility of connecting states with different or equal parity. For instance, it has been proven that drivings like $\mathcal{H}_D \sim (a^\dagger + a)$ and $\mathcal{H}_D \sim \sigma^x$ connect states belonging to different subspaces [Wan+16], this happens because the matrix element $\langle \sigma, \pm | \mathcal{H}_D | \sigma', \mp \rangle \neq 0$. Moreover, for a driving like $\mathcal{H}_D \sim \sigma^z$, only states with equal parity can be connected since the matrix element $\langle \sigma, \pm | \mathcal{H}_D | \sigma', \pm \rangle \neq 0$.

6.4 Two photon process mediated by the quantum Rabi model

Here we propose the implementation of a two-photon process mediated by the QRS, which relies on its anharmonicity and the selection rules previously discussed. In particular, we provide specific resonance conditions between multi-modes cavities and the QRS to achieve the phase matching condition analogue to the usual parametric down-conversion process in optical systems.

Let us consider the following set of parameters for the QRS $\omega_q = 0.8\ \omega_{\rm cav}$ and $g = 0.6\ \omega_{\rm cav}$. In this case, as shown in Fig 6.1, the first three energy levels form a cascade Ξ system similar to Rydberg atoms studied in cavity quantum electrodynamics [BRH87]. The ground and the second excited state have parity $p = +1$, while the first excited state has parity $p = -1$ (see Fig 6.1(b)). According to with the type of interaction between the multi-mode cavities with the QRS (c.f. Eq. (B.3)), a single photon will not be able to produce a transition between the second excited state $|2,+\rangle$ with the ground state $|0,+\rangle$ since it is forbidden by parity. However, these states can be connected through a second-order process. The latter may occur when the sum of frequencies of the modes belonging to a cavity matches that of the energy transition between the ground and the second excited state of the QRS, i.e. $\omega_1^\ell + \omega_2^\ell = \nu_{20}$. Moreover, the frequency of each mode must be far-off-resonance with respect to the frequency of the first excited state $\omega_{1,2}^\ell \gg \nu_{10}$. Under these conditions, the intermediate level can be adiabatically eliminated leading to the effective Hamiltonian

$$\mathcal{H}_{\rm eff}^\ell = \mathcal{H}_{\rm QRS} + \mathcal{H}_{\rm c} + \sum_{\ell,\ell'=1}^{N} \mathcal{J}_\ell^{\ell'} (b_\ell^\dagger c_{\ell'}^\dagger \mathcal{S}^- + b_\ell c_{\ell'} \mathcal{S}^+), \tag{6.6}$$

which describes simultaneous two-photon processes in both cavities. Here, $S^+ = |2,+\rangle\langle 0,+|$ corresponds to the ladder operator of the QRS in the effective two-level basis. Furthermore, the effective coupling strength $\mathcal{J}_\ell^{\ell'}$ is defined as follows

$$\mathcal{J}_\ell^{\ell'} = J_1^\ell J_2^{\ell'} \chi_{01}\chi_{21}\left[\frac{1}{\Delta_{10}^2} + \frac{1}{\Delta_{21}^2}\right]. \tag{6.7}$$

Here, we define the matrix element of the operator a in the QRS basis as $\chi_{kj}^{\pm} = \langle k,+|a|j,-\rangle$ and the QRS-mode detuning $\Delta_{kj}^{1,2} = \omega_{1,2}^\ell - \nu_{kj}$. The Hamiltonian in Eq. (6.6) gives rise to several parametric down conversion processes mediated by the QRS, i.e., by starting with one excitation on the QRS of energy ν_{20}, it may produce a pair of photons of frequencies ω_1 and ω_2. The photons generated by this scheme will distribute on the multi-mode cavities according to the relation $\omega_1^\ell + \omega_2^{\ell'} = \nu_{20}$. Depending on the number of cavities N, this condition enables us to generate two

uncorrelated single-photons ($N = 1$), or producing identical entangled states of different frequency such as Bell states ($N = 2$) or W states ($N \geq 3$). For the cases, $N = \{1, 2, 3\}$ the effective Hamiltonians read

$$\mathcal{H}^1_{\text{eff}} = \mathcal{J}^1_2 \left[b^\dagger_1 c^\dagger_1 \mathcal{S}^- + b_1 c_2 \mathcal{S}^+ \right]. \tag{6.8a}$$

$$\mathcal{H}^2_{\text{eff}} = \mathcal{J}^1_2 \left[b^\dagger_1 c^\dagger_1 + b^\dagger_2 c^\dagger_2 + b^\dagger_1 c^\dagger_2 + b^\dagger_2 c^\dagger_1 \right] \mathcal{S}^- + \text{H.c.} \tag{6.8b}$$

$$\mathcal{H}^3_{\text{eff}} = \mathcal{J}^1_2 \left[b^\dagger_1 c^\dagger_1 + b^\dagger_2 c^\dagger_2 + b^\dagger_3 c^\dagger_3 + b^\dagger_1 c^\dagger_2 + b^\dagger_1 c^\dagger_3 + b^\dagger_2 c^\dagger_1 + b^\dagger_2 c^\dagger_3 + b^\dagger_3 c^\dagger_1 + b^\dagger_3 c^\dagger_2 \right] \mathcal{S}^- + \text{H.c.} \tag{6.8c}$$

The protocol works as follows: we initially consider the entire system in its ground state i.e., $|\Psi(0)\rangle = |0, +\rangle \bigotimes_{\ell,\ell'}^N |0_\ell, 0_{\ell'}\rangle$. Afterwards, one may excite the QRS with a microwave pulse with frequency $\nu = \nu_{20}$. This interaction can be modeled by the Hamiltonian $\mathcal{H}_D = \Omega \cos(\nu_{20} t)\sigma^z$. Notice that $\mathcal{H}_D$ preserves the $\mathbb{Z}_2$ symmetry of the QRS, thus enabling transitions between states of equal parity. The state of the system, after an interaction time $t = \pi/\Omega$, is given by $|\Psi(\pi/\Omega)\rangle = |2, +\rangle \bigotimes_{\ell,\ell'}^N |0_\ell, 0_{\ell'}\rangle$. Then, the system evolves under the Hamiltonian (6.2) for a time $t_S = \pi/(2\mathcal{J}^1_2)$, $t_B = \pi/(4\mathcal{J}^1_2)$, or $t_W = \pi/(6\mathcal{J}^1_2)$, for generating uncorrelated single photons, pair of Bell states, or pair of W states, respectively. As a result, the QRS excitation generates two photons distributed on the cavities satisfying the relation $\omega^\ell_1 + \omega^{\ell'}_2 = \nu_{20}$. The wavefunctions of the system after algebraic manipulation read

$$|\Psi(\pi/\Omega + \pi/2\mathcal{J}^1_2)\rangle_S = |+, 0\rangle \otimes |1_{\omega_1}\rangle \otimes |1_{\omega_2}\rangle, \tag{6.9a}$$

$$|\Psi(\pi/\Omega + \pi/4\mathcal{J}^1_2)\rangle_B = |+, 0\rangle \otimes |\Psi^+_{\omega_1}\rangle \otimes |\Psi^+_{\omega_2}\rangle, \tag{6.9b}$$

$$|\Psi(\pi/\Omega + \pi/6\mathcal{J}^1_2)\rangle_W = |+, 0\rangle \otimes |W_{\omega_1}\rangle \otimes |W_{\omega_2}\rangle, \tag{6.9c}$$

where $|\Psi^+_{\omega_n}\rangle$ is the Bell state for photons of frequency ω_n distributed over different resonators, that is, $|\Psi^+_{\omega_n}\rangle = \frac{1}{\sqrt{2}}[|1_{\omega_n}\rangle|0_{\omega_n}\rangle + |0_{\omega_n}\rangle|1_{\omega_n}\rangle]$. Also, the state $|W_{\omega_n}\rangle$ stands for a W state of a single photon of frequency ω_n distributed over different cavities.

In Fig. 6.2 we show the numerical calculations of the above mentioned protocol. Here, we compute the population evolution of states $|\Psi(0)\rangle$, and states $|\Psi\rangle_S$, $|\Psi\rangle_B$, and $|\Psi\rangle_W$ given in Eqs. (6.9). The parametric interaction can produce either uncorrelated photon states of different frequency or identical entangled states of modes belonging to distinct cavities. Furthermore, the simulations show that the state generation time decreases as $1/N$. This can be explained by analysing the structure of Eqs. (6.8). As the effective Hamiltonians describe a quantum dynamics in a reduced 2-dimensional Hilbert space, the matrix elements between the initial state $|\Psi(0)\rangle$ and $|\Psi\rangle_S$, $|\Psi\rangle_B$,

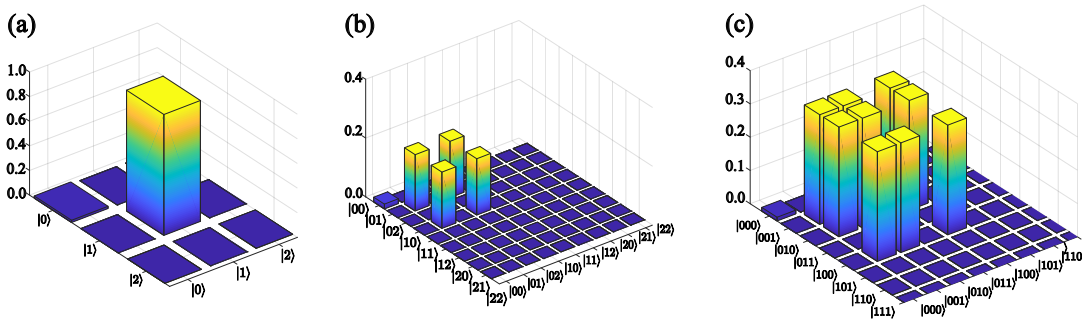

Figure 6.3: **Density matrix field mode**. Reconstructed density matrices associated with the modes ω_1, i.e. ρ_{ω_1}, for the case there the system is composed by $N = 1$ (a), $N = 2$ (b) and $N = 3$ (c) multimode cavities. At the specific state generation times t_S, t_B, and t_W, the dominant amplitudes correspond to the states $|1_{\omega_1}\rangle$, $|\Psi^+_{\omega_1}\rangle$ and $|W_{\omega_1}\rangle$, respectively.

and $|\Psi\rangle_W$ are proportional to the normalization of the desired state, that is, $\sqrt{N} \times \sqrt{N}$, where $N = 1$ stands for single photons, $N = 2$ for Bell states, and $N \geq 3$ for W states. In other words, the matrix elements of the effective Hamiltonians are proportional to the number of multimode cavities. By considering the following parameters for the QRS, $\omega_{\rm cav} = 2\pi \times 13.12$ GHz [Bou+09], qubit frequency $\omega_q = 0.8\omega_{\rm cav}$, light-matter coupling strength $g = 0.6\omega_{\rm cav}$, they allow us to estimate $|\chi_{10}| = 0.8188$ and $|\chi_{21}| = 1.235$. In addition, we choose $\omega_1^n = 0.25\nu_{20}$, $\omega_2^n = 0.75\nu_{20}$, $J_1^n = 0.0075\nu_{20}$, and $J_2^n = 0.0053\nu_{20}$. In this case, the state generation times are about $t_S \approx 25.10(8)$ [ns], $t_B \approx 12.55(4)$ [ns], $t_W \approx 8.369(4)$ [ns] for $N = 3$, and $t_W \approx 6.28$ [ns] for $N = 4$, see Fig. 6.2.

6.5 Copies of density matrices

In the above section, we have demonstrated that our system can generate identical copies of pure microwave photon states ($N = 1, 2, 3$). Here, we demonstrate that even including loss mechanisms our protocol can still generate copies of density matrices with high fidelity. Since our proposal includes an ultrastrongly coupled light-matter system, the dissipative dynamics will be described by the master equation [BGB11]

$$\begin{aligned}\dot{\rho}(t) &= i[\rho(t), \mathcal{H}] + \sum_{\ell=1}^{N} \kappa_\ell \mathcal{D}[b_\ell]\rho(t) + \sum_{n=1}^{M}\sum_{\ell=1}^{N} \kappa_\ell \mathcal{D}[c_\ell]\rho(t) \\ &+ \sum_{\sigma,\sigma>\sigma'} (\Gamma_\kappa^{\sigma\sigma'} + \Gamma_\gamma^{\sigma\sigma'} + \Gamma_{\gamma_\phi}^{\sigma\sigma'})\mathcal{D}[|\sigma, p\rangle\langle\sigma', p'|]\rho(t). \end{aligned} \tag{6.10}$$

	$N=1$	$N=2$	$N=3$
$\mathcal{F}(\rho_{\omega_1},\rho_{\omega_2})$	0.9898	0.9818	0.9832
$\mathcal{F}_S$	0.9892	-	-
$\mathcal{F}_B$	-	0.9945	-
$\mathcal{F}_W$	-	-	0.9904

Table 6.1: **Fidelity quantum states**. Summarized Fidelity values between the states ρ_{ω_ℓ} obtained through of the master Equation (6.11) with the fictitious states $\rho_{\rm probe}$ and $\rho_{\rm tensor}$ for the case where the QRS is coupled to $n=\{1,2,3\}$ multi-modes cavity.

Here, $\mathcal{H}$ is the Hamiltonian of Eq. (6.2) and $\mathcal{D}[O]\rho = 1/2(2O\rho O^\dagger - \rho O^\dagger O - O^\dagger O\rho)$ is the Liouvillian operator. Furthermore, κ_ℓ^n stands for photon loss rate for each cavity mode. $\Gamma_\kappa^{\sigma\sigma'}$, $\Gamma_\gamma^{\sigma\sigma'}$ and $\Gamma_{\gamma_\phi}^{\sigma\sigma'}$ are the dressed decay rates associated with the QRS, and they are defined as $\Gamma_\kappa^{\sigma\sigma'} = \frac{\kappa}{\omega_{\rm cav}}\nu_{\sigma\sigma'}|{\rm X}_{\sigma\sigma'}|^2$, $\Gamma_\gamma^{\sigma\sigma'} = \frac{\gamma}{\omega_q}\nu_{\sigma\sigma'}|\sigma^x_{\sigma\sigma'}|^2$ and $\Gamma_{\gamma_\phi}^{\sigma\sigma'} = \frac{\gamma_\phi}{\omega_q}\nu_{\sigma\sigma'}|\sigma^z_{\sigma\sigma'}|^2$, where κ, γ and γ_ϕ are the bare photon leakage rate, relaxation rate, and depolarizing noise rates, respectively.

To study the robustness of our protocol under loss mechanisms, first, we will examine the generation of copies of density matrices for the cases of $N=1,2,3$ multimode cavities. As mentioned in the previous section, the whole system is initialized in the state $|\Psi(0)\rangle = |0,+\rangle\bigotimes_{\ell,\ell'}^N|0_\ell,0_{\ell'}\rangle$. Then, we let the system to evolve under Eq. (6.10) for three different times: $t_S = \pi/(2\mathcal{J}_2^1)$, $t_B = \pi/(4\mathcal{J}_2^1)$, and $t_W = \pi/(6\mathcal{J}_2^1)$, for $N=1$, $N=2$, and $N=3$ multimode cavities, respectively. Once the corresponding density matrix $\rho(t)$ is obtained, we trace over the QRS and modes ω_2 (ω_1) to obtain the reduced density matrix ρ_{ω_1} (ρ_{ω_2}) which contains only degrees of freedom associated with the mode ω_1 (ω_2) distributed on different multimode cavities. Table 6.1, first row, shows the fidelity between both reduced density matrices $\mathcal{F}(\rho_{\omega_1},\rho_{\omega_2}) = {\rm Tr}(\rho_{\omega_1}\rho_{\omega_2})$. These results allow us to conclude that both quantum states are identical up to 99% fidelity for a single cavity, and up to 98% fidelity for two and three cavities. Table 6.1 also shows the fidelities of generating the states of Eqs. (6.9), that is, $\mathcal{F}_S = {\rm Tr}(\rho(t_S)\rho_S)$, $\mathcal{F}_B = {\rm Tr}(\rho(t_B)\rho_S)$, and $\mathcal{F}_W = {\rm Tr}(\rho(t_W)\rho_S)$, where $\rho(t)$ have been numerically calculated from Eq. (6.10). In Fig. 6.3 we plot the reconstructed density matrices for each case. The high fidelities of our protocol are mainly due to the fast state generation times as compared with the loss rates. Our numerical calculations has been carried out with realistic circuit QED parameters at temperature ${\rm T} = 15\ {\rm mK}$ [FD+16a]. For the QRS decay rates we consider values $\kappa = 2\pi\times 0.10\ {\rm MHz}$, $\gamma = 2\pi\times 15\ {\rm MHz}$ and $\gamma_\phi = 2\pi\times 7.69\ {\rm MHz}$ and for the cavities $\kappa_\ell^n = \kappa$.

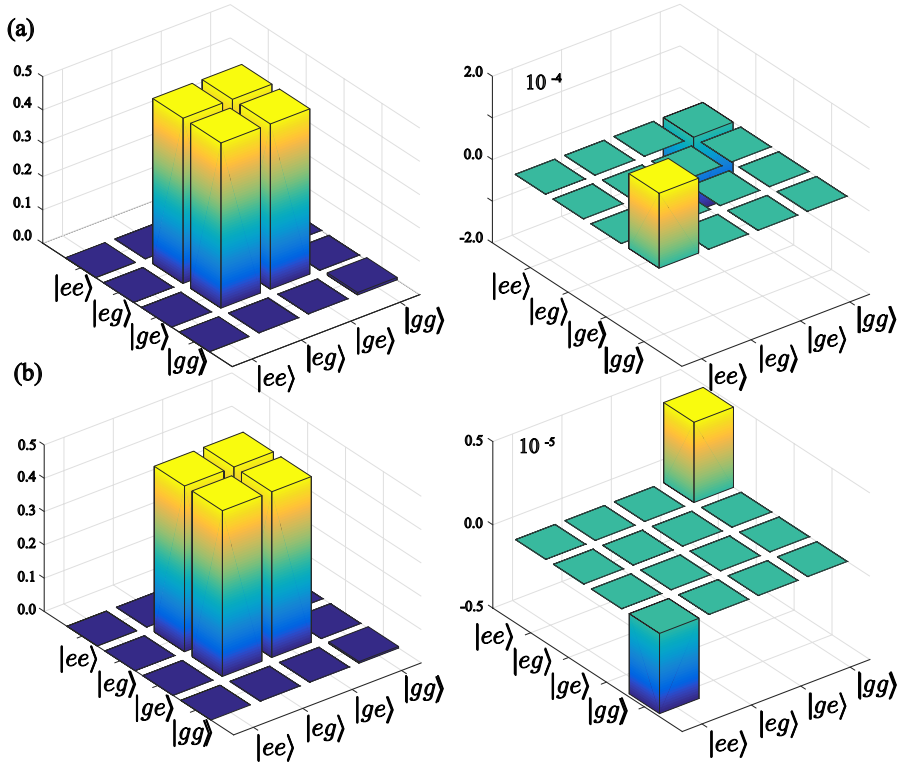

Figure 6.4: **Density matrix two-level systems**. Real and imaginary part of the reduced density matrix composed by the two qubits coupled to the field mode of frequency (a) ω_1 and ω_2. The fidelity between the simulated state with the Bell state $|\psi^+\rangle = (|eg\rangle + |eg\rangle)/\sqrt{2}$ is (a) $\mathcal{F} = 0.9960$ and (b) $\mathcal{F} = 0.9976$.

6.6 Entanglement Swapping Between Distant superconducting qubits

I this section, we transfer the entanglement generated into the field modes towards distant superconducting circuits. Let us consider a pair of two-level systems coupled at the end of each cavity. Notice that as the cavities are $\lambda/4$ transmission line resonator, the superconducting qubits corresponds to flux qubit to guarantee strong coupling with the resonators. In such a case, we describe the system with the following Hamiltonian

$$\mathcal{H}_{\rm ES} = \mathcal{H} + \sum_{\ell=1}^{2} \frac{\omega_{q\ell}^{n}}{2}\sigma_{\ell}^{z} + \sum_{\ell=1}^{2} \lambda_{\ell}\sigma_{\ell}^{x}(\mathcal{B}_{\ell}^{\dagger} + \mathcal{B}_{\ell}), \tag{6.11}$$

where $\mathcal{H}$ is the Hamiltonian defined in Eq. (6.2). Moreover, σ_{ℓ}^{x} (σ_{ℓ}^{z}) is the Pauli matrix describing the two-level systems. $\mathcal{B}_{\ell}$ is the extended cavity operators. Depending on whether the superconducting qubits coupled to the first or the second mode the operators can be $\mathcal{B}_{\ell} = b_{\ell}, c_{\ell}$, respectively.

Finally, λ_ℓ is the coupling strength between the qubit and the field mode. The system dynamics is described by the following master equation

$$\dot{\rho}(t) = [\text{Eq.}(10)] + \sum_{\ell=1}^{N} \gamma_\ell \mathcal{D}[\sigma_\ell^-]\rho(t) + \sum_{\ell=1}^{N} \gamma_{\phi_\ell} \mathcal{D}[\sigma_\ell^z]\rho(t). \tag{6.12}$$

The last two terms on the master equation describe the loss mechanisms acting on the two-level system, i.e., relaxation on the qubit at a rate γ and depolarising noise at rate γ_ϕ. The entanglement swapping protocol is the following; we initialise the whole system in its ground state

$$\rho_0 = |0,+\rangle\langle 0,+| \bigotimes_{\ell,\ell'}^{N} |0_\ell, 0_{\ell'}\rangle\langle 0_\ell, 0_{\ell'}| \bigotimes_{\ell}^{N} |g_\ell\rangle\langle g_\ell|, \tag{6.13}$$

We dispersively couple the two-level systems with the field modes on the cavities ($\omega_\ell^{1,2} \gg \omega_{q\ell}$). Next, we drive the QRS to prepare in the second excited state $|2,+\rangle$

$$\rho_1 = |2,+\rangle\langle 2,+| \bigotimes_{\ell,\ell'}^{N} |0_\ell, 0_{\ell'}\rangle\langle 0_\ell, 0_{\ell'}| \bigotimes_{\ell}^{N} |g_\ell\rangle\langle g_\ell|, \tag{6.14}$$

This state is the initial condition of our scheme. Afterwards, we let evolve the system under the Hamiltonian in Eq. (6.11). As we dispersively coupled the qubits, they do not evolve. After a time $t = \pi/(2\mathcal{J}_{\text{eff}})$, the system evolves to

$$\rho_2 = |0,+\rangle\langle 0,+| \bigotimes_{\ell}^{N} |\Psi_{\omega_\ell}^+\rangle\langle \Psi_{\omega_\ell}^+| \bigotimes_{\ell}^{N} |g_\ell\rangle\langle g_\ell|. \tag{6.15}$$

The next step is to avoid the generated photons coming back to the QRS. In such a case, we tune far-off resonance the QRS by changing the qubit frequency forming the QRS. We have done this change through an external magnetic flux. Next, we put in resonance the external two-level system with either field mode $\omega_\ell^{1,2}$. In such a case, for a time $t = \pi/(2\lambda_\ell)$, the system evolves to

$$\rho_3 = |0,+\rangle\langle 0,-| \bigotimes |\Psi_{\omega_\ell}^+\rangle\langle \Psi_{\omega_\ell}^+| \bigotimes |\Psi_{\omega_{\ell'}}^+\rangle\langle \Psi_{\omega_{\ell'}}^+|. \tag{6.16}$$

Here, $|\Psi_{\omega_\ell}\rangle = (|g_1 e_2\rangle + |e_1 g_2\rangle)/\sqrt{2}$ is Bell state of the pair of qubits. Fig. (6.4) shows the real and imaginary part of the reduced density matrix for the pair of qubits after performing the protocol. As the figure shows, even though the loss mechanisms act on the system, the entanglement on

the modes can be transferred to the qubits with high fidelity. For the two-level systems coupled to the first mode (ω_1^ℓ), the fidelity is $\mathcal{F} = 0.9960$, and $\mathcal{F} = 0.9976$ when the qubit is resonant with the second mode (ω_2^ℓ). This transfer occurs at the time scale of $t_{S_1} = 23.08$ [ns] and $t_{S_2} = 16.32$ [ns], respectively.

6.7 Conclusion

In summary, we have shown the usefulness of the QRS to generate photons. Based on the selection rules and the anharmonicity present of the QRS with an analogue to the phase matching condition observed in the parametric frequency conversion. It is possible to generate two photons starting to one excitation on the QRS. Depending on the number of multi-mode cavities in our setup, we can create two uncorrelated photons states or like-copies of maximally entangled states of photons (Bell or W states). In addition, we also demonstrate that by increasing the number of cavities coupled to the QRS, the time of the distribution of the photons decrease. Open a possibility to generate many-body microwave photonic state. Furthermore, by coupling an ancillary three-level system to one cavity a controlled phase gate can be implemented. The application of this gate on the system allow us to generate higher entangled state. Finally, we propose a possible implementation using current technologies in superconducting circuits.

Conclusion

In summary, this theses has addressed the problem concerning with energy transport mediated by a hybrid light-matter system in the ultra-strong coupling regime, termed as quantum Rabi system (QRS). The novel features exhibited by the energy spectrum of this system as anharmonicity of its energy levels and internal selection rules imposed by the parity symmetry have permitted us to develop protocols to generate and transport excitations. Moreover, we have also presented the possible implementation of these protocols within the near-terms quantum architecture termed as superconducting circuit and circuit quantum electrodynamics.

In chapter 5 we have developed a quantum protocol to perform high-fidelity transport of either excitations or quantum states between a pair of two-level systems mediated by a QRS initially prepared in a thermal state. The QRS is formed by two qubits, each of them built by a Josephson-based circuit ultrastrongly coupled to a quantized field mode confined in a transmission line resonator. The additional two-level systems are composed by a transmon qubit coupled capacitively at the edges of the resonator forming the QRS.

The quantum protocol consists of preparing the entire system in a thermal state. Due to the system parameters, the thermal state of the whole system is represented by the QRS in a thermal state factorised from the two-level systems, which are prepared in their ground state. Afterwards, with a classical driving in one of the two-level system, it is possible to generate one excitation or an arbitrary quantum state on it. Letting evolve the system, we show that even though the mediator is in the thermal state, it is still possible to achieve high-fidelity state transfer. The efficiency of this protocol relies on the selection rules presents on the QRS together with a specific resonance condition on the two-level systems. We show that the main detrimental effect on the transport is the working temperature instead of the losses mechanism acting on the entire system. In fact, in the presence of them, the state transfer fidelity of an arbitrary quantum state on the Bloch sphere reach 97.9% of efficiency.

In chapter 6 we have proposed a method to generate and transport quantum copies of mi-

crowave photons in extended resonators mediated by a QRS. The QRS system is formed by a Josephson-based electronic circuit ultratrongly coupled to a quantized field mode confined in a transmission line resonator. The extended resonator are composed by transmission line resonators supporting two distinct modes.

The generation scheme considers specific resonance condition between the extended resonator and the QRS. Under this condition, the effective model governing the system dynamics consists of two-photon transition mediated by the QRS, similar to the observed in the parametric down-conversion process. In such a case, depending on the number of coupled cavities, our scheme can generate in a deterministic manner, a pair of uncorrelated photons states of different frequency, a product of Bell and W states of spatially distant resonators. Moreover, we also demonstrate improved generation times when increasing the number of multi-modes cavities. Furthermore, we also show the generation of genuine multipartite-entanglement states between field modes and ancillary two-level system.

Bibliography References

[AA+18] Albarrán-Arriagada, F. et al. “Spin-1 models in the ultrastrong-coupling regime of circuit QED”. In: *Phys. Rev. A* 97 (2 2018), p. 022306.

[Abd+08] Abdumalikov, Abdufarrukh A. et al. “Vacuum Rabi splitting due to strong coupling of a flux qubit and a coplanar-waveguide resonator”. In: *Phys. Rev. B* 78 (18 2008), p. 180502.

[Abd+10] Abdumalikov, A. A. et al. “Electromagnetically Induced Transparency on a Single Artificial Atom”. In: *Phys. Rev. Lett.* 104 (19 2010), p. 193601.

[All+10] Allman, M. S. et al. “rf-SQUID-Mediated Coherent Tunable Coupling between a Superconducting Phase Qubit and a Lumped-Element Resonator”. In: *Phys. Rev. Lett.* 104 (17 2010), p. 177004.

[AN10] Ashhab, S. and Nori, Franco. “Qubit-oscillator systems in the ultrastrong-coupling regime and their potential for preparing nonclassical states”. In: *Phys. Rev. A* 81 (4 2010), p. 042311.

[AR63] Anderson, P. W. and Rowell, J. M. “Probable Observation of the Josephson Superconducting Tunneling Effect”. In: *Phys. Rev. Lett.* 10 (6 1963), pp. 230–232.

[BA17] Blais, Christian Kraglund Andersen and Alexandre. “Ultrastrong coupling dynamics with a transmon qubit”. In: *New Journal of Physics* 19.2 (2017), p. 023022.

[Bau+16] Baust, A. et al. “Ultrastrong coupling in two-resonator circuit QED”. In: *Phys. Rev. B* 93 (21 2016), p. 214501.

[BCS57] Bardeen, J., Cooper, L. N., and Schrieffer, J. R. “Theory of Superconductivity”. In: *Phys. Rev.* 108 (5 1957), pp. 1175–1204.

[Ber+05] Bertet, P. et al. “Dephasing of a Superconducting Qubit Induced by Photon Noise”. In: *Phys. Rev. Lett.* 95 (25 2005), p. 257002.

[Ber+10] Bergeal, N. et al. “Analog information processing at the quantum limit with a Josephson ring modulator”. In: *Nature Physics* 6 (2010). Article, 296 EP –.

[BGB10] Boissonneault, Maxime, Gambetta, J. M., and Blais, Alexandre. “Improved Superconducting Qubit Readout by Qubit-Induced Nonlinearities”. In: *Phys. Rev. Lett.* 105 (10 2010), p. 100504.

[BGB11] Beaudoin, Félix, Gambetta, Jay M., and Blais, A. “Dissipation and ultrastrong coupling in circuit QED”. In: *Phys. Rev. A* 84 (4 2011), p. 043832.

[Bis10] Bishop, Lev S. “Circuit quantum electrodynamics”. In: *arXiv:1007.3520* (2010).

[Bla+04] Blais, Alexandre et al. “Cavity quantum electrodynamics for superconducting electrical circuits: An architecture for quantum computation”. In: *Phys. Rev. A* 69 (6 2004), p. 062320.

[Boa+07] Boaknin, E et al. “Dispersive microwave bifurcation of a superconducting resonator cavity incorporating a Josephson junction”. In: *arXiv cond-mat/0702445* (2007).

[Bos+17] Bosman, Sal J. et al. “Approaching ultrastrong coupling in transmon circuit QED using a high-impedance resonator”. In: *Phys. Rev. B* 95 (22 2017), p. 224515.

[Bos03] Bose, Sougato. “Quantum Communication through an Unmodulated Spin Chain”. In: *Phys. Rev. Lett.* 91 (20 2003), p. 207901.

[Bou+09] Bourassa, J. et al. “Ultrastrong coupling regime of cavity QED with phase-biased flux qubits”. In: *Phys. Rev. A* 80 (3 2009), p. 032109.

[Bou+12] Bourassa, J. et al. “Josephson-junction-embedded transmission-line resonators: From Kerr medium to in-line transmon”. In: *Phys. Rev. A* 86 (1 2012), p. 013814.

[BP+02] Breuer, Heinz-Peter, Petruccione, Francesco, et al. *The theory of open quantum systems*. Oxford University Press on Demand, 2002.

[Bra11] Braak, D. “Integrability of the Rabi Model”. In: *Phys. Rev. Lett.* 107 (10 2011), p. 100401.

[BRH87] Brune, M., Raimond, J. M., and Haroche, S. “Theory of the Rydberg-atom two-photon micromaser”. In: *Phys. Rev. A* 35 (1 1987), pp. 154–163.

[Bru+87] Brune, M. et al. “Realization of a two-photon maser oscillator”. In: *Phys. Rev. Lett.* 59 (17 1987), pp. 1899–1902.

[Bru+92] Brune, M. et al. “Manipulation of photons in a cavity by dispersive atom-field coupling: Quantum-nondemolition measurements and generation of “Schrödinger cat” states”. In: *Phys. Rev. A* 45 (7 1992), pp. 5193–5214.

[Cas+10a] Casanova, J. et al. “Deep Strong Coupling Regime of the Jaynes-Cummings Model”. In: *Phys. Rev. Lett.* 105 (26 2010), p. 263603.

[Cas+10b] Casanova, J. et al. “Short-time-interaction quantum measurement through an incoherent mediator”. In: *Phys. Rev. A* 81 (6 2010), p. 062126.

[CBC05] Ciuti, Cristiano, Bastard, Gérald, and Carusotto, Iacopo. “Quantum vacuum properties of the intersubband cavity polariton field”. In: *Phys. Rev. B* 72 (11 2005), p. 115303.

[CC06] Ciuti, Cristiano and Carusotto, Iacopo. “Input-output theory of cavities in the ultrastrong coupling regime: The case of time-independent cavity parameters”. In: *Phys. Rev. A* 74 (3 2006), p. 033811.

[Chi+04] Chiorescu, I. et al. “Coherent dynamics of a flux qubit coupled to a harmonic oscillator”. In: *Nature* 431 (2004), 159 EP –.

[Chr+04] Christandl, Matthias et al. “Perfect State Transfer in Quantum Spin Networks”. In: *Phys. Rev. Lett.* 92 (18 2004), p. 187902.

[Chr+05] Christandl, Matthias et al. “Perfect transfer of arbitrary states in quantum spin networks”. In: *Phys. Rev. A* 71 (3 2005), p. 032312.

[CI+18] Campagne-Ibarcq, P. et al. “Deterministic Remote Entanglement of Superconducting Circuits through Microwave Two-Photon Transitions”. In: *Phys. Rev. Lett.* 120 (20 2018), p. 200501.

[Cir+97] Cirac, J. I. et al. “Quantum State Transfer and Entanglement Distribution among Distant Nodes in a Quantum Network”. In: *Phys. Rev. Lett.* 78 (16 1997), pp. 3221–3224.

[CW08] Clarke, John and Wilhelm, Frank K. “Superconducting quantum bits”. In: *Nature* 453 (2008), 1031 EP –.

[Cyr73] Cyrot, M. “Ginzburg-Landau theory for superconductors”. In: *Reports on Progress in Physics* 36.2 (1973), p. 103.

[CZ95] Cirac, J. I. and Zoller, P. “Quantum Computations with Cold Trapped Ions”. In: *Phys. Rev. Lett.* 74 (20 1995), pp. 4091–4094.

[Dev+98] Devoret, V. Bouchiat et al. “Quantum coherence with a single Cooper pair”. In: *Physica Scripta* 1998.T76 (1998), p. 165.

[Dev97] Devoret, MH. *Quantum fluctuations in electrical circuits Fluctuations Quantique: Les Houches, Session LXIII, 1995 ed S Reynaud et al*. Amsterdam: Elsevier, 1997.

[DF61] Deaver, Bascom S. and Fairbank, William M. “Experimental Evidence for Quantized Flux in Superconducting Cylinders”. In: *Phys. Rev. Lett.* 7 (2 1961), pp. 43–46.

[DHC15] Duan, Liwei, He, Shu, and Chen, Qing-Hu. “Concise analytic solutions to the quantum Rabi model with two arbitrary qubits”. In: *Annals of Physics* 355 (2015), pp. 121–129.

[Dic54] Dicke, R. H. “Coherence in Spontaneous Radiation Processes”. In: *Phys. Rev.* 93 (1 1954), pp. 99–110.

[Dir27] Dirac, Paul Adrien Maurice. “The quantum theory of the emission and absorption of radiation”. In: *Proc. R. Soc. Lond. A* 114.767 (1927), pp. 243–265.

[DJ92] Deutsch, David and Jozsa, Richard. “Rapid solution of problems by quantum computation”. In: *Proc. R. Soc. Lond. A* 439.1907 (1992), pp. 553–558.

[DL+09] De Liberato, S. et al. “Extracavity quantum vacuum radiation from a single qubit”. In: *Phys. Rev. A* 80 (5 2009), p. 053810.

[DN61] Doll, R. and Näbauer, M. “Experimental Proof of Magnetic Flux Quantization in a Superconducting Ring”. In: *Phys. Rev. Lett.* 7 (2 1961), pp. 51–52.

[DQB14] Didier, Nicolas, Qassemi, Farzad, and Blais, Alexandre. “Perfect squeezing by damping modulation in circuit quantum electrodynamics”. In: *Phys. Rev. A* 89 (1 2014), p. 013820.

[DS13] Devoret, M. H. and Schoelkopf, R. J. “Superconducting Circuits for Quantum Information: An Outlook”. In: *Science* 339.6124 (2013), p. 1169.

[DWM04] Devoret, Michel H, Wallraff, Andreas, and Martinis, John M. “Superconducting qubits: A short review”. In: *arXiv preprint cond-mat/0411174* (2004).

[ECZ97] Enk, S. J. van, Cirac, J. I., and Zoller, P. “Ideal Quantum Communication over Noisy Channels: A Quantum Optical Implementation”. In: *Phys. Rev. Lett.* 78 (22 1997), pp. 4293–4296.

[Eic+11] Eichler, C. et al. “Observation of Two-Mode Squeezing in the Microwave Frequency Domain”. In: *Phys. Rev. Lett.* 107 (11 2011), p. 113601.

[Eic+14] Eichler, C. et al. “Quantum-Limited Amplification and Entanglement in Coupled Nonlinear Resonators”. In: *Phys. Rev. Lett.* 113 (11 2014), p. 110502.

[Eve+04] Everitt, M. J. et al. “Superconducting analogs of quantum optical phenomena: Macroscopic quantum superpositions and squeezing in a superconducting quantum-interference device ring”. In: *Phys. Rev. A* 69 (4 2004), p. 043804.

[EW13] Egger, D. J. and Wilhelm, F. K. “Multimode Circuit Quantum Electrodynamics with Hybrid Metamaterial Transmission Lines”. In: *Phys. Rev. Lett.* 111 (16 2013), p. 163601.

[FD+10] Forn-Díaz, P. et al. “Observation of the Bloch-Siegert Shift in a Qubit-Oscillator System in the Ultrastrong Coupling Regime”. In: *Phys. Rev. Lett.* 105 (23 2010), p. 237001.

[FD+16a] Forn-Díaz, P. et al. “Broken selection rule in the quantum Rabi model”. In: *Scientific Reports* 6 (2016). Article, 26720 EP –.

[FD+16b] Forn-Díaz, P. et al. “Ultrastrong coupling of a single artificial atom to an electromagnetic continuum in the nonperturbative regime”. In: *Nature Physics* 13 (2016), 39 EP –.

[Fel+14] Felicetti, S. et al. “Photon transfer in ultrastrongly coupled three-cavity arrays”. In: *Phys. Rev. A* 89 (1 2014), p. 013853.

[Fel+15] Felicetti, S. et al. “Parity-dependent State Engineering and Tomography in the ultrastrong coupling regime”. In: *Scientific Reports* 5 (2015). Article, 11818 EP –.

[Fer32] Fermi, Enrico. “Quantum Theory of Radiation”. In: *Rev. Mod. Phys.* 4 (1 1932), pp. 87–132.

[Fey06] Feynman, Richard Phillips. *QED: The strange theory of light and matter*. Princeton University Press, 2006.

[GAF10] Grynberg, Gilbert, Aspect, Alain, and Fabre, Claude. *Introduction to Quantum Optics: From the Semi-classical Approach to Quantized Light*. Cambridge: Cambridge University Press, 2010.

[GAN14] Georgescu, I. M., Ashhab, S., and Nori, Franco. "Quantum simulation". In: *Rev. Mod. Phys.* 86 (1 2014), pp. 153–185.

[Gar11] Garraway, Barry M. "The Dicke model in quantum optics: Dicke model revisited". In: *Philosophical Transactions of the Royal Society A: Mathematical, Physical and Engineering Sciences* 369.1939 (2011), p. 1137.

[Gas+17] Gasparinetti, Simone et al. "Correlations and Entanglement of Microwave Photons Emitted in a Cascade Decay". In: *Phys. Rev. Lett.* 119 (14 2017), p. 140504.

[Gin50] Ginzburg, VI. "On the theory of superconductivity". In: *Zh. eksper. teor. Fiz.* 20 (1950), pp. 1064–1082.

[Gir11] Girvin, Steven M. "Circuit qed: Superconducting qubits coupled to microwave photons". In: *Proceedings of the 2011 Les Houches Summer School* (2011).

[GKL13] Greentree, Andrew D, Koch, Jens, and Larson, Jonas. "Fifty years of Jaynes–Cummings physics". In: *Journal of Physics B: Atomic, Molecular and Optical Physics* 46.22 (2013), p. 220201.

[Gor59] Gorkov, Lev Petrovich. "Microscopic derivation of the Ginzburg-Landau equations in the theory of superconductivity". In: *Sov. Phys. JETP* 9.6 (1959), pp. 1364–1367.

[Gro96] Grover, Lov K. "A Fast Quantum Mechanical Algorithm for Database Search". In: *Proceedings of the Twenty-eighth Annual ACM Symposium on Theory of Computing*. STOC '96. Philadelphia, Pennsylvania, USA: ACM, 1996, pp. 212–219.

[GS89] Gerlach, Walther and Stern, Otto. "Walther Gerlach (1889-1979): Eine Auswahl aus seinen Schriften und Briefen". In: ed. by Bachmann, Hans-Reinhard and Rechenberg, Helmut. Berlin, Heidelberg: Springer Berlin Heidelberg, 1989. Chap. Der experimentelle Nachweis der Richtungsquantelung im Magnetfeld, pp. 26–29.

[Gu+17] Gu, Xiu et al. "Microwave photonics with superconducting quantum circuits". In: *Physics Reports* 718-719 (2017), pp. 1–102.

[Guo+14] Guo, Jie Peng et al. "Solution of the two-qubit quantum Rabi model and its exceptional eigenstates". In: *Journal of Physics A: Mathematical and Theoretical* 47.26 (2014), p. 265303.

[Gut+01] Guthöhrlein, G. R. et al. "A single ion as a nanoscopic probe of an optical field". In: *Nature* 414 (2001), 49 EP –.

[Göp+08] Göppl, M. et al. "Coplanar waveguide resonators for circuit quantum electrodynamics". In: *Journal of Applied Physics* 104.11 (2008), p. 113904.

[Hao+15] Hao, Jie Peng et al. "Algebraic structure of the two-qubit quantum Rabi model and its solvability using Bogoliubov operators". In: *Journal of Physics A: Mathematical and Theoretical* 48.28 (2015), p. 285301.

[Har+12] Hartmann, M. Leib et al. "Networks of nonlinear superconducting transmission line resonators". In: *New Journal of Physics* 14.7 (2012), p. 075024.

[Hei27] Heisenberg, W. "Über den anschaulichen Inhalt der quantentheoretischen Kinematik und Mechanik". In: *Zeitschrift für Physik* 43.3 (1927), pp. 172–198.

[HJ+16] Hadfield, Robert H, Johansson, Göran, et al. *Superconducting Devices in Quantum Optics*. Springer, 2016.

[Hof+11] Hoffman, A. J. et al. "Dispersive Photon Blockade in a Superconducting Circuit". In: *Phys. Rev. Lett.* 107 (5 2011), p. 053602.

[HRB] Häffner, H., Roos, C.F., and Blatt, R. "Quantum computing with trapped ions". In: *Physics Reports* 469.4 (), pp. 155 –203.

[HTK12] Houck, Andrew A., Türeci, Hakan E., and Koch, Jens. “On-chip quantum simulation with superconducting circuits”. In: *Nature Physics* 8 (2012), 292 EP –.

[Ito74] Itoh, T. “Analysis of Microstrip Resonators”. In: *IEEE Transactions on Microwave Theory and Techniques* 22.11 (1974), pp. 946–952.

[Izm+04] Izmalkov, A. et al. “Evidence for Entangled States of Two Coupled Flux Qubits”. In: *Phys. Rev. Lett.* 93 (3 2004), p. 037003.

[JC63] Jaynes, E. T. and Cummings, F. W. “Comparison of quantum and semiclassical radiation theories with application to the beam maser”. In: *Proceedings of the IEEE* 51.1 (1963), pp. 89–109.

[Jos62] Josephson, B. D. “Possible new effects in superconductive tunnelling”. In: *Physics Letters* 1.7 (1962), pp. 251–253.

[Kit66] Kittel, Charles. *Introduction to solid state*. Vol. 162. John Wiley & Sons New Jersey, 1966.

[KM80] Knight, P. L. and Milonni, P. W. “The Rabi frequency in optical spectra”. In: *Physics Reports* 66.2 (1980), pp. 21–107.

[KO11] Kamerlingh Onnes, H. “The resistance of pure mercury at helium temperatures”. In: *Commun. Phys. Lab. Univ. Leiden, b* 120 (1911).

[Koc+07] Koch, Jens et al. “Charge-insensitive qubit design derived from the Cooper pair box”. In: *Phys. Rev. A* 76 (4 2007), p. 042319.

[Kos09] Koshino, Kazuki. “Down-conversion of a single photon with unit efficiency”. In: *Phys. Rev. A* 79 (1 2009), p. 013804.

[Kur+18] Kurpiers, P. et al. “Deterministic quantum state transfer and remote entanglement using microwave photons”. In: *Nature* 558.7709 (2018), pp. 264–267.

[Kya+15a] Kyaw, T. H. et al. “Creation of quantum error correcting codes in the ultrastrong coupling regime”. In: *Phys. Rev. B* 91 (6 2015), p. 064503.

[Kya+15b] Kyaw, T. H. et al. “Scalable quantum memory in the ultrastrong coupling regime”. In: *Scientific Reports* 5 (2015). Article, 8621 EP –.

[Kya+17] Kyaw, Thi Ha et al. “Parity-preserving light-matter system mediates effective two-body interactions”. In: *Quantum Science and Technology* 2.2 (2017), p. 025007.

[Lad+10] Ladd, T. D. et al. “Quantum computers”. In: *Nature* 464 (2010). Review Article, 45 EP –.

[Lan+11] Lang, C. et al. “Observation of Resonant Photon Blockade at Microwave Frequencies Using Correlation Function Measurements”. In: *Phys. Rev. Lett.* 106 (24 2011), p. 243601.

[Lan13] Langford, Nathan K. “Circuit qed-lecture notes”. In: *arXiv:1310.1897* (2013).

[Lee+17] Lee, Qiongtao Xie et al. “The quantum Rabi model: solution and dynamics”. In: *Journal of Physics A: Mathematical and Theoretical* 50.11 (2017), p. 113001.

[Liu+14] Liu, Yu-xi et al. “Controllable microwave three-wave mixing via a single three-level superconducting quantum circuit”. In: *Scientific Reports* 4 (2014). Article, 7289 EP –.

[LL73] Louisell, William Henry and Louisell, William H. *Quantum statistical properties of radiation*. Vol. 7. Wiley New York, 1973.

[LLP80] Landau, Lev Davidovich, Lifshitz, Evgenii M, and Pitaevskii, LP. *Statistical physics, part I*. 1980.

[Mar+02] Martinis, John M. et al. “Rabi Oscillations in a Large Josephson-Junction Qubit”. In: *Phys. Rev. Lett.* 89 (11 2002), p. 117901.

[Mar07] Marquardt, Florian. “Efficient on-chip source of microwave photon pairs in superconducting circuit QED”. In: *Phys. Rev. B* 76 (20 2007), p. 205416.

[MCCM14] Moya-Cessa, B. M. Rodríguez-Lara, Chilingaryan, S. A., and M., H. “Searching for structure beyond parity in the two-qubit Dicke model”. In: *Journal of Physics A: Mathematical and Theoretical* 47.13 (2014), p. 135306.

[MG05] Moon, K. and Girvin, S. M. “Theory of Microwave Parametric Down-Conversion and Squeezing Using Circuit QED”. In: *Phys. Rev. Lett.* 95 (14 2005), p. 140504.

[MO33] Meissner, Walther and Ochsenfeld, Robert. “Ein neuer effekt bei eintritt der supraleitfähigkeit”. In: *Naturwissenschaften* 21.44 (1933), pp. 787–788.

[Naj10] Najm, Farid N. *Circuit simulation*. John Wiley & Sons, 2010.

[Nak12] Nakamura, Y. “Microwave quantum photonics in superconducting circuits”. In: *IEEE Photonics Conference 2012*. 2012, pp. 544–545.

[Nar+16] Narla, A. et al. “Robust Concurrent Remote Entanglement Between Two Superconducting Qubits”. In: *Phys. Rev. X* 6 (3 2016), p. 031036.

[NB09] Nazarov, Yuli V. and Blanter, Yaroslav M. *Quantum Transport: Introduction to Nanoscience*. Cambridge: Cambridge University Press, 2009.

[NC11] Nataf, Pierre and Ciuti, Cristiano. “Protected Quantum Computation with Multiple Resonators in Ultrastrong Coupling Circuit QED”. In: *Phys. Rev. Lett.* 107 (19 2011), p. 190402.

[Nie+10] Niemczyk, T. et al. “Circuit quantum electrodynamics in the ultrastrong-coupling regime”. In: *Nature Physics* 6 (2010), 772 EP –.

[Nis+07] Niskanen, A. O. et al. “Quantum Coherent Tunable Coupling of Superconducting Qubits”. In: *Science* 316.5825 (2007), p. 723.

[NPT99] Nakamura, Y., Pashkin, Yu A., and Tsai, J. S. “Coherent control of macroscopic quantum states in a single-Cooper-pair box”. In: *Nature* 398 (1999), 786 EP –.

[NWF04] Nori, Yu-xi Liu, Wei, L. F., and Franco. “Generation of nonclassical photon states using a superconducting qubit in a microcavity”. In: *EPL (Europhysics Letters)* 67.6 (2004), p. 941.

[OIK08] Ogden, C. D., Irish, E. K., and Kim, M. S. “Dynamics in a coupled-cavity array”. In: *Phys. Rev. A* 78 (6 2008), p. 063805.

[Orl+99] Orlando, T. P. et al. “Superconducting persistent-current qubit”. In: *Phys. Rev. B* 60 (22 1999), pp. 15398–15413.

[OW13] Oliver, William D. and Welander, Paul B. “Materials in superconducting quantum bits”. In: 38.10 (2013), pp. 816–825.

[Pes18] Peskin, Michael E. *An introduction to quantum field theory*. CRC Press, 2018.

[PL+13] Perez-Leija, Armando et al. “Coherent quantum transport in photonic lattices”. In: *Phys. Rev. A* 87 (1 2013), p. 012309.

[Plo+07] Ploeg, S. H. W. van der et al. “Adiabatic Quantum Computation With Flux Qubits, First Experimental Results”. In: *IEEE Transactions on Applied Superconductivity* 17.2 (2007), pp. 113–119.

[Poz09] Pozar, David M. *Microwave engineering*. John Wiley & Sons, 2009.

[Rab36] Rabi, I. I. “On the Process of Space Quantization”. In: *Phys. Rev.* 49 (4 1936), pp. 324–328.

[Rab37] Rabi, I. I. “Space Quantization in a Gyrating Magnetic Field”. In: *Phys. Rev.* 51 (8 1937), pp. 652–654.

[RBH01] Raimond, J. M., Brune, M., and Haroche, S. “Manipulating quantum entanglement with atoms and photons in a cavity”. In: *Rev. Mod. Phys.* 73 (3 2001), pp. 565–582.

[RCLV15] Rotondo, Pietro, Cosentino Lagomarsino, Marco, and Viola, Giovanni. “Dicke Simulators with Emergent Collective Quantum Computational Abilities”. In: *Phys. Rev. Lett.* 114 (14 2015), p. 143601.

[Rid+12] Ridolfo, A. et al. “Photon Blockade in the Ultrastrong Coupling Regime”. In: *Phys. Rev. Lett.* 109 (19 2012), p. 193602.

[RJ95] Ruiz, Claudio Pita and Jesús, Claudio de. *Cálculo vectorial*. Prentice-Hall Hispanoamericana, 1995.

[RLM13] Rodríguez-Lara, S. A. Chilingaryan and M., B. “The quantum Rabi model for two qubits”. In: *Journal of Physics A: Mathematical and Theoretical* 46.33 (2013), p. 335301.

[Rom+12] Romero, G. et al. “Ultrafast Quantum Gates in Circuit QED”. In: *Phys. Rev. Lett.* 108 (12 2012), p. 120501.

[Ros+18] Rosenblum, S. et al. “A CNOT gate between multiphoton qubits encoded in two cavities”. In: *Nature Communications* 9.1 (2018), p. 652.

[Rso] “The electromagnetic equations of the supraconductor”. In: *Proceedings of the Royal Society of London. Series A - Mathematical and Physical Sciences* 149.866 (1935), p. 71.

[RSR07] Retzker, A., Solano, E., and Reznik, B. “Tavis-Cummings model and collective multiqubit entanglement in trapped ions”. In: *Phys. Rev. A* 75 (2 2007), p. 022312.

[Sag+11] Sage, Jeremy M. et al. “Study of loss in superconducting coplanar waveguide resonators”. In: *Journal of Applied Physics* 109.6 (2011), p. 063915.

[Sai+14] Saira, O.-P. et al. “Entanglement Genesis by Ancilla-Based Parity Measurement in 2D Circuit QED”. In: *Phys. Rev. Lett.* 112 (7 2014), p. 070502.

[SB+16] Sánchez-Burillo, E. et al. “Full two-photon down-conversion of a single photon”. In: *Phys. Rev. A* 94 (5 2016), p. 053814.

[Sch+17] Schuetz, M. J. A. et al. “High-fidelity hot gates for generic spin-resonator systems”. In: *Phys. Rev. A* 95 (5 2017), p. 052335.

[Sch07] Schuster, David Isaac. *Circuit quantum electrodynamics*. Yale University, 2007.

[SEW91] Scully, Marian O., Englert, Berthold-Georg, and Walther, Herbert. “Quantum optical tests of complementarity”. In: *Nature* 351 (1991), 111 EP –.

[SG08] Schoelkopf, R. J. and Girvin, S. M. “Wiring up quantum systems”. In: *Nature* 451 (2008), 664 EP –.

[Sho07] Shore, Bruce W. “Sir Peter Knight and the Jaynes-Cummings model”. In: *Journal of Modern Optics* 54.13-15 (2007), pp. 2009–2016.

[Sim04] Simons, Rainee N. *Coplanar waveguide circuits, components, and systems*. Vol. 165. John Wiley & Sons, 2004.

[SJS10] Strauch, Frederick W., Jacobs, Kurt, and Simmonds, Raymond W. “Arbitrary Control of Entanglement between two Superconducting Resonators”. In: *Phys. Rev. Lett.* 105 (5 2010), p. 050501.

[SK93] Shore, Bruce W. and Knight, Peter L. “The Jaynes-Cummings Model”. In: *Journal of Modern Optics* 40.7 (1993), pp. 1195–1238.

[SM00] Sørensen, Anders and Mølmer, Klaus. “Entanglement and quantum computation with ions in thermal motion”. In: *Phys. Rev. A* 62 (2 2000), p. 022311.

[SM99] Sørensen, Anders and Mølmer, Klaus. “Quantum Computation with Ions in Thermal Motion”. In: *Phys. Rev. Lett.* 82 (9 1999), pp. 1971–1974.

[SMFZ99] Solano, E., Matos Filho, R. L. de, and Zagury, N. “Deterministic Bell states and measurement of the motional state of two trapped ions”. In: *Phys. Rev. A* 59 (4 1999), R2539–R2543.

[Sol+17] Solano, Jie Peng et al. “Dark-like states for the multi-qubit and multi-photon Rabi models”. In: *Journal of Physics A: Mathematical and Theoretical* 50.17 (2017), p. 174003.

[SSS17] Srinivasan, M. Steffen, Sandberg, M., and S. “Recent research trends for high coherence quantum circuits”. In: *Superconductor Science and Technology* 30.3 (2017), p. 030301.

[Str12] Strauch, Frederick W. “All-Resonant Control of Superconducting Resonators”. In: *Phys. Rev. Lett.* 109 (21 2012), p. 210501.

[Sun+15] Sundaresan, Neereja M. et al. “Beyond Strong Coupling in a Multimode Cavity”. In: *Phys. Rev. X* 5 (2 2015), p. 021035.

[SWF17] Shao, Wenjun, Wu, Chunfeng, and Feng, Xun-Li. “Generalized James’ effective Hamiltonian method”. In: *Phys. Rev. A* 95 (3 2017), p. 032124.

[SWM10] Saffman, M., Walker, T. G., and Mølmer, K. “Quantum information with Rydberg atoms”. In: *Rev. Mod. Phys.* 82 (3 2010), pp. 2313–2363.

[SYZ14] Su, Qi-Ping, Yang, Chui-Ping, and Zheng, Shi-Biao. “Fast and simple scheme for generating NOON states of photons in circuit QED”. In: *Scientific Reports* 4 (2014). Article, 3898 EP –.

[SZ97] Scully, Marlan O. and Zubairy, M. Suhail. *Quantum Optics*. Cambridge: Cambridge University Press, 1997.

[TC68] Tavis, Michael and Cummings, Frederick W. “Exact Solution for an N-Molecule—Radiation-Field Hamiltonian”. In: *Phys. Rev.* 170 (2 1968), pp. 379–384.

[TC69] TAVIS, MICHAEL and CUMMINGS, FREDERICK W. “Approximate Solutions for an N-Molecule-Radiation-Field Hamiltonian”. In: *Phys. Rev.* 188 (2 1969), pp. 692–695.

[Tin04] Tinkham, Michael. *Introduction to superconductivity*. Courier Corporation, 2004.

[TRK92] Thompson, R. J., Rempe, G., and Kimble, H. J. “Observation of normal-mode splitting for an atom in an optical cavity”. In: *Phys. Rev. Lett.* 68 (8 1992), pp. 1132–1135.

[UM17] Uri, Vool and Michel, Devoret. “Introduction to quantum electromagnetic circuits”. In: *International Journal of Circuit Theory and Applications* 45.7 (2017), pp. 897–934.

[Und+12] Underwood, D. L. et al. “Low-disorder microwave cavity lattices for quantum simulation with photons”. In: *Phys. Rev. A* 86 (2 2012), p. 023837.

[Wal+00] Wal, Caspar H. van der et al. “Quantum Superposition of Macroscopic Persistent-Current States”. In: *Science* 290.5492 (2000), p. 773.

[Wal+04] Wallraff, A. et al. “Strong coupling of a single photon to a superconducting qubit using circuit quantum electrodynamics”. In: *Nature* 431 (2004), 162 EP –.

[Wan+09] Wang, H. et al. “Improving the coherence time of superconducting coplanar resonators”. In: *Applied Physics Letters* 95.23 (2009), p. 233508.

[Wan+11] Wang, H. et al. “Deterministic Entanglement of Photons in Two Superconducting Microwave Resonators”. In: *Phys. Rev. Lett.* 106 (6 2011), p. 060401.

[Wan+14] Wang, Hui et al. “Solutions to the quantum Rabi model with two equivalent qubits”. In: *EPL (Europhysics Letters)* 106.5 (2014), p. 54001.

[Wan+16] Wang, Yimin et al. “Holonomic quantum computation in the ultrastrong-coupling regime of circuit QED”. In: *Phys. Rev. A* 94 (1 2016), p. 012328.

[Wer+08] Werlang, T. et al. “Rabi model beyond the rotating-wave approximation: Generation of photons from vacuum through decoherence”. In: *Phys. Rev. A* 78 (5 2008), p. 053805.

[WK10] Wilhelm, Seth T. Merkel and K., Frank. “Generation and detection of NOON states in superconducting circuits”. In: *New Journal of Physics* 12.9 (2010), p. 093036.

[WY07] Wu, Ying and Yang, Xiaoxue. “Strong-Coupling Theory of Periodically Driven Two-Level Systems”. In: *Phys. Rev. Lett.* 98 (1 2007), p. 013601.

[Xio+15] Xiong, Shao-Jie et al. “Efficient scheme for generation of photonic NOON states in circuit QED”. In: *Optics letters* 40.10 (2015), pp. 2221–2224.

[Yan+16] Yan, Fei et al. “The flux qubit revisited to enhance coherence and reproducibility”. In: *Nature Communications* 7 (2016). Article, 12964 EP –.

[Yao+11] Yao, N. Y. et al. “Robust Quantum State Transfer in Random Unpolarized Spin Chains”. In: *Phys. Rev. Lett.* 106 (4 2011), p. 040505.

[YN03] You, J. Q. and Nori, Franco. “Quantum information processing with superconducting qubits in a microwave field”. In: *Phys. Rev. B* 68 (6 2003), p. 064509.

[YN11] You, J. Q. and Nori, Franco. “Atomic physics and quantum optics using superconducting circuits”. In: *Nature* 474 (2011). Review Article, 589 EP –.

[Yos+16] Yoshihara, Fumiki et al. “Superconducting qubit-oscillator circuit beyond the ultrastrong-coupling regime”. In: *Nature Physics* 13 (2016), 44 EP –.

[YTN03] You, J. Q., Tsai, J. S., and Nori, Franco. “Controllable manipulation and entanglement of macroscopic quantum states in coupled charge qubits”. In: *Phys. Rev. B* 68 (2 2003), p. 024510.

[Yur+88] Yurke, B. et al. “Observation of 4.2-K equilibrium-noise squeezing via a Josephson-parametric amplifier”. In: *Phys. Rev. Lett.* 60 (9 1988), pp. 764–767.

[Yur+89] Yurke, B. et al. “Observation of parametric amplification and deamplification in a Josephson parametric amplifier”. In: *Phys. Rev. A* 39 (5 1989), pp. 2519–2533.

[Zag+08] Zagoskin, A. M. et al. “Controlled Generation of Squeezed States of Microwave Radiation in a Superconducting Resonant Circuit”. In: *Phys. Rev. Lett.* 101 (25 2008), p. 253602.

[Zha+16] Zhao, Yan-Jun et al. “Engineering entangled microwave photon states through multiphoton interactions between two cavity fields and a superconducting qubit”. In: *Scientific Reports* 6 (2016). Article, 23646 EP –.

[Zue+09] Zueco, David et al. “Qubit-oscillator dynamics in the dispersive regime: Analytical theory beyond the rotating-wave approximation”. In: *Phys. Rev. A* 80 (3 2009), p. 033846.

Appendices

Appendix A

Incoherent-mediator for quantum state transfer in the ultrastrong coupling regime: Effective Hamiltonian

Here, we derive the effective Hamiltonian described in the main manuscript where a two-qubit quantum Rabi system interacts with two additional qubits. We write the QRS Hamiltonian in its diagonal form ($\hbar = 1$)

$$H_{\rm QRS} = \sum_{j=0}^{\infty} \nu_j |\psi_j\rangle\langle\psi_j|, \tag{A.1}$$

where ν_j is the jth eigenfrequency associated with the jth eigenstate $|\psi_j\rangle$. Also, we make use of the completeness relation for eigenstates $|\psi_j\rangle$ to write the Hamiltonian (2) of the main manuscript as

$$H = \sum_{j=0}^{\infty} \nu_j |\psi_j\rangle\langle\psi_j| + \sum_{n=1}^{N=2} \frac{\omega_n}{2} \tau_n^z + \sum_{n=1}^{N=2} \sum_{j,k} \lambda_n \chi_{jk} \tau_n^x |\psi_j\rangle\langle\psi_k|, \tag{A.2}$$

where we have defined $\chi_{jk} = \langle\psi_j|(a + a^\dagger)|\psi_k\rangle$. To derive the effective qubit-qubit Hamiltonian, we consider the Hamiltonian (A.2) in the interaction picture with respect to the free part $H_0 =$

$\sum_{j=0}^{\infty}\nu_j|\psi_j\rangle\langle\psi_j| + \sum_{n=1}^{N=2}(\omega_n/2)\tau_n^z$. This leads to the Hamiltonian

$$\bar{H}_I(t) = \sum_{n,j,k}\lambda_n\chi_{jk}|\psi_j\rangle\langle\psi_k|\big(\tau_n^+ e^{i\Delta_{kj}^n t} + \tau_n^- e^{-i\mu_{kj}^n t}\big), \tag{A.3}$$

where the detuning parameters are defined as $\Delta_{kj}^n = \omega_n - \nu_{kj}$ and $\mu_{kj}^n = \omega_n + \nu_{kj}$, abd $\nu_{kj} = \nu_k - \nu_j$ are energy differences of the QRS. In addition, the effective Hamiltonian is given by

$$\bar{H}_{\text{eff}}(t) = \frac{1}{2}[\bar{H}_I(t), W(t)], \tag{A.4}$$

where the function $W(t)$ is defined by the following integral

$$W(t) = -i\int_{t_0}^{t}\bar{H}_I(t')dt'. \tag{A.5}$$

From the Hamiltonian (A.3) it is straightforward to obtain $W(t)$ as

$$W(t) = \sum_{n=1}^{N=2}\sum_{j,k}\left(\lambda_n\chi_{jk}\tau_n^-|\psi_j\rangle\langle\psi_k|\frac{(e^{-i\mu_{kj}^n t}-1)}{\mu_{kj}^n} - \lambda_n\chi_{jk}\tau_n^+|\psi_j\rangle\langle\psi_k|\frac{(e^{i\Delta_{kj}^n t}-1)}{\Delta_{kj}^n}\right). \tag{A.6}$$

Hence, the derivation of the effective Hamiltonian (A.4) depends only on the commutator between terms (A.6) and (A.3). In this case, the most relevant commutator are given by

$$\left[\tau_n^{\pm}|\psi_j\rangle\langle\psi_k|, \tau_m^{\pm}|\psi_p\rangle\langle\psi_q|\right] = \tau_n^{\pm}\tau_m^{\pm}(\delta_{kp}|\psi_j\rangle\langle\psi_q| - \delta_{jq}|\psi_p\rangle\langle\psi_k|) \tag{A.7a}$$

$$\left[\tau_n^{\pm}|\psi_j\rangle\langle\psi_k|, \tau_m^{\mp}|\psi_p\rangle\langle\psi_q|\right] = \tau_n^{\pm}\tau_m^{\mp}\delta_{kp}|\psi_j\rangle\langle\psi_q| - \tau_m^{\mp}\tau_n^{\pm}\delta_{jq}|\psi_p\rangle\langle\psi_k|. \tag{A.7b}$$

Thus, the effective Hamiltonian reads

$$\begin{aligned}
\bar{H}_{\text{eff}}(t) = \quad & \frac{1}{2}\sum_{n,n'}\sum_{j,k}\lambda_n\lambda_{n'}\chi_{jk}\times\Bigg[\\
& \sum_p\chi_{pj}|\psi_p\rangle\langle\psi_k|\Bigg(\frac{e^{i\Delta_{kj}^n t}(e^{i\Delta_{jp}^{n'}t}-1)\tau_n^+\tau_{n'}^+}{\Delta_{jp}^{n'}} - \frac{e^{i\Delta_{kj}^n t}(e^{i\mu_{jp}^{n'}t}-1)\tau_{n'}^-\tau_n^+}{\mu_{jp}^{n'}} \\
& + \frac{e^{-i\mu_{kj}^n t}(e^{i\Delta_{jp}^{n'}t}-1)\tau_{n'}^+\tau_n^-}{\Delta_{jp}^{n'}} - \frac{e^{-i\mu_{kj}^n t}(e^{-i\mu_{jp}^{n'}t}-1)\tau_n^-\tau_{n'}^-}{\mu_{jp}^{n'}}\Bigg) \\
& - \sum_q\chi_{kq}|\psi_j\rangle\langle\psi_q|\Bigg(\frac{e^{i\Delta_{kj}^n t}(e^{i\Delta_{qk}^{n'}}t-1)\tau_n^+\tau_{n'}^+}{\Delta_{qk}^{n'}} - \frac{e^{i\Delta_{kj}^n t}(e^{i\mu_{qk}^{n'}t}-1)\tau_{n'}^+\tau_n^-}{\mu_{qk}^{n'}} \\
& + \frac{e^{-i\mu_{kj}^n t}(e^{i\Delta_{qk}^n t}-1)\tau_n^-\tau_{n'}^+}{\Delta_{qk}^{n'}} - \frac{e^{-i\mu_{kj}^n t}(e^{-i\mu_{qk}^{n'}t}-1)\tau_n^-\tau_{n'}^-}{\mu_{qk}^{n'}}\Bigg)\Bigg].
\end{aligned} \tag{A.8}$$

It is noteworthy that in our system, the frequency terms μ_{kj}^{n}, Δ_{kj}^{n} and $\nu_{k,k'}$ are larger than the effective coupling terms $\lambda_n\lambda_{n'}\chi_{jk}\chi_{pj}/\Delta_{kj}^{n'}$ and $\lambda_n\lambda_{n'}\chi_{jk}\chi_{pj}/\mu_{kj}^{n'}$. Therefore, we can be safely neglect these fast oscillating terms in a secular approximation. In this case, the effective Hamiltonian in the Schrödinger picture reads

$$\begin{aligned} H_{\text{eff}} &= H_0 + \frac{1}{2}\sum_{n,n'}\sum_{j,k}\lambda_n\lambda_{n'}|\chi_{jk}|^2(|\psi_k\rangle\langle\psi_k| - |\psi_j\rangle\langle\psi_j|) \times \\ &\left(\frac{\tau_n^+\tau_{n'}^+}{\Delta_{jk}^{n'}} - \frac{\tau_n^+\tau_{n'}^-}{\mu_{jk}^{n'}} + \frac{\tau_n^-\tau_{n'}^+}{\Delta_{jk}^{n'}} - \frac{\tau_n^-\tau_{n'}^-}{\mu_{jk}^{n'}}\right). \end{aligned} \tag{A.9}$$

In addition, as the effective Hamiltonian contains terms of the form $\tau_n^{\pm}\tau_{n'}^{\pm}$, that are zero when $n = n'$, we can split the sum into two parts, one for equal indexes n and n', and one for the opposite case. In this situation, we obtain an effective qubit-qubit interaction between the leftmost and rightmost qubits

$$\begin{aligned} H_{\text{eff}} = H_0 + \frac{1}{2}\sum_{j,k}|\chi_{jk}|^2(|\psi_k\rangle\langle\psi_k| - |\psi_j\rangle\langle\psi_j|)\left[\sum_n \lambda_n^2\left(\frac{\tau_n^-\tau_{n'}^+}{\Delta_{jk}^{n'}} - \frac{\tau_n^+\tau_{n'}^-}{\mu_{jk}^{n'}}\right)\right] \\ +\frac{1}{2}\sum_{j,k}|\chi_{jk}|^2(|\psi_k\rangle\langle\psi_k| - |\psi_j\rangle\langle\psi_j|)\left[\sum_{n,n'}\lambda_n\lambda_{n'}\left(\frac{1}{\Delta_{jk}^{n'}} + \frac{1}{\Delta_{jk}^{n'}} - \frac{1}{\mu_{jk}^{n'}} - \frac{1}{\mu_{jk}^{n'}}\right)\tau_n^x\tau_{n'}^x\right]. \end{aligned} \tag{A.10}$$

Finally, if we truncate to the two lowest energy levels of the QRS, we obtain the effective Hamiltonian

$$H_{\text{eff}} = H_0 + \frac{1}{2}|\chi_{10}|^2\mathbf{Z}_p \otimes \mathbf{S}_{12}, \tag{A.11}$$

where $|\chi_{10}|^2 = |\langle\psi_0|(a^\dagger + a)|\psi_1\rangle|^2$, $\mathbf{Z}_p = |\psi_1\rangle\langle\psi_1| - |\psi_0\rangle\langle\psi_0|$, $\mathbf{S}_{12} = \lambda_1\lambda_2(1/\mu_{10}^1 + 1/\mu_{10}^2 - 1/\Delta_{10}^1 - 1/\Delta_{10}^2)\tau_1^x\tau_2^x + 2\sum_{n=1}^2\lambda_n^2(\tau_n^+\tau_n^-/\Delta_{10}^n - \tau_n^-\tau_n^+/\mu_{10}^n)$, and $\tau_n^{\pm} = (\tau_n^x \pm i\tau_n^y)/2$. The detunings are defined as $\Delta_{10}^n = \omega_n - \nu_{10}$ and $\mu_{10}^n = \omega_n + \nu_{10}$, where ω_n corresponds to the nth qubit frequency that interacts with the QRS.

Appendix B

Parity-assisted Generation of Nonclassical States of Light in Superconducting Circuits: Effective Hamiltonian

Here, we derive the effective Hamiltonian given in Eq. (6.8) in the chapter 6. We have done the derivation by considering the dispersive treatment beyond of RWA [Kya+17; Zue+09]. Let us consider the Hamiltonian given in the Eq (1) in the main manuscript

$$\mathcal{H} = \mathcal{H}_{\rm QRS} + \mathcal{H}_{\rm c} + \mathcal{H}_I, \tag{B.1}$$

$$\mathcal{H}_{\rm c} = \sum_{\ell=1}^{N} (\omega_1^\ell b_\ell^\dagger b_\ell + \omega_2^\ell c_\ell^\dagger c_\ell), \tag{B.2}$$

$$\mathcal{H}_I = \sum_{\ell=1}^{N} \left[J_1^\ell (b_\ell^\dagger + b_\ell) + J_2^\ell (c_\ell^\dagger + c_\ell)\right](a + a^\dagger), \tag{B.3}$$

which describe the interaction between a QRS with N multi-modes cavities, each of them supporting $M = 2$ modes. To obtain the effective Hamiltonian, first, we express the QRS Hamiltonian in its diagonal form

$$\mathcal{H}_{\rm QRS} = \sum_{j,p}^{\infty} \nu_j |j,p\rangle\langle j,p|, \tag{B.4}$$

where ν_j is the jth eigenfrequency from the jth eigenstate $|j,p\rangle$ with j is increasing in energy, and p is the parity of the state. Now we write the interacting term of the Hamiltonian in Eq. (B.1) in the QRS basis leading to

$$\mathcal{H}_I = \sum_{\ell=1}^{N} \sum_{j,k,p,q} (J_1^\ell \chi_{jk} b_\ell^\dagger |j,p\rangle\langle k,q| + J_2^\ell \chi_{jk} c_\ell^\dagger |j,p\rangle\langle k,q|) + \text{h.c}, \tag{B.5}$$

we are defined χ_{jk} as the matrix element of the annihilation operator of the QRS $\chi_{jk} = \langle j,p|a|k,q\rangle$. Now, we write the Hamiltonian (B.5) in the interaction picture with respect to the free Hamiltonian $\mathcal{H}_0$ defined as $\mathcal{H}_0 = \mathcal{H}_{\text{QRS}} + \mathcal{H}_{\text{c}}$. The interacting Hamiltonian reads

$$\bar{\mathcal{H}}_I = \sum_{\ell=1}^{N} \sum_{j,k,p,q} \left(J_1^\ell \chi_{jk} e^{-i\Delta_{kj}^{\ell 1} t} b_\ell^\dagger |j,p\rangle\langle k,q| + J_2^\ell \chi_{kj} e^{-i\Delta_{kj}^{\ell 2} t} c_\ell^\dagger |j,p\rangle\langle k,q|\right) + \text{h.c.} \tag{B.6}$$

Here, we have defined the detuning between the QRS with and the ℓth field mode as $\Delta_{kj}^{\ell n} = \omega_n^\ell - \nu_{kj}$. The effective Hamiltonian is given by

$$\bar{\mathcal{H}}_{\text{eff}}^\ell(t) = \frac{1}{2}\big[\bar{\mathcal{H}}_I(t), \mathcal{W}(t)\big]. \tag{B.7}$$

The function $\mathcal{W}(t)$ is defined as

$$\mathcal{W}(t) = -i\int_0^t dt' \bar{\mathcal{H}}_I(t') \tag{B.8}$$

$$\mathcal{W}(t) = \sum_{\ell=1}^{N} \sum_{j,k,p,q} \left[\frac{J_1^\ell \chi_{kj}(e^{-i\Delta_{kj}^{\ell 1} t} - 1)}{\Delta_{kj}^{\ell 1}} b_\ell^\dagger |j,p\rangle\langle k,q| + \frac{J_2^\ell \chi_{kj}(e^{i\Delta_{kj}^{\ell 2} t} - 1)}{\Delta_{kj}^{\ell 2}} c_\ell^\dagger |j,p\rangle\langle k,q|\right] + \text{h.c.} \tag{B.9}$$

Notice that, form Ref [SWF17]. For Hamiltonians with the following structure

$$\bar{\mathcal{H}}_I(t) = \sum_m \left[\hat{\mathcal{O}}_m e^{i\Delta_m t} + \hat{\mathcal{O}}_m^\dagger e^{-i\Delta_m t}\right], \tag{B.10}$$

the effective Hamiltonian is given by the relation

$$\bar{\mathcal{H}}_{\text{eff}}^\ell(t) = \sum_m \frac{1}{\Delta_m}\big[\hat{\mathcal{O}}, \hat{\mathcal{O}}^\dagger\big], \tag{B.11}$$

Thus, the effective Hamiltonian in the Schŕodinger picture reads

$$\mathcal{H}_{\rm eff}^{\ell} = \mathcal{H}_0 + \frac{1}{2}\sum_{\ell,\ell'=1}^{N} J_1^{\ell} J_2^{\ell'} (b_{\ell}^{\dagger} c_{\ell'} + b_{\ell} c_{\ell'}^{\dagger} - \mathbb{I}) \mathcal{A}_{\ell',n'} + \frac{1}{2}\sum_{\ell,\ell'=1}^{N} J_1^{\ell} J_2^{\ell'} b_{\ell}^{\dagger} c_{\ell'}^{\dagger} \mathcal{B}_{\ell',n'} + \text{h.c}, \tag{B.12}$$

where the operators $\mathcal{A}_{\ell',n'}$ and $\mathcal{B}_{\ell',n'}$ are associated with the QRS system and they are defined as

$$\mathcal{A}_{\ell',n'} = \sum_{\sigma,\rho} \frac{\chi_{\sigma\rho}^2}{\Delta_{\sigma\rho}^{\ell' n'}} \Big[|\rho,p\rangle\langle\rho,p| - |\sigma,q\rangle\langle\sigma,q| \Big] \tag{B.13}$$

$$\mathcal{B}_{\ell',n'} = \sum_{\sigma,k,\rho} \frac{\chi_{k\sigma}\chi_{\rho\sigma}}{\Delta_{\sigma\rho}^{\ell' n'}} |\rho,p\rangle\langle k,q| - \sum_{\sigma,j,\rho} \frac{\chi_{j\rho}\chi_{\rho\sigma}}{\Delta_{\sigma\rho}^{\ell' n'}} |j,p\rangle\langle\sigma,q| \tag{B.14}$$

In the three level approximation of the QRS, these operators are given by

$$\mathcal{A}_{\ell' n'} = \Omega_{10}^{\ell n} |0,+\rangle\langle 0,+| + \Omega_{21}^{\ell n} |2,+\rangle\langle 2,+|, \tag{B.15}$$

$$\mathcal{B}_{\ell' n'} = \mathcal{J}_{\ell,\ell'}^{n,n'} |0,+\rangle\langle 2,+|. \tag{B.16}$$

The effectives coupling strength $\Omega_{jk}^{\ell n}$ and $\mathcal{J}_{\ell,\ell'}^{n,n'}$ are defines as

$$\Omega_{jk}^{\ell n} = \frac{2\nu_{jk}[\chi_{kj}]^2}{(\nu_{jk})^2 - (\omega_{\ell}^{n})^2}, \tag{B.17}$$

$$\mathcal{J}_{n,n'}^{\ell,\ell'} = \frac{J_n^{\ell} J_{n'}^{\ell'} \chi_{01}\chi_{21}}{2} \left[\frac{1}{\Delta_{10}^{\ell' n'}} - \frac{1}{\Delta_{21}^{\ell' n'}} \right]. \tag{B.18}$$

For system parameters $\omega_1^n = 0.25\nu_{20}$, $\omega_2^n = 0.75\nu_{20}$, $J_1^n = 0.0075\nu_{20}$, and $J_2^n = 0.0053\nu_{20}$, we obtain that $\Omega_{jk}^{\ell n} \ll \mathcal{J}_{\ell,\ell'}^{n,n'}$ ($\mathcal{J}_{\ell,\ell'}^{n,n'}$ is at least two order of magnitude larger than $\Omega_{jk}^{\ell n}$). Thus, the frequency of their respective process are fast oscillating and can be neglected in a secular approximation. Leading to the effective Hamiltonian

$$\mathcal{H}_{\rm eff}^{\ell} = \mathcal{H}_{\rm QRS} + \mathcal{H}_{\rm c} + \sum_{\ell,\ell'=1}^{N} \mathcal{J}_{\ell}^{\ell'} (b_{\ell}^{\dagger} c_{\ell'}^{\dagger} \mathcal{S}^{-} + b_{\ell} c_{\ell'} \mathcal{S}^{+}), \tag{B.19}$$

which describes simultaneous two-photon processes in both cavities. Here, $S^{+} = |2,+\rangle\langle 0,+|$ corresponds to the ladder operator of the QRS in the effective two-level basis. For the cases,

$N = \{1, 2, 3\}$ the effective Hamiltonians read

$$\mathcal{H}^1_{\text{eff}} = \mathcal{J}^1_2 \left[b^\dagger_1 c^\dagger_1 \mathcal{S}^- + b_1 c_2 \mathcal{S}^+ \right]. \tag{B.20a}$$

$$\mathcal{H}^2_{\text{eff}} = \mathcal{J}^1_2 \left[b^\dagger_1 c^\dagger_1 + b^\dagger_2 c^\dagger_2 + b^\dagger_1 c^\dagger_2 + b^\dagger_2 c^\dagger_1 \right] \mathcal{S}^- + \text{H.c.} \tag{B.20b}$$

$$\mathcal{H}^3_{\text{eff}} = \mathcal{J}^1_2 \left[b^\dagger_1 c^\dagger_1 + b^\dagger_2 c^\dagger_2 + b^\dagger_3 c^\dagger_3 + b^\dagger_1 c^\dagger_2 + b^\dagger_1 c^\dagger_3 + b^\dagger_2 c^\dagger_1 + b^\dagger_2 c^\dagger_3 + b^\dagger_3 c^\dagger_1 + b^\dagger_3 c^\dagger_2 \right] \mathcal{S}^- + \text{H.c.} \tag{B.20c}$$